Understanding and Engineering the Photophysics of Single CdSe Nanocrystals

by

Inhee Chung

B.S. Chemistry

Pohang University of Science and Technology, 1999

Submitted to the Department of Chemistry

in Partial fulfillment of the requirements for

the Degree of

Doctor of Philosophy

At the

MASSACHUSETTS INSTITUTE OF TECHNOLOGY

June 2004

© 2004 MASSACHUSETTS INSTITUTE OF TECHNOLOGY

Signature of Author_____

Department of Chemistry
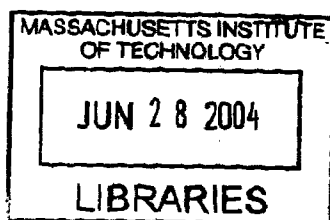
May 17, 2004

Certified by_____

Moungi G. Bawendi

Professor of Chemistry

Thesis Advisor

Accepted by_____

Robert W. Field

Chairman, Departmental Committee on Graduate Students

1

This doctoral thesis has been examined by a committee of the Department of Chemistry as follows:

Professor Keith A. Nelson
Chairman

Professor Moungi G. Bawendi
Thesis Supervisor

Professor Sylvia T. Ceyer

Understanding and Engineering the Photophysics of Single CdSe Nanocrystals

by

Inhee Chung

Submitted to the Department of Chemistry on May 17, 2004 in Partial Fulfillment of the Requirements for the Degree of Doctor of Philosophy in Chemistry

ABSTRACT

This thesis focuses on uncovering the photophysics of CdSe semiconductor quantum dots (QDs) at the single QD level, and correlating the phenomenological behavior observed at the single QD level to that observed at the ensemble level. Understanding the photophysics of QDs can potentially allow the specific optical properties of QDs to be applied in various ways. For example, through the study of the emission polarization of single QDs a 2D transition polarization property was discovered at room temperature. This enables us to monitor the 3D orientational dynamics of a target system by rigidly attaching a single QD to the system. Semiconductor QDs offer many advantages over other chromophores in a variety of applications because of their relatively narrow emission line width, an absorption spectrum that is well suited for multiplexed fluorescence detection, and their optical stability. However, fluorescence blinking phenomena in single colloidal QDs have been largely regarded as a undesirable optical properties. We have began to understand the phenomenology of the fluorescence blinking through a study of the statistics that are embedded in the fluorescence intensity time traces of collection of QDs. We have developed a statistical description of fluorescence blinking of single QDs and connected the blinking statistics to the fluorescence time traces of a collection of QDs. This study has shown that the fluorescence behavior of a collection of QDs is ergodic and moreover that it contains all the statistical information observed at the single QD level.

Thesis Supervisor: Moungi G. Bawendi, Ph.D.
Title: Professor of Chemistry

For my beloved family: Umma, Abba, and Yunhee

Table of Contents

List of Figures

7

List of Tables

Chapter 0. Introduction

0.1. The quantum confinement effect

When a photon with energy greater than the bandgap is absorbed in a semiconducting material, an electron-hole pair (a.k.a. an exciton) is created, followed by a radiative or non-radiative recombination. When the size of the semiconducting material is decreased to a size smaller than the Bohr radius, the confined carriers behave like particles in a box and simple quantum mechanical calculations predict their energies as a function of the size. Unlike the bulk, quantum confinement leads to discrete energy states, which vary as a function of the size and shape of the semiconductor.

Among colloidal semiconducting quantum dots (QDs), Cadmium Selenide (CdSe) QDs represent a benchmark system for the study of colloidal nanocrystals. CdSe QDs have been successfully synthesized using wet-chemical methods. They are of high optical quality and their radii can be tuned between 1 and 6 nm (the Bohr radius of CdSe is 5.6 nm). With the advent of single molecule spectroscopy, the study of individual QDs has deepened our understanding of the photophysical properties of these QDs. In order to fully utilize QDs as optical emitters, their fundamental photophysics need to be meticulously studied. Many chapters in this thesis are motivated by a desire to thoroughly understand the fundamental photophysics of single CdSe QDs, by revisiting previously discovered phenomena as well as discovering new physics.

0.2. Single QDs

0.2.1. A brief Introduction to the Photo-physics of CdSe QDs

Numerous theoretical studies have explained the size dependence of the energy levels of excitons confined by the physical volume of a nanocrystal [1-5]. The relative size of the exciton Bohr radius compared to that of the QD is the key criterion to determine if an exciton is located in the weak or strong confined regime. When the ratio between the Bohr radius, a, and the QD radius, R, is less than one ($a / R < 1$), then the electron and the hole are weakly confined. In this regime, the weakly confined exciton gains little kinetic energy from the 3D confinement. In this case, an infinite-potential-well model within the single-band effective approximation can be applied. On the other hand, when $a / R >> 1$, the 3D quantum confinement effect is very strong and the confined electron-hole pair is considered as one quasi-particle. Then the exciton is strongly affected by the presence of the spatial boundaries and the actual height of the boundaries. The excitonic Bohr radius of CdSe QDs is 5.6nm. In the strongly confined regime, the energy is dominated by the confinement which is dependent on $1/R^2$. This $1/R^2$ dependence gives rise to a blue-shift in the first absorption peak of CdSe QDs, with decreasing size. Since the effect from coulomb interaction ($\propto 1/R$) is smaller than the kinetic part, the electron and the hole are reasonably uncoupled in QDs. This uncoupled behavior between the electron and the hole gives the total energy as the sum of their energies added to the bulk band gap energy, E_g.

$$E_T = E_g + \frac{\hbar^2 k^2 n_{e,l_e}}{2m_e{}^*} + \frac{\hbar^2 k^2 n_{h,l_h}}{2m_h{}^*} \qquad (0.1)$$

Where Eg is 1.74 eV (1.84 eV) for CdSe at 300 K (10 K). The particle in a sphere model, using effective masses for the electron and the hole works well to describe the discrete absorption features seen in CdSe QDs [6,7].

0.2.2. Optical Properties of Single CdSe QDs

CdSe QDs are known for their size-dependent optical properties with absorption and emission wavelengths that are tunable across the visible range (~ 450-700 nm). The optical properties of single CdSe QDs have been widely studied with the advent of single QDs spectroscopy, using intensified CCD cameras for parallel data acquisition from single QDs [8,9], and single photon-counting measurements for lifetime [10] or quantum optics [11] experiments at the single QD level. Single QD spectroscopy demonstrated its excellence in giving access to single QDs photophysical parameters, which are hidden in the inhomogeneously broadened emission spectra or in the intensity signal from a collection of QDs. Single QD spectroscopy also opened the way to investigate the emission polarization of single CdSe QDs. Early studies suggested that the emitting transition dipole is 2-D degenerate, unlike organic dyes that mostly feature 1-D transition dipoles. Room temperature measurements of the emission polarization of single QDs enabled us to study the orientational dynamics of QDs embedded in or attached to an interesting system (such as glassy materials and bio-molecules) [9]. At low temperature (~ 10K), single QD emission spectra show a longitudinal optical (LO) phonon

12

progression with an averaged peak-to-peak energy spacing, equivalent to the energy spacing of bulk CdSe. Quantum-confined Stark effects were also investigated in strongly confined single CdSe QDs, where excitons are delocalized, and therefore highly polarizable[8]. Spectral diffusion was speculated to originate from the fluctuating environment, due to heating as an example. Single QDs embedded in glassy matrices have shown intermittency in their fluorescence time traces. The measured duration times when single QDs are emitting (on-times) and not emitting (off-times) followed power-law statistics [15]. Charging experiments and theoretical studies of blinking phenomena have led to a tentative model that a charged QD does not emit [12].

0.2.3. The blinking Statistics of CdSe QDs.

As described above, spectroscopic studies on single CdSe QDs have revealed many interesting photo-physical phenomenona, but many of them are still unexplained. The blinking statistics of CdSe QDs is one of them. The waiting times of switching events follow power-law statistics. Theoretical studies have attempted to explain the power-law statistics by utilizing a random walk model [14], or a trap distribution of charge carriers [15], but none of them have delivered an exact explanation. While the general statistics of the fluorescence blinking phenomena of single QDs in glass matrices are reported, the power-law statistics have not been fully described.

In nature, power-law statistics are observed for numerous systems, such as, long-range correlations in DNA sequences [16] and time intervals between consecutive earthquakes [17]. An important parameter of power-law distributions is the scaling

range. In power-law statistics for the duration of an event, the lower power-law cut-off could be the smallest duration time of that event. However this lower cut-off could be experimentally limited by the resolution of a detector or by the noise. The upper cut-off could be the largest duration time of that event. But in most cases, the upper cut-off is limited by human time scales.

For the case of single CdSe QDs, fluorescence intermittency obeys the power-law statistics $p(t) \propto t^{-\alpha-1}$ that are in the regime of Lèvy's statistics. Indeed, early experiments on single CdSe QDs showed that $\alpha \approx 0.5$. Therefore the mean and variance of waiting times for switching from on to off or off to on diverge if no cut-offs are included (an unbounded power-law). An on-time upper cut-off was observed in previous experiments on single CdSe QDs. On the other hand, no off-time upper cut-off was observed in the off-time power-law distribution. If this cut-off was to exist, it should be longer that the on-time counterpart. If there was no off-time upper cut-off, the fluorescence from a collection of QDs should completely vanish after a long period of time. But experimental investigations show that the fluorescence from a collection of QDs reaches a final non-zero steady state value. This not only proves that the upper cut-off time exists but also completes the off-time power-law distribution by giving us access to the off-time upper cut-off. One important message from this viewpoint is that the fluorescence decay often observed from collections of QDs, which was previously assigned to a photo-bleaching effect, can now be explained using purely statistical considerations.

With the presence of upper cut-offs, the statistics of fluorescence intermittency in the CdSe QD are now ergodic. In fact, we were uncertain about this ergodicity, so we decided to use 'a collection', rather than using 'an ensemble' to indicate many QDs. We

believe that having the full representation of the power-law statistics of the on- and off-waiting times from single QD fluorescence time traces will lead us to understand the microscopic blinking mechanisms as well as engineering the fluorescence blinking.

0.3. Thesis Overview.

This thesis concentrates on the photo-physical phenomena of single dots and collections of CdSe QDs. Chapter 1 describes room temperature emission polarization measurements from single CdSe QDs. The 2-D characteristic in the polarization enables monitoring the 3-D orientational dynamics of single QDs as a function of time. This enables the study of the rotational dynamics of glassy polymers at their glass transition.

The work in Chapter 2, as a first step for the rest of the thesis, was motivated by the intensity fluctuation in the fluorescence time trace of a QD-microsphere composite. We first started our work by investigating the effect of the experimental binning on the power-law statistics. As a result, we found that the power-law statistics are preserved through the binning. We also connected the blinking statistics of single QDs to the fluorescence intensity time trace of a collection of QDs. This work was done by Monte Carlo simulation and fluorescence measurements on single QDs and collections of QDs. We then modified the single QD power-law statistics to incorporate the cut-offs.

The florescence intensity time trace of a collection of QDs is described with a probability, $f_{on}(t)$, for a QD to emit at time t. With the condition of symmetric lower cut-offs, we were able to isolate three regions in the intensity time trace of the collection of QDs: a first early flat region which corresponds to a 50 % chance to have a QD in an on

state at time t, followed by a second power law decay region and a third steady state region where the intensity fluctuates around a mean value.

In chapter 3 we present the theoretical aspects of the effect of the lower cut-offs on the fluorescence intensity time traces of single QDs. Chapter 4 describes how the binning affects the fluorescence time traces of single QDs. Chapter 5 presents the effect of the excitation intensity on the fluorescence time trace: the thermal relaxation time of the QD system is defined. This thermal relation time was experimentally measured for overcoated QDs dispersed in hexane solution and solid QDs-polymer composite. In Chapter 6, we report the dependence of the excitation intensities on upper cut-off values. Chapter 7 explains the effect of the power-law statistics on the relative standard deviation (at the steady state) of the fluorescence intensities of a collection of QDs.

0.4. References

1. L. Brus, Appl. Phys. A 1991, 53, 456.
2. Al. L. Efros and A. L. Efros, Fiz. Tekh. Poluprovodn. **16**, 1209 (1982) Sov. Phys. Semicond. **16**, 772 (1982) ; D. J. Norris, M. G. Bawendi, Phys. Rev. B 1996, 53, 16 338.; D. J. Norris. A. L. Efros, M. Rosen, M. G. Bawendi, Phys. Rev. B 1996, 53, 16 347.; A. L. Efros, M. Rosen, M. Kuno, M. Nirmal, D. J. Norris, M. G. Bawendi, Phys. Rev. B 1996, 54, 4843.
3. L. E. Brus, J. Chem. Phys. **79**, 5s566 (1983).
4. S. V. Nair, S. Sinha and K. C. Rustagi, Phys. Rev. B **35**, 4098 (1987); T. Takagahara, **36**, 9293 (1987).
5. S. Schmidt-Rink, D. A. B. Miller and D. S. Chemla, Phys. Rev. B **35**, 8113 (1986); E. Hanamura, **38**, 1228 (1988)
6. C.B.Murray, D.J. Norris and M.G. Bawendi, J. Am. Chem. Soc. 115, 8706(1993), Norris, M. G.; Bawendi, M. G. Structure in the Lowest Absorption Feature of CdSe Quantum Dots.*J. Chem. Phys.* 1995, *103*, 5260-5268.
7. M.G. Bawendi, P.J. Carroll, W.L. Wilson and L.E.Brus, J.Chem.Phys. 96,946(1992), Norris, M. G.; Bawendi, M. G. Structure in the Lowest Absorption Feature of CdSe Quantum Dots.*J. Chem. Phys.* 1995, *103*, 5260-5268. Efros, Al. L.; Rosen, M.; Kuno, M.; Nirmal, M.; Norris,D. J.; Bawendi, M. G. Band-edge exciton in quantum
dots of semiconductors with a degenerate valence band: Dark and Bright exciton states. *Phys. Rev. B* 1996, *54*, 4843-4856.
8. A. L. Efros, Sov. Phys. Semicond. 1982, 16, 772.; L. E. Brus, J. Chem. Phys. 1984, 80, 4403.; [22] S. A. Empedocles, D. J. Norris, M. G. Bawendi, Phys. Rev. Lett. 1996, 77, 3873.
9. Empedocles, S. A. & Bawendi, M. G. (1997) *Science* **278**, 2114–2117.; Chung I, Shimizu KT, Bawendi MG: Room temperature measurements of the 3D orientation of single CdSe quantum dots using polarization microscopy. *Proceedings of the National Academy of Sciences of the United States of America* 2003, **100**:405-408.
10. Fisher BR, Eisler H-J, Stott NE, and Bawendi MG: Emission Intensity Dependence and Single-Exponential Behavior In Single Colloidal Quantum Dot Fluorescence Lifetimes, *Journal of Phys. Chem. B* 2004, **108**:143-148.
11. Lounis B, Single Nanoobjects as Triggered Single Photons Sources, Single Molecules Volume 2, Issue 4, 2001. Pages 289-290
12. Woo W-K, Shimizu KT, Jarosz MV, Neuhauser RG, Leatherdale CA, Rubner MA, Bawendi MG: Reversible charging of CdSe nanocrystals in a simple solid-state device. *Advanced Materials* 2002,14:1068-1071.
13. Shimizu KT, Neuhauser RG, Leatherdale CA, Empedocles SA, Woo WK, Bawendi MG: Blinking statistics in single semiconductor nanocrystal quantum dots. *Physical Review B: Condensed Matter and Materials Physics* 2001, 63; M. Kuno, D. P. Fromm, H. F. Hamann, A. Gallagher, and D. J. Nesbitt, J. Chem. Phys. 112, 3117 (2000).
14. A. L. Efros and M. Rosen, Phys. Rev. Lett. 78, 1110 (1997).
15. M. Kuno, D. P. Fromm, S. T. Johnson, A. Gallagher, D. J. Nesbitt "Modeling distributed kinetics in isolated semiconductor quantum dots,", *Phys. Rev. B* **67**, 125304 (2003).

16. A. Arneodo, E. Bacry, P/V. Graves, and J.F. Muzy, Phys. Rev. Letter. **74**, 3293 (1995).

17. K. Christensen, L. Danon, T. Scanlon, and P. Bak, Unified Scaling Law for Earthquakes. Proc. Natl. Acad. Sci. USA. **99**, 2509-2513 (2002).

Chapter 1. Room Temperature Measurements of the 3-D Orientation of Single CdSe Quantum Dots using Polarization Microscopy

1.1. Introduction

Optical investigations of transition dipole orientations have uncovered behavior ranging from structural changes in biological systems [1] to fast and slow relaxation dynamics at the molecular level in glassy matrices [2]. Most of these studies rely on organic dye molecules that have absorbing and emitting transition dipoles that are linear dipoles (non-degenerate, or linear emitters). In general, conventional far-field microscopy of such species can provide information only about the in-plane orientation of the chromophores through the projection of the transition dipole onto the focal plane. Insight into the full three-dimensional (3-D) orientation of optical probes should provide further detailed information about complex processes in the condensed phase. Scanning near-field microscopy and aberrated or defocused wide-field microscopy have been used in conjunction with linear emitters, providing information about the 3-D orientation of transition dipoles of single molecules [3-6]. These methods require especially high spatial resolution resulting in a smaller field of view and in greater acquisition times. A theoretical method to determine the 3-D orientation of a single molecule's transition dipole under a polarization microscope setup was as well developed [7]. Recently, scanning confocal microscopy has been used to image single absorbing transition dipoles by annular illumination in order to enhance the longitudinal component of the excitation source [8]. While easier to apply than the previous techniques, it can still be difficult to discern subtle changes in orientation, since the orientation information depends on a fit between theoretical and experimental image patterns of the transition dipoles.

A chromophore with a two-fold degenerate dipole (2-D or circular emitter) intrinsically contains 3-D orientation information. For a randomly oriented circular emitter, the 2-D polarization is projected as an elliptical shape on the sample plane where the ellipticity and direction of the long axis depend on the 3-D orientation of the transition dipole relative to the optical axis. Recently, CdSe QDs were shown to have a 2-D transition dipole at cryogenic temperatures [4]. Here we demonstrate that a 2-D transition dipole is also observed at room temperature (RT) where biological applications can be pursued [9,17].

Quantum confinement of the exciton in CdSe colloidal QDs results in discrete, atomic-like electronic energy levels. Numerous experimental studies on ensembles of QDs have suggested that the lowest lying states that participate in the emission process are doubly degenerate in the plane perpendicular to the c-axis [9-12]. This degeneracy is responsible for the previously observed 2-D transition dipole in emission at 10K. In this letter, we show that single CdSe QDs also have a 2-D transition dipole at room temperature. We use this finding to design an optical setup that can track the rotational motion of multiple single QDs simultaneously, in various host matrices, and at different temperatures.

1.2. Experimental

The emitting transition dipoles of 1-D and 2-D chromophores were probed using far-field polarization microscopy at room temperature. The samples were illuminated and the image collected using an oil-immersion microscope objective (N.A. of 1.25). Single DiI molecules (1,1'-dioctadecyl-3,3,3',3'-tetramethylindocarbocyanite

perchlorate) were chosen as a well-known organic dye molecule with a 1-D (linear) transition dipole. The CdSe QDs were prepared following the method of Murray *et al* [16] and overcoated with a few layers of ZnS [19]. A dilute solution of QDs (or DiI molecules) was spin-cast in a polymethylmethacrylate (PMMA) matrix onto a glass substrate. The fluorescence signal from individual QDs was split into its parallel and perpendicular polarization components by a polarization displacement prism.

In order to monitor orientation dynamics in real time, we used a modified optical layout that measures two polarization anisotropy values from four polarization components of the emission from multiple individual QDs simultaneously. First, the emission signal was split into two parallel beams by a set of three prisms. One of the beams was then rotated by 45° with a polarization rotator as shown in Fig. 1.1(a). These parallel beams were then split further according to their polarization using a polarization displacement prism to yield the 0°, 90°, 45°, and 135° polarization components of the emission for each QD as seen in Fig. 1.1(b). Two polarization anisotropy values were defined by the (0°, 90°), and (45°, 135°) components, respectively, for each QD. Since every pair of in-plane and out-of plane angles produces a pair of anisotropy values, a data analysis program was written to match the observed anisotropy values to the pair of two angles that defines the QD orientation. The time trace of anisotropy values then translates into a corresponding angular rotational time trace.
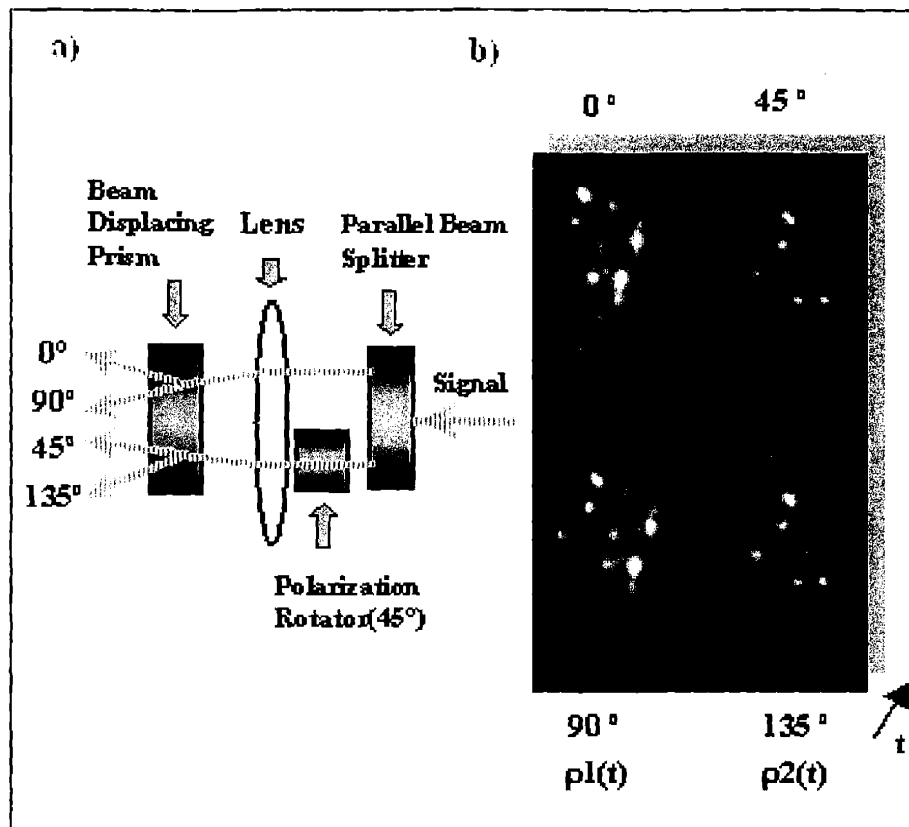
Figure 1.1. (a) Schematic of the apparatus used to obtain the image in (b). The fluorescence signal is split into two parallel beams. One beam is then rotated by 45° with a polarization rotator. The two beams are then passed through a polarization beam displacing prism to yield the 0°, 90°, 45°, and 135° polarization components of the image. (b) Four polarization components (0°, 90°, 45°, 135°) of the same QDs obtained simultaneously. Two components (0°, 90°) define one anisotropy value and the other two (45°, 135°) define the second anisotropy value. A series of these images creates a time series of anisotropy values.

1.3. 2-D Emitting Transition Dipoles of Single CdSe QDs at RT: Results

In order to identify the nature of the transition dipole for CdSe QDs, polarization anisotropy (ρ) values, defined as $\rho = \dfrac{I_{par} - I_{per}}{I_{par} + I_{per}}$, where $I_{par(per)}$ is the parallel (perpendicular) polarization component of emission intensity, were obtained. Figs. 1.2(a) and 1.2(b) show the orthogonal polarization components of the fluorescence from single

QDs and DiI molecules, respectively. Most of the QD images show both polarization components as in Fig. 1.2(a), while those from DiI molecules seldom show a complimentary pair in the orthogonal polarization. As an example, in Fig. 1.2(a) and 1.2(b), this is shown in the photo-emission images in orthogonal polarization from a QD and a DiI molecule inside two vertical circles, respectively.

a)   **b)**
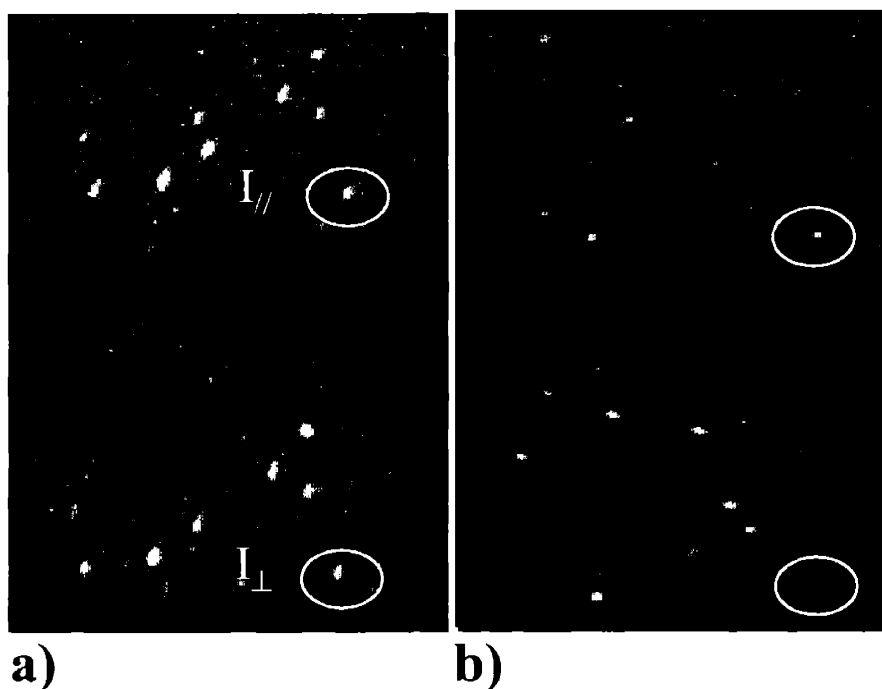
Figure 1.2. Polarized fluorescence images of single (a) CdSe QDs (2.8 nm radius) and (b) DiI molecules. The emission is split into two images with orthogonal polarization components using a polarization displacement prism. These images are used to obtain polarization anisotropy values. The intensity images of orthogonal polarization pairs of photo-emission from a QD and a DiI molecule are shown inside two vertical circles in (a) and (b).

The different statistical distributions of anisotropy values clearly reveal the different nature of the emitting transition dipoles between QDs and DiI molecules. Care was taken to properly prepare samples where the possibility for any rotational or

translational motion of the QDs (or DiIs) was greatly reduced and random distributions of orientations were ensured. Anisotropy values of the QDs and DiI molecules were nearly constant for the entire acquisition time, except for when the dots were in their "off" state (not luminescing), where noise then dominated the data. This verified that the particles in the PMMA matrix were frozen at their initial positions and that we were looking at single chromophores. Without careful background subtraction and rejection of QD dark periods, averaged anisotropy values may be reduced to zero, leading to misleadingly small values for the degree of polarization.

Histograms of the theoretical and experimental polarization anisotropy values of DiI molecules and QDs are shown in Figs. 1.3(a) and 1.3(c) and, 1.3(b) and 1.3(d), respectively. The theoretical distributions were calculated using transition dipole models based on Ref. [9]. I_{par} and I_{per} functions were defined in terms of the in-plane (ϕ) and out-of-plane (θ) angles accordingly. Anisotropy values (ρ) were generated assuming a random distribution of chromophore orientations. Since the projection of one dipole depends on the incident light cone which is determined by the N.A. of an objective, the anisotropy values were corrected for the collection angle (59.6°) of the microscope objective [14-15]. Experimental distributions of anisotropy values for QDs and DiI molecules were consistent with theoretical predictions for 1-D and 2-D transition dipoles, respectively, as shown in Fig. 1.2(a) and (b). Experimental and theoretical distributions of the polarization anisotropy values were not statistically different according to a chi-squared test.
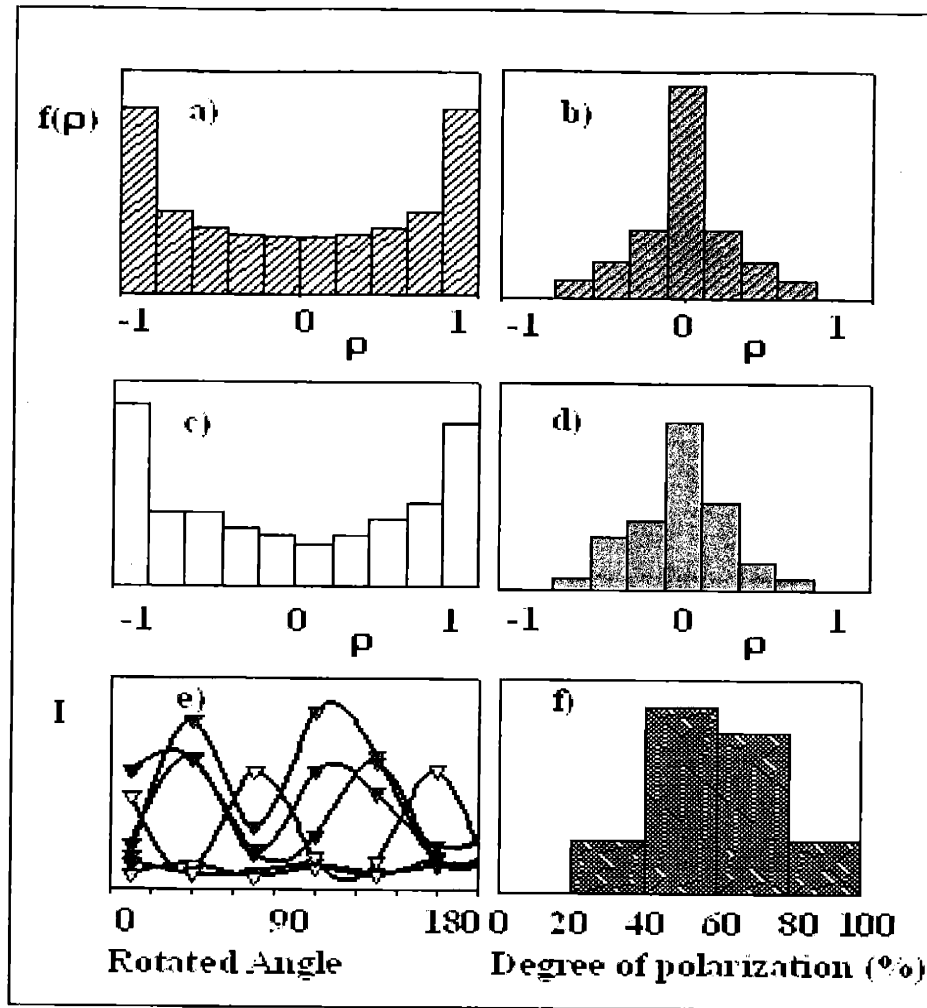
Figure 1.3. Theoretical histograms of the probability density, f(ρ), of polarization anisotropy values ρ for (a) 1-D and (b) 2-D transition dipoles, assuming that the emitters are randomly oriented. These histograms demonstrate good agreement with experimental results for (c) DiI (1-D dipole) and (d) CdSe QDs (2-D dipole). The intensity (I) variations while rotating the detection polarization angles from five QDs are plotted in (e). The experimental distribution of the degree of polarization (DOP) (f) is additional evidence of the 2-D character of the transition dipole of a CdSe QD. The distribution was obtained from 21 individual QDs. The shape of this distribution at room temperature is similar to that at low temperature.

Further evidence for a 2-D transition dipole in single QDs is shown in Figs. 1.3(e) and (f). By sequentially rotating the polarization displacement prism from 0° to 180°, changes in anisotropy values from the same single QD were plotted to show a sinusoidal pattern over rotated angles as shown in Fig. 1.3(e). Moreover, the degree-of-polarization

25

values, defined as $\frac{I_{max}-I_{min}}{I_{max}}$, for individual QDs were extrapolated out at the maxima of oscillatory plots. Fig. 1.3(f) demonstrates that the distribution of degree-of-polarization values for the randomly oriented set of QDs at room temperature is very much consistent with a 2-D transition dipole [4], in contrast with previous work [13]. The experimental mean value of the degree-of-polarization was measured to be 0.59 with the standard deviation, ±0.28, as compared to the simulated mean value of 0.50(±0.36) for generic 2-D transition dipoles.

We also investigated size-dependent emission properties of QDs with 1.3 nm, 1.8 nm and 2.8 nm radii. All three sizes of QDs showed statistically the same distribution of polarization anisotropy values as the 2-D theoretical analogue. According to theory, only the highest energy state among the five band-edge fine structure states is predicted to have a 1-D emitting transition dipole [12]. The polarization measurements above show that the contribution of the singly defined uppermost state to the emission polarization at room temperature is insignificant in our size range. This is consistent with simple calculations based on the energy spacing between the lowest optically active state and the uppermost state, combined with their oscillator strengths, [18] that predicts that ~ 10% of the population in the uppermost state at room temperature.

1.4. Polarization of Single QDs as 3-D Orientation Probes

The projection of the 2-D transition dipole onto the sample plane can provide out-of-plane and in-plane angle information about the QD orientation from measuring the ellipticity of the projection and the direction of the major axis [9]. However, to obtain

both the in-plane and out-of-plane angle and consequently the full 3-D orientation, two anisotropy values are needed. Fig. 1.3(a) shows four QDs, each with four different polarization components from our optical setup. Although the fluorescence image is divided into four components, the signal-to-noise ratio is still excellent.

As a proof-of-concept experiment to show that QDs can serve as a local probe of orientational dynamics, dilute concentrations of QDs were embedded in a few polymer/solvent mixtures and the individual QD rotational dynamics (~10–20Hz) were monitored. As an example, Fig. 1.4(a) maps the temperature dependent rotational dynamics of QDs in a hexadecane/PMMA system for 300 sec with 10 Hz acquisition rate. Each mark on the spherical map corresponds to the QD crystalline axis orientation and the lines connect between two sequential positions. The longitude and latitude correspond to in-plane (ϕ) and out-of-plane (θ) angles, respectively. At temperatures lower than the melting point (18°C) of hexadecane, we would expect QDs not to fluctuate much from their original position, while at temperatures above the melting point, the QDs should show more rotational diffusion. The blue plots demonstrate low temperature motion (10°C) while green and red plots show two sequential segments of the high temperature motion (27°C). Periods where the dot is in its "off" state (not emitting) have been removed from the plots. As expected, the low temperature data (blue plots) show little motion compared to the jumps of the green and red plots at the higher temperature.
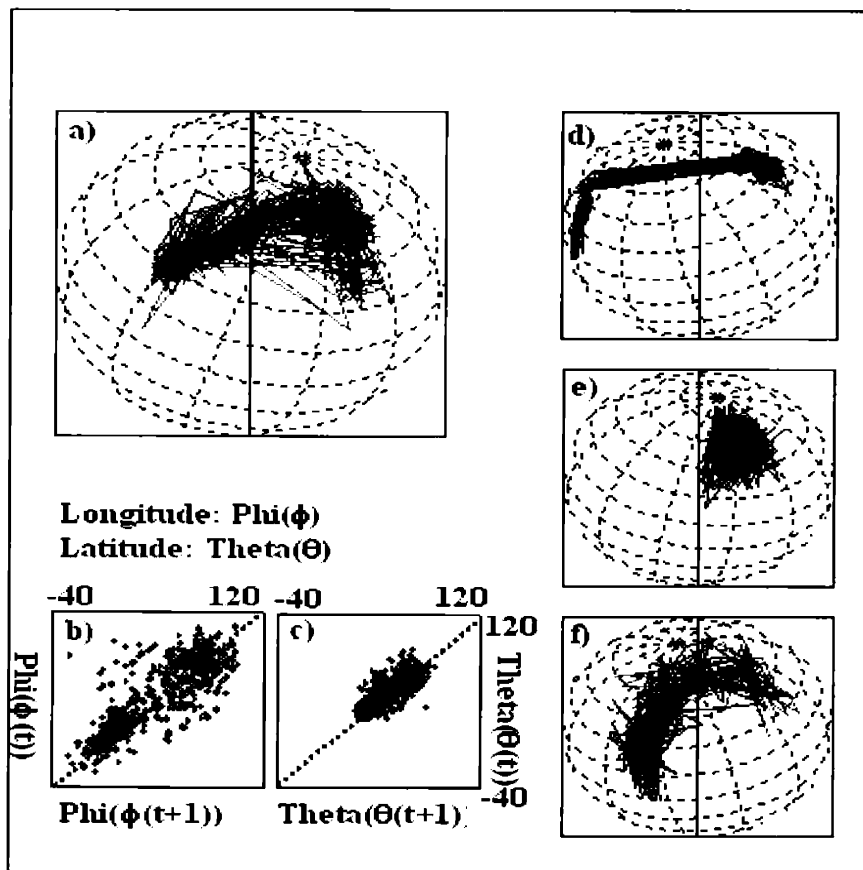
Figure 1.4. (a) Projection map of the temperature dependent rotational dynamics of a QD over 300s with 10Hz acquisition rate. Hexadecane (Mp = 18°C) mixed with PMMA was used as a matrix. The temperature was increased and sequentially measured in three traces: blue (10°C), green (27°C), and red (27°C). (b)-(c) Lag plots [$\phi(t)$ vs. $\phi(t+1)$ and ($\theta(t)$ vs. $\theta(t+1)$)] show that the positions correlate in time and that the deviations from the center values of (b) in-plane angle (ϕ) and (c) out-of-plane angle (θ) are larger at temperatures above the melting point than below. The colors correspond to those seen in (a). (d) Rotational movement of a QD in a viscous polymer matrix, poly(phenyl-glycidil)-ether-co-aldehyde, at room temperature. In sequence, three distinctive dynamics were observed and grouped with different colors (blue, green and red sequentially). (e) Rotational movements in a polymer that is less viscous than in (d) shows larger fluctuations. (f) Rotational dynamics in hexadecane/PMMA matrix.

This is well demonstrated in the lag plots of the out-of plane angle and the in-plane angle in Fig. 1.4(b) and 1.4(c), respectively. The plots [$\phi(t)$ vs. $\phi(t+1)$ and ($\theta(t)$ vs. $\theta(t+1)$), where (t+1) corresponds to one data point farther in time that at time t, show that the rotational dynamics are correlated in time since the data points are clustered along the

diagonal. At low temperature, the cluster (blue plots) is tightly bound along the diagonal but as the temperature is raised, two new clusters (green and red) are formed at different positions along the diagonal. The deviation from the diagonal distribution is a measure of the extent of fluctuation. Though the in-plane and out-of-plane angles were not constant at 10 °C (blue plots), the extent of the fluctuations was much smaller than at 27 °C (green and red). Compared to the lag plot of the out-of-plane angle in Fig. 1.4(c), the in-plane angle in Fig 1.4(b) shows more motion in general, thus indicating different dynamics for each angular motion. This may be explained if this particular QD was not perfectly embedded inside the matrix, but resided close to an interface.

Fig. 1.4(d) shows the rotational movement of a QD in a viscous polymer matrix, poly(phenyl-glycidil)-ether-*co*-aldehyde, at room temperature. As a function of time, three distinctive dynamics were observed and grouped in different colors. The dynamics in the blue track demonstrate little fluctuation around a single mean, but sudden jumping migration is observed in the green track. Due to the shape symmetry of the projected transition dipoles, changes of theta and phi by $\pm\pi$ will produce the same anisotropy values but this degeneracy can uncouple the rotational motion assuming continuous change of angle sets as long as the dynamics is sufficiently slow. Fig. 1.4(e) demonstrates rather large fluctuations around a single mean value of the rotational motion of a QD in polymer that is less viscous than in Fig. 1.4(d). It is clear that statistical studies from a number of QDs are necessary to appropriately understand these systems because a single QD cannot be reprsentative of the dynamics occurring in the entire host matrix. Fig. 1.4(f) shows rotational dynamics in a hexadecane/PMMA matrix. This plot clearly shows the migration from one type of trajectory motion in blue to another in green.

From these experiments, we can conclude that in order to fully understand the physics of dynamical properties of various host matrices, the rotational motions of many QDs must be simultaneously observed.

1.5. Conclusion

The appeal of CdSe QDs over conventional dye molecules is three-fold: (1) the 2-D transition dipole of QDs enables the application of simple far-field microscopy to monitor 3-D dynamical motion in real time, (2) QDs are photo physically more stable than organic dyes, and (3) simultaneous detection of different colored QDs can be performed with one excitation source. The 2-D transition dipole property of QDs enables the use of simple far-field microscopy to gain powerful 3-D orientation data. By using the emission polarization and optical properties of QDs, the rotational motion of many QDs can be monitored simultaneously in various matrices and in real time. These QDs may find use in better understanding the collective microscopic orientational motions in a variety of systems.

1.6. References

1. Bopp, M.A., Sytnik, A., Howard, T.D., Cogdell, R.J. & Hochstrasser, R.M. (1999) PNAS **96**, 11271-11276.

2. Deschenes, L.A. & Vanden Bout, D.A. (2001) Science **292**, 255-258.

3. Betzig, E. & Chichester, R. (1993) Science **262**, 1422-1425.

4. Sepiol, J., Jasny, J., Keller, J. & Wild, U. P. (1997) Chem. Phys. Lett. **273**, 444-448.

5. Dickson, R. M., Norris, D. J., & Moerner, W. E. (1998) Phys. Rev. Lett. **81**, 5322-5325.

6. Bartko, A. P. & Dickson, R. M. (1999) J. Phys. Chem. B **103**, 3053-3056.

7. Fourkas, J. T.(2001) Optics Letters **26**, 211-213

8. Sick, B., Hecht, B. & Novotny, L. (2000) Phys. Rev. Lett. **85**, 4482-4485.

9. Empedocles, S. A. & Bawendi, M. G. (1997) Science **278**, 2114-2117.

10. Efros, Al. L. (1992) Phys. Rev. B **46**, 7448-7458.

11. Efros, Al. L, Rosen, M, Kuno, M, Nirmal, M, Norris D. J. & Bawendi M. G. (1996) Phys. Rev. B **54**, 4843-4856.

12. Norris, D. J., Efros, Al. L., Rosen, M. & Bawendi, M. G. (1996) Phys. Rev. B **53**, 16347-16354.

13. Hu, J., Li, L.S., Yang, W., Manna, L., Wang, L.W. & Alivisatos, A.P. (2001) Science **292**, 2060-2063.

14. Fattinger, C. H. & Lukosz, W. (1984) J. Lumin. **31&32**, 933-935.

15. Lukosz, W. (1981) J. Opt. Soc. Am., **71**(6), 744-754.

16. Murray, C. B., Norris, D. J. & Bawendi, M. G. (1993) J. Am. Chem. Soc. **115**, 8706-8715.

17. Dahan, M., Laurence T., Pinaud F., Chemla D. S., Alivisatos A. P., Sauer, M. & Weiss, S. (2001) Optics Letters **26** (11), 825-827

18. Nirmal, M., Norris, D. J., Kuno,M., Bawendi, M. G., Rosen,M & Efros, A. L. (1995) Phys. Rev. Lett. **75**, 3728-3731.

19. Dabbousi, B. O., Rodriguez-Viejo, J., Mikulec, F. V., Heine, J. R., Mattoussi, H., Ober, R., Jensen, K. F. & Bawendi, M. G. (1997) J. Phys. Chem. B **101**, 9463-9475.

Chapter 2. Connecting Single Quantum Dot Intermittency and Fluorescence Intensity Decays from Collections of Dots

2.1. Introduction

Although advances in single fluorophore spectroscopy [1-3] have catalyzed detailed studies of individual fluorophores, connecting the dynamical behavior of a collection of fluorophores to that of the individual fluorophores is not always apparent, yet the phenomenology observed at the ensemble level must reflect the underlying microscopic dynamics. For example, while fluorescence spectroscopy on single colloidal semiconductor quantum dots (QDs) has uncovered interesting fluorescence intermittency [4-5] phenomena, the implications of this intermittency to observations at the ensemble level have not been obvious. Inversely, it has not been clear how observations at the ensemble level can contribute to our understanding of the dynamics at the single dot level. Yet understanding this connection is likely to be very important if we are to begin to understand the microscopic reasons for intermittency, and also because the performance of QDs in applications ranging from biological imaging [6,7] to opto-electronic devices [8,9] increasingly appears to be strongly affected by the intermittency. The working hypothesis for colloidal QDs is that the intermittency results as the QD switches between an emissive, neutral state (bright or "on") and a non-emissive, ionized, charged state (dark or "off") [4,10-12]. Probability distributions for the lengths of on(off)-times have been experimentally shown to follow power-law statistics [4,5]. Interestingly, the characteristic powers for the on(off)-time distributions have been observed to be similar

and insensitive to environmental changes[5]. The measured powers, in the absence of bounds to the time range of the distribution, place the blinking effect in Lévy's statistical regime, where the mean and the variance of the distribution diverge [13]. Upper bounds [5] have been observed only for the on-times, but they must also exist for the off-times. Otherwise, the emission intensities of all collections of QDs would eventually go to zero, which they do not. Emission intensities do exhibit a decay in time, but to a steady state. This decay has often been attributed to a permanent photochemical process. Although such processes can and do occur, decays observed under our experimental conditions are reversible. We show here that intermittency by itself predicts and explains both the rate of decay and the ultimate steady state level. Indeed, the behavior of a collection of QDs must reflect the underlying statistics of single QDs. This can be experimentally realized by exciting a collection of QDs that are immobile under the same conditions of high excitation power used to observe single QDs. Dahan and coworkers [14] have explained the experimental intensity decay of a collection of QDs from single QD statistics by taking a slightly higher on-time power than the off-time power, which results in non-ergodic behavior as expected from unbounded Lévy statistics, but this predicts a decay to zero intensity. Here we show that the experimentally observed intensity decay to a steady state in the fluorescence of a collection of immobile QDs implies that both on- and off-times must have upper bounds in their distributions and reflects underlying ergodic behavior. In this letter, we propose a phenomenological model that introduces lower and upper bounds to the on(off)-time power-law distributions of single QD fluorescence intermittency. We use Monte-Carlo simulations and analytical studies to show that this model is consistent with the intensity decay to a steady state observed in collections of

34

immobile QDs. Finally, we show that parameters of the underlying single QD phenomenological model that would be inaccessible from single QD experiments can be obtained from experiments on collections of QDs.

2.2. Experiments and Results

Experimental time traces of fluorescence intermittency by necessity use a time binning process. We begin by showing that the measured statistics of on(off)-times are not fundamentally affected by the choice of the bin-size, as long as it is sufficiently smaller than any experimentally observed long time bound. For the purposes of this discussion, we define an "intrinsic" intensity time trace as a time series of emitted photons prior to an experimental binning process. We use the simplifying assumption that (1) an off-state is a charged state that is "dark," (2) a photon is emitted after each absorption process during an on-state, and (3) the shortest time scale is then determined by the excitation flux. This shortest time scale becomes an operational measure of the lower bound to the distributions of on(off)-times. This intrinsic time trace effectively has a bin-size determined by the inverse value of the excitation flux, returning a value of "1" if the QD is neutral (i.e. fluoresces when interrogated), or "0" if it is dark. As defined, the intrinsic time trace is then perfectly binary, as shown in the trace of Fig. 2.2.1(a), obtained using a Monte-Carlo simulation described below. Re-binning this time trace, as is effectively done experimentally, diminishes its binary characteristic as shown in Fig. 2.2.1(b). The new bin-size then sets a new operational lower bound for the on(off)-time

distributions. On(off)-times in the re-binned time trace are defined relative to an arbitrary intensity threshold.
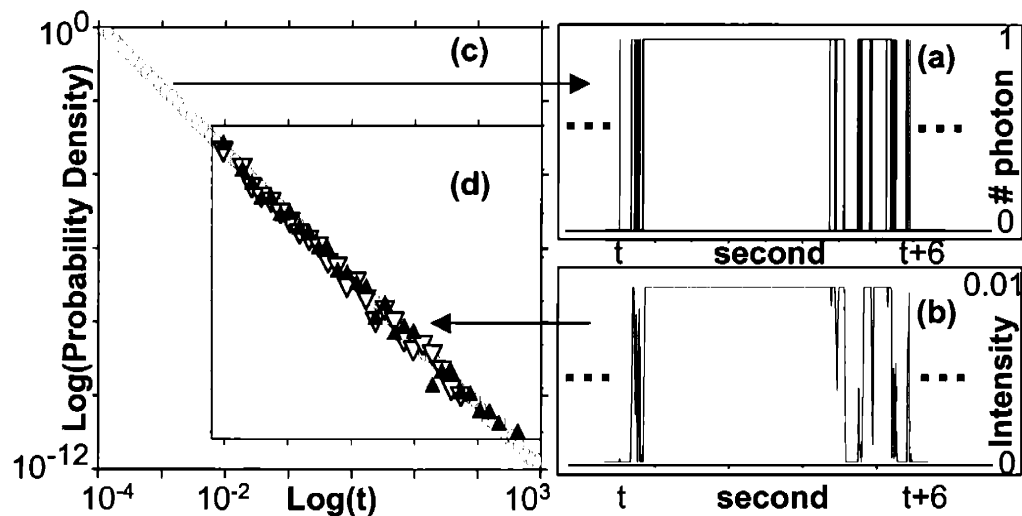
Figure 2.2.1. (a) Small portion of a simulated intrinsic time trace, constructed from the on(off)-time power-law probability distributions of Eq. 2.1 as described in the text. (b) Portion of the time trace [same portion as in (a)] after re-binning with a bin-size of 10^{-2} sec. (c) Probability density distributions for on- and off-times (overlapping open circles) from Eq. 2.1, used to generate the time traces in (a) and (b), with powers $- \mu_{on(off)} - 1 = -1.5$. (d) Probability density distributions for on- (open triangles) and off-(closed triangles) times, extracted from the re-binned trace, a small portion of which is shown in (b). The intensity threshold defining on-times is set to zero.

To explore the effects of re-binning and the choice of intensity threshold, we simulate intrinsic time traces assuming bounded power-law statistics for the distributions of on(off) times:

$$p_{on(off)}(t)dt = 0 \quad (t < t^{min}_{on(off)}), \quad p_{on(off)}(t)dt = 0 \quad (t^{max}_{on(off)} < t)$$

$$p_{on(off)}(t)dt = C_{on(off)} \cdot t^{-\mu_{on(off)}-1} dt \quad (t^{min}_{on(off)} < t < t^{max}_{on(off)})$$

(2.1)

where $p_{on(off)}(t)dt$ are on(off)-time probability density functions, $C_{on(off)}$ are normalization factors, and $[t^{min}_{on(off)}, t^{max}_{on(off)}]$ defines the time interval for which power-law statistics hold. Consistent with experimental observations, we chose $\mu_{on(off)} = 0.5$,

[10,11] and $t_{on(off)}^{min} = 10^{-4}$ sec (the initial bin-size). We arbitrarily set $t_{on(off)}^{max} = 10^3$ sec, an order of magnitude larger than the longest experimentally observed off-time (itself restricted by the length of an experimental time trace). Simulations were typically run to generate time traces spanning $3 \cdot 10^5$ sec. Fig. 2.2.1(a) shows a small (6 sec) snapshot of an intrinsic time trace generated by this simulation, Fig. 2.2.1(b) shows the same snapshot after re-binning, with a bin-size of 10^{-2} sec. Fig. 2.2.1(c) (open circles) shows the probability density distributions of on(off)-times used to generate the intrinsic trace. The probability density distributions of on- and off-times extracted after re-binning are shown as open and closed triangles in Fig. 2.2.1(d), using an intensity threshold set to 0 to define on and off events. Changing the intensity thresholds did not change the measured power-law statistics. Simulations were also performed to test different intrinsic power-law statistics with $0 < \mu_{on(off)} < 1$, defined in the same range $[10^{-4}, 10^3]$ (sec). We found in every case that the intrinsic power-law statistics were preserved through the re-binning process.

Experimental on-time distributions are observed to deviate from a pure power-law at longer times. This deviation is observed as a decay away from the power-law, or as an abrupt cut-off of the power-law distribution if the time trace is not long enough to statistically acquire enough of the long on-time events in this decay. Figure 2.2.2(a) shows experimental probability density distributions of on-times (triangles) and off-times (straight line), collected from various QDs [5] at room temperature. At low temperature (10K) and low laser excitation flux [5], the on-time power-law was observed to extend as far as the off-time power-law within the experimental window available. The deviation from power-law implies that the on-time power-law statistics are in parallel with

additional channels for charging the QDs that effectively act as upper bounds to the power-law. These additional channels are affected by the surface environment of the QDs, the temperature, and the excitation intensity [5]. Protecting the surface of the QDs increases the probability of observing longer on-times, delaying the start of deviation from power-law statistics.
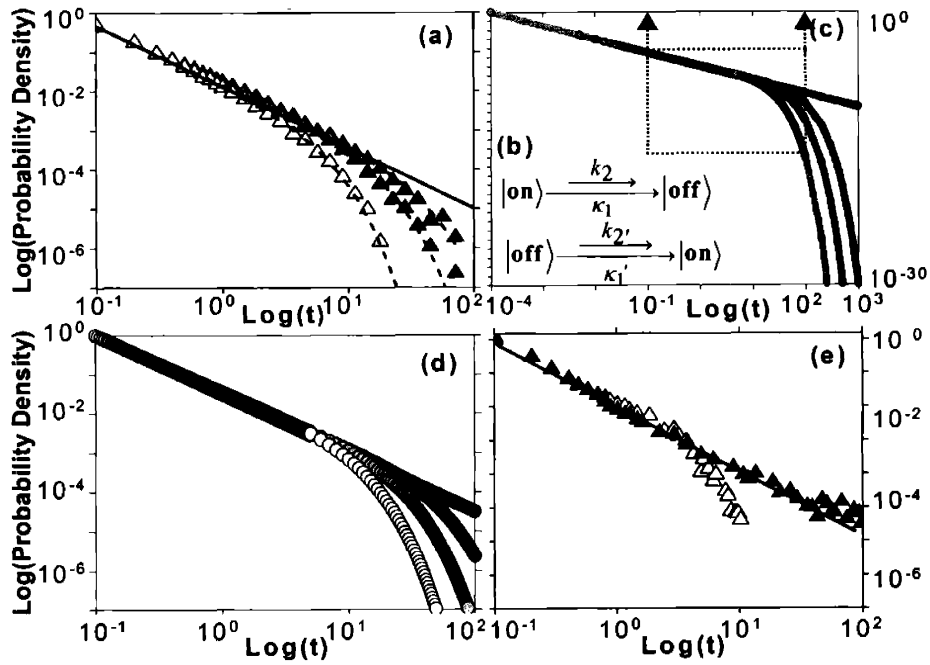
Figure 2.2.2. (a) Experimental probability density distributions of the on-times (triangles) for 1.5 nm-radius (black) and 2.5 nm-radius (gray) (CdSe)ZnS (core)shell QDs, and 2.5 nm-radius CdSe QDs (white). Their off-time distributions are indistinguishable on this graph and plotted as a solid line. The dashed lines are fits using Eq. 2.2, giving τ_{on}=16.4, 7.8, and 2.7 sec, respectively. The bin-size in these experiments was 10^{-1} sec. (b) Phenomenological half-reaction schemes for the two switching channels between on- and off-states, as described in the text. (c) Calculated probability density distributions using Eq. 2.2 with τ_{on} = 20, 5, and 2 sec, τ_{off} =10^{3} sec, and $t^{min}_{on(off)}$=10^{-4} sec. The dotted box indicates the experimental time range of [10^{-1}, 10^{2}] sec. (d) Calculated probability density distributions in the dotted box of (c), re-normalized for comparison with the experimental data in (a). (e) Probability density distributions for on-times (open triangles) and off-times (black triangles) obtained from a simulated time trace using Monte Carlo Methods from Eq. 2.2, using τ_{on} = 2 and τ_{off} = 10^{3} sec, and re-binned (bin-size = 10^{-1} sec).

38

Upper bounds or deviations from power-law statistics for the off-times have not been observed experimentally, because these bounds are apparently significantly larger than those for the on-times, as is seen below in our analysis of decays of collections of QDs.

We now construct a phenomenological model that incorporates the experimental observations as follows. We construct waiting time distributions with the half-reactions schemes as seen in Fig. 2.2.2(b), where each half-reaction consists of two parallel switching channels. One channel gives rise to a power-law distribution (resulting for example from an appropriate distribution of rate constants $\kappa_{1(1')}$ [11]), and the other is exponential with rate constants $k_{2(2')}$. The waiting time distributions, $p_{nf(fn)}(t)dt$, are the probability densities for observing a switch from an on-state to an off-state (nf), or vice versa (fn) after residing in an on- or off-state for time t. Consequently

$$p_{nf(fn)}(t) = \frac{dP_{on(off)}(t)}{dt}$$, where $1 - P_{on(off)}(t)$ are the cumulative distribution functions

for on(off)-times (i.e. the probability that a QD is still remained in the previous state) and

$$1 - P_{on(off)} = C_{on(off)} \cdot t^{-\mu_{on(off)}} \cdot exp(-t/\tau_{on(off)}) \quad (t_{on(off)}^{min} < t), P_{on(off)} = 0 \quad (t < t_{on(off)}^{min}) \quad (2.2)$$

with $\mu_{on(off)} = 0.5$ to match experiments, and with $t_{on(off)}^{min}$ as an operationally defined lower bounds as described previously. The exact values of $t_{on(off)}^{min}$ do not affect our results, as long as they are significantly smaller than both the length of a complete time trace and $\tau_{on(off)}$. The exponential term in the probability distribution effectively acts as an upper bound to the power-law. The presence of a lower bound and the exponential cut-off enables calculation of normalization factors, $C_{on(off)}$. We use this model to fit the experimental data of Fig. 2.2.2(a) (dashed lines), extracting τ_{on} values of 16.4, 7.8, and

2.7 sec for 1.5 nm radius (CdSe)ZnS [(core)shell] QDs, 2.5 nm radius (CdSe)ZnS QDs, and 2.5 nm radius CdSe QDs, respectively. Fig. 2.2.2(c) shows calculated probability density functions, $p_{nf(fn)}(t)$, based on Eq. 2.2 with on(off)-time probability distributions created with τ_{on} = 20, 5, and 2 sec, τ_{off} = 10^3 sec (chosen to be larger than the experimentally observed longest off-time) and $t_{on(off)}^{min}$ = 10^{-4} sec. Restricting the data between 10^{-1} sec and 10^2 sec and re-scaling shows that the calculated probability densities of Fig. 2.2.2(d) compare well with their corresponding experimental counterparts in Fig. 2.2.2(a). These statistics are also robust to re-binning. An intrinsic time trace constructed using Monte-Carlo methods from Eq. 2.2 using τ_{on} = 2 sec and τ_{off} = 10^3 sec was re-binned using a bin-size of 10^{-1} sec. The on(off)-time statistics of the re-binned time trace were then obtained and plotted in Fig. 2.2.2(e), which closely matches the experimental white triangle plot in Fig. 2.2.2(a).

With a phenomenological model for single QD statistics put forth, we now turn to the behavior of the fluorescence intensity from collections of immobile and dilute (non-interacting) QDs. Figure 2.2.3(a) shows intensity time traces from samples of CdSe and (CdSe)ZnS QDs, normalized to the initial intensity. The samples are in the dark until t=0, the starting point when they are illuminated with the laser. Both samples show fluorescence intensity decays, reaching steady state values at ~ 680 and 3,900 sec, respectively. The existence of a steady state implies that the power-law distribution of off-times must also have an upper bound. Otherwise the intensity evolutions would statistically "age", decaying to zero, with all the QDs displaying non-ergodic behavior by eventually residing in nearly infinitely long off-states. The intensity time trace of a collection of immobile, dilute QDs can be identically mapped onto the probability of

finding a single QD in an on-state. We can therefore analyze this ensemble experiment within the context of our phenomenological model for the statistics of single QDs. We will proceed two ways. We will derive analytical expressions for the probability of finding a QD in an on-state, and we will also simulate time traces for many individual QDs using Monte-Carlo methods, and add these traces together.

Analytical expressions for the probability of a QD being in an on-state can be derived from the waiting time distributions $p_{nf(fn)}(t)$. This probability, defined as $f_{on}(t)$, can be expressed in its Laplace transform,

$$f_{on}(s) = \frac{\alpha \cdot p_{nf}(s) \cdot (1 - p_{fn}(s)) + (1 - \alpha) \cdot (1 - p_{nf}(s))}{1 - p_{fn}(s) \cdot p_{nf}(s)} \cdot \frac{1}{s} \qquad (2.3)$$

where α is the proportion of QDs that are on at $t = 0$. To solve for $f_{on}(s)$, we divide the time into three segments as shown in Fig. 2.2.3(b): $t < \tau_{on}$, $\tau_{on} < t < \tau_{off}$, and $\tau_{off} < t$. We obtain the following results, as explained below, where $\langle t_{on(off)} \rangle$ is the expectation value for on(off)-times.

$$f_{on}(t) = 0.5 \qquad\qquad t_{on(off)}^{min} \ll t < \tau_{on}$$

$$f_{on}(t) \approx t^{-(1 - \mu_{off})} \qquad \tau_{on} \ll t < \tau_{off} \qquad (2.4)$$

$$f_{on}(t) = \frac{< t_{on} >}{< t_{on} > + < t_{off} >} \qquad t > \tau_{off}$$

When $t_{on(off)}^{min} \ll t < \tau_{on}$, both waiting time distributions are identical, giving $f_{on}(t) = 0.5$. When $\tau_{on} < t < \tau_{off}$, a mean on-time can be calculated, so that for t large compared to τ_{on}, a small-s expansion from Eq. 2.3 gives $p_{nf}(s) \sim 1 - s \langle t_{on} \rangle$, while $p_{fn}(t)$ is still a power-law. Since the on-time distribution converges while the off-time

41

distribution is still a power-law in this region, the probability f_{on} (t) decays like the

off-time power-law. Finally, when $\tau_{off} < t$, mean values can be obtained for both on and

off-times, yielding $p_{nf(fn)}(s) \sim 1 - s \left\langle t_{on(off)} \right\rangle$, which results in the probability of

a QD being in an on-state reaching a steady state.
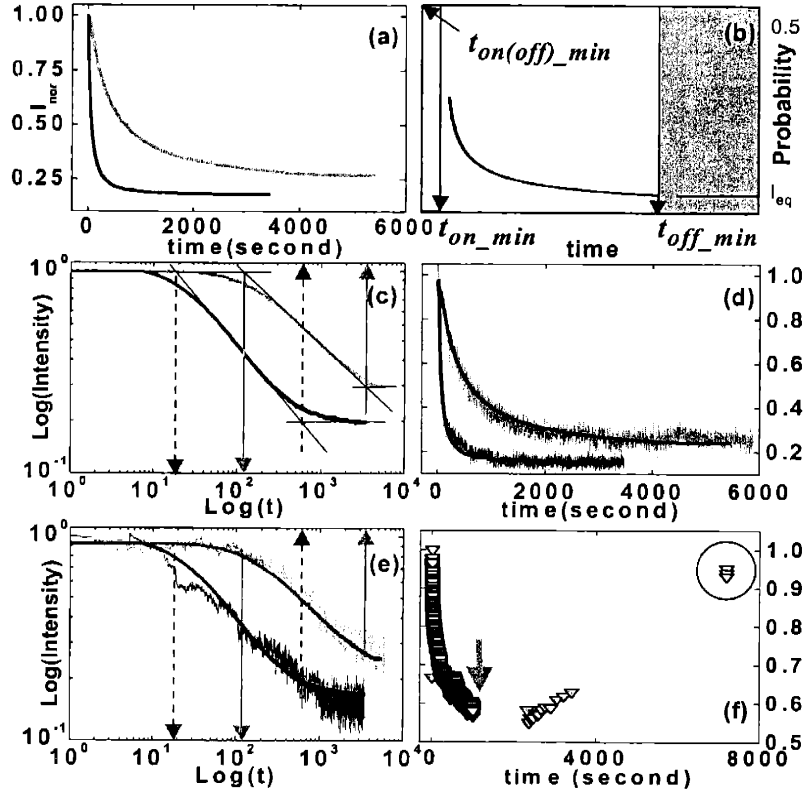
Figure 2.2.3. (a) Normalized fluorescence intensity time traces from collections of QDs, consisting of (CdSe)ZnS (core)shell (gray) and CdSe (black) QDs, both with core radii of 2.5 nm. (b) Plot of the analytical form for $f_{on}(t)$ (Eq. 2.3). (c) Log-log plots of the experimental intensity time traces in (a). The beginning and end points of the power-law decays for the two plots are indicated by arrows pointing up for the beginning points, and pointing down for the end points, respectively. These points are obtained as the intersections of the two slopes. These points correspond to τ_{on} and τ_{off}. (d) Intensity time traces obtained from adding 5,000 traces of different QDs generated using Monte-Carlo simulations. The smooth solid lines are the experimental data in (a) for comparisons. (e) Log-log plots of the simulated intensity time traces in (d) with plots in (c) overlayed. (f) Observed fluorescence intensity recovery after an initial decay, as described in the text, obtained from a collection of 2.4nm radius (CdSe)ZnS (core)shell QDs. The arrow indicates the time at which continuous excitation was stopped.

42

These analytical forms for $f_{on}(t)$ are especially interesting because they directly

link the intensity time trace of a collection of QDs to the statistical parameters that

describe the phenomenology of single QD on(off)-time distributions. In other words,

experiments on collections of QDs can be used to extract the phenomenological

parameters of single QD statistical models. This is particularly powerful because

experiments on collections of QDs can access regimes (such as long effective time traces,

or low laser flux intensities) that are inaccessible with single QD experiments. The main

result is that $f_{on}(t)$ should behave as a power-law for $\tau_{on} < t < \tau_{off}$, and should level out

to a constant defined by τ_{on} and τ_{off} for $t > \tau_{off}$. This is confirmed experimentally by

taking the experimental decays of Fig. 2.2.3(a) and replotting them on a log-log scale in

Fig. 2.2.3(c). After an initial flat region, the two curves show a power-law decay with a

power of approximately -0.5 (as expected from single dot statistics) starting at t~14 and

110 sec after the first excitation. The two plots begin to deviate from a power-law at t ~

680 and 3,900 sec and enter a steady state region, as predicted by Eq. 2.3. The beginning

and end of the power-law regime thus correspond to experimental values for the single

QD phenomenological constants τ_{on} and τ_{off}. This represents the first experimental

observation of an effective bound for the length of off-times. As an illustration of the

significance of this result, we estimate that it would require a single QD intensity time

trace that is ~10^6 sec (2 weeks) long to extract such a value of τ_{off} ~3,900 sec. The steady

state saturation intensities for $t > \tau_{off}$ are obtained experimentally as $I_{sat}= 0.10$ and 0.13

for the two curves, which compares well with the prediction of Eq. 2.3, which, using the

experimentally determined values for τ_{on} and τ_{off}, predicts $I_{sat}=$ 0.092 and 0.13, respectively [15].

To further complete the picture, we simulate the intensity time trace of a collection of QDs by summing the time traces of many individual QDs. We use the values of τ_{on} and τ_{off} experimentally obtained above to generate intensity time traces for 5,000 QDs by Monte Carlo methods, using a bin-size of 10^{-1} sec. The summation of these traces is shown in Figs. 2.2.3(d) and 2.2.3(e). The simulated time traces overlap well with the experimental traces. The intensity fluctuations observed in the simulated traces are consequences of the finite number of QDs in the collection, with each QD blinking.

If the experimental intensity decays of collections of QDs in Fig. 2.2.3 are the result of underlying single QD statistics, then this intensity decay should be reversible. This is illustrated in Fig. 2.2.3(f). The initial intensity decay in the presence of continuous excitation is first observed. The excitation light was removed at t=1,400 sec (marked by an arrow), and the fluorescence intensity was then sampled with short excitation events. The intensity as shown inside a circle is observed to have almost completely recovered after 6,400 sec. This recovery also indicates that the switch from an off- to an on-state needs not be light-induced.

2.3. Conclusion

In conclusion, we have shown that bounds to the power-law probability distributions for on- and off-times in QD blinking statistics are critical in understanding fluorescence intermittency in these single fluorophore experiments. These bounds allow us to quantitatively correlate the properties of single QDs to the observation of intensity decays in collections of QDs, under conditions where permanent photochemical darkening processes appears to be insignificant. We have shown that experiments on collections of QDs can now also be used to extract parameters of single QD statistics that could not have been obtained otherwise. These new parameters are likely to have a microscopic origin. A systematic exploration of how these parameters vary as a function of local dot environment may be the key to understanding intermittency at the microscopic level.

2.4. References

[1] W. E. Moerner and L. Kador, Phys. Rev. Lett. **62**, 2535 (1989).

[2] M. Orrit and J. Bernard, Phys. Rev. Lett. **65**, 2716 (1990).

[3] E. Betzig and R. J. Chichester, Science **262**, 1422 (1993).

[4] M. Kuno, D. P. Fromm, H. F. Hamann, A. Gallagher, and D. J. Nesbitt, J. Chem. Phys. **112**, 3117 (2000). ; M. Kuno, D. P. Fromm, H. F. Hamann, A. Gallagher, and D. J. Nesbitt, J. Chem. Phys. **115**, 1028 (2001).

[5] K. T. Shimizu, R. G. Neuhauser, C. A. Leatherdale, S. A. Empedocles, W. K. Woo, and M. G. Bawendi, Phys. Rev. B **63**, 205316 (2001).

[6] M. Dahan, S. Levi, C. Luccardini, P. Rostaing, B. Riveau, A. Triller, Science **302**, 442 (2003)

[7] D. S. Lidke, P. Nagy, R. Heintzmann, D. J. Arndt-Jovin, J. N. Post, H. E. Grecco, E. A. Jares-Erijman, T. M. Jovin, Nature Biotechnology **22**, 198 (2004)

[8] N. Tessler, V. Medvedev, M. Kazes, S. H. Kan, U. Banin, Science **295**, 1506 (2002)

[9] W. K. Woo, K. T. Shimizu, M. V. Jarosz, R. G. Neuhauser, C. A. Leatherdale, M. A. Rubner, M. G. Bawendi, Advanced Materials **14**, 1068 (2002)

[10] Al. L. Efros and M. Rosen, Phys. Rev. Lett. **78**, 1110 (1997).

[11] M. Kuno, D. P. Fromm, S. T. Johnson, A. Gallagher, D. J. Nesbitt, *Phys. Rev. B* **67**, 125304 (2003).

[12] Y. Jung, E. Barkai, and R. J. Silbey, *Chem. Phys.* **284** (1-2): 181-194 (2002).

[13] F. Bardou, J. P. Bouchaud, A. Aspect, and C. Cohen-Tannoudji, *Lévy Statistics and Laser Cooling* (Cambridge University Press, Cambridge, England, 2001).

[14] X. Brokmann, J.-P. Hermier, G. Messin, P. Desbiolles, J.-P. Bouchaud, and M. Dahan, Phys. Rev. Lett. **90** 120601 (2003).

[15] Note that Eq. 2.3 has $I(t = 0) = 0.5$, while we normalized Fig. 2.2.3 to have $I(t = 0) = 1.0$. This is taken into account in our comparison.

Chapter 3. Theoretical viewpoints on the relationship of the power-law cut-off values and the fluorescence intensity time traces

3.1. Introduction

In Chapter 2, we learned that the seven parameters that describe the blinking statistics of single QDs explain the photo-decay and the final steady-state that appears in the fluorescence time trace of collections of single QDs. The seven parameters are: the initial proportion of neutral QDs, α, the on- and off-time lower and upper cut-offs, t_{on}^{min}, t_{off}^{min}, t_{on}^{max} and t_{off}^{max}, and the on- and off-time powers, μ_{on} and μ_{off}. μ_{on} and μ_{off} are obtained from analyzing single QD time traces. From the experimental blinking statistics for single QDs, we obtained the average values $\mu_{on} \approx \mu_{off} \cong 0.5$. The parameters, μ_{off}, t_{on}^{max} and t_{off}^{max}, can be directly obtained from the fluorescence time traces of collections of QDs. On the other hand, t_{on}^{min}, t_{off}^{min} and α are not seen in the fluorescence time traces of a collection of QDs when the bin-size, t_b, is much larger than t_{on}^{min} and t_{off}^{min}. (see Chapter 4) In Chapter 2, we hypothesized that t_{on}^{min} and t_{off}^{min} are light-induced, and for simplicity, we further assumed $t_{on}^{min} \cong t_{off}^{min}$. However, there are some indications that the relative values of t_{on}^{min} and t_{off}^{min} can be indirectly estimated from the fluorescence time traces of collections of some QDs at some excitation period.

48

When $t_{on}^{min} \cong t_{off}^{min}$, the inital part ($0 \ll t < t_{on}^{max}$) of the fluorescence time trace of a collection of QDs is described by $f_{on}(t) = 0.5$ with the condition $t_b \gg t_{on(off)}^{min}$. We define the constant $f_{on}(t)$ region as the quasi-equilibrium state which is a temporary equilibrium.
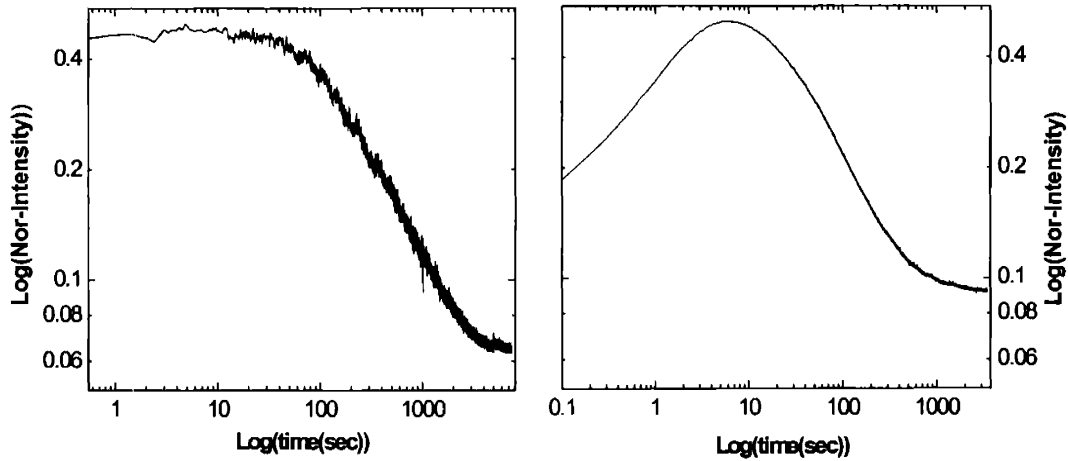
Figure 3.1. (a) Log-log plot of the fluorescence time trace of a collection of CdSe(ZnS) QDs at the excitation intensity of 8 kW/cm^2. The first absorption peak of the QDs/hexane solution was at 592 nm and the diluted solution was spin-coated on a bare glass substrate. (b) Log-log plot of the fluorescence time trace of a collection of core-shell CdSe(ZnS) at 30 kW/cm^2. The first ABS peak was at 570 nm and the sample preparation was the same as (a).

Figure 3.1(a) demonstrates the quasi-equilibrium state where $f_{on}(t) = 0.5$ when $t < 40$ sec from the fluorescence intensity time trace of a collection of CdSe(ZnS) QDs. Although the $f_{on}(t) = 0.5$ region is often acquired for CdSe and CdSe(ZnS) QDs on bare glass substrates or polymer matrices, different quasi-equilibrium states and initial dynamic features are also observed. (see Chapter 6) For example, Figure 3.1(b) does not show the quasi-equilibrium state. Instead, the early dynamics show photo-brightening for 6 sec, directly followed by a photo-decay, without the appearance of a stable quasi-

49

equilibrium. As shown in this chapter, the difference between the first two examples originates from different values of t_{on}^{min} and t_{off}^{min}.

In this chapter, we theoretically model fluorescence time traces by the time evolution of $f_{on}(t)$, constructed using an intrinsic bin-size smaller than t_{on}^{min} and t_{off}^{min}, and by varying the three parameters, α, t_{on}^{min} and t_{off}^{min}, while fixing the other four parameters as $t_{on}^{max} = 10\ (10^2)$ and $t_{off}^{max} = 10^2(10^3)\sec$, and $\mu_{on(off)} = 0.5$. We observe how these three parameters, α, t_{on}^{min} and t_{off}^{min}, affect the initial dynamics, quasi-equilibrium state and the steady-state. Rather than utilizing Monte-Carlo Simulations as done in Chapter 2, we will numerically calculate the inverse Laplace transform of $f_{on}(s)$. This direct conversion does not incorporate the experimental binning, but we explain how binning affects the initial dynamics of $f_{on}(t)$. The function $f_{on}(t)$ will be constructed using an intrinsic bin-size of 10^{-8} sec, and effects due to thermal relaxation will not be taken into account. (see Chapter 5)

3.2. Results

3.2.1. $t_{on}^{min} \cong t_{off}^{min}$
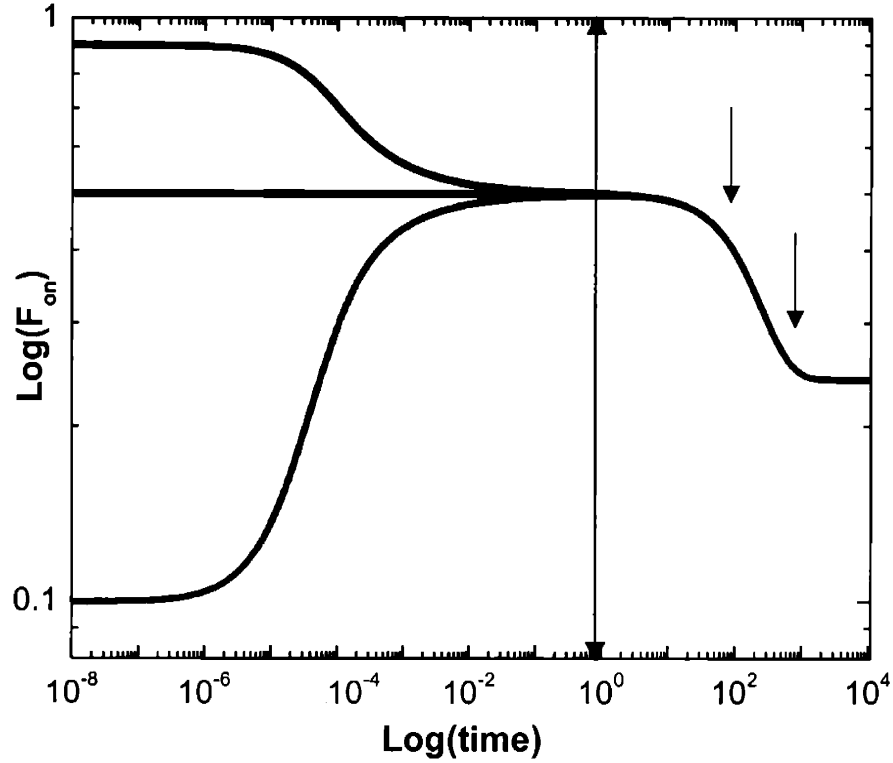
Figure 3.2.1. $t_{on}^{min} = t_{off}^{min} = 10^{-4}$ sec, and $t_{on}^{max} = 10^2$, $t_{off}^{max} = 10^3$ sec with α as (a) 90% (red), (b) 50% (black) and (a) 10% (green).

Figure 3.2.1(a)-(c) are constructed using $t_{on}^{min} \cong t_{off}^{min} = 10^{-4}$ sec ,

$t_{on}^{max} = 10^2$ and $t_{off}^{max} = 10^3$ sec and α = 10% (green), 50% (black) and 90% (red), respectively. The intrinsic bin-size is arbitrarily set at 10^{-8} sec. $f_{on}(t)$ is found to be constant with $f_{on}(t) = \alpha$, from 10^{-8} sec to 10^{-6} sec, as seen in the yellow box. When t approaches $t_{on}^{min} = 10^{-4}$ sec, $f_{on}(t)$ decays (when α = 0.9) or rises (when α = 0.1) to the

51

quasi-equilibrium state which appears exactly at $f_{on}(t) = 0.5$. This constant $f_{on}(t) = 0.5$ value begins to deviate as time approaches $t = t_{on}^{max}$. Irrespective of α, which is the QTQY value (see Chapter 5), the quasi-equilibrium states are characterized by $f_{on}(t) = 0.5$ as shown for the three time traces in this Figure. t_{on}^{max} and t_{off}^{max} are precisely observed as indicated by the arrows at 10^2 and 10^3 sec, respectively. A common steady state appears for the three time traces at $f_{on}(t) = 0.24$. Theoretically the $f_{on}(t)$ values at the quasi-equilibrium state, $f_{on}^{qe}(t)$, and steady state, $f_{on}^{ss}(t)$, can be given as:

$$f_{on}^{qe} = \frac{\left\langle t_{on} \right\rangle_{t_{on}^{min}}^{\infty}}{\left\langle t_{on} \right\rangle_{t_{on}^{min}}^{\infty} + \left\langle t_{off} \right\rangle_{t_{off}^{min}}^{\infty}}$$

$$f_{on}^{ss} = \frac{\left\langle t_{on} \right\rangle_{t_{on}^{min}}^{t_{on}^{max}}}{\left\langle t_{on} \right\rangle_{t_{on}^{min}}^{t_{on}^{max}} + \left\langle t_{off} \right\rangle_{t_{off}^{min}}^{t_{off}^{max}}} \qquad (3.2.1)$$

where $\left\langle t_{on} \right\rangle_{t_{on}^{min}}^{\infty}$ and $\left\langle t_{off} \right\rangle_{t_{off}^{min}}^{\infty}$ are the mean values of the on- and off-times within the range of $t_{on}^{min}, t_{off}^{min} < t < \infty$, respectively. In addition, $\left\langle t_{on} \right\rangle_{t_{on}^{min}}^{t_{on}^{max}}$ and $\left\langle t_{off} \right\rangle_{t_{off}^{min}}^{t_{off}^{max}}$ are the mean values of the on- and off-times within the range of $t_{on}^{min}, t_{off}^{min} < t < t_{on}^{max}, t_{off}^{max}$, respectively. This Equation 3.2.1, and the functional forms for $\left\langle t_{on(off)} \right\rangle$ yield $f_{on}^{qe} = 0.50$ and $f_{on}^{ss} = 0.24$.

52

The double-sided arrow shows the position of an arbitrary experimental bin-size,

$t_b = 1\sec$. In this case, the early dynamics shown until $t = 1\sec$ are averaged within the

first bin and not observed. With $t_b \cong 1\sec$, all three time traces in Figure 3.2.1 map onto

an observed time trace that would only show the quasi-equilibrium state at $f_{on}(t) = 0.5$

followed by a decay to a steady state. When t_{on}^{max} is not sufficiently larger than t_{on}^{min}, as

described below, the quasi-equilibrium state at $f_{on}(t) = 0.5$ is not reached. Figure 3.2.1(d)

demonstrates how the time traces are affected when t_{on}^{min} approaches t_{on}^{max}. The green

line is for $\alpha = 0.5$. The black, dark gray, gray, and light gray curves are constructed using

$\alpha = 0.9$ and 0.1, as in Figure 3.1, with $t_{on(off)}^{min}$ values at 10^{-6}, 10^{-4}, 10^{-2}, and 10^{-1} sec,

respectively. When $t_{on}^{max} / t_{on}^{min} \leq 10^4$, the quasi-equilibrium states are no longer reached.
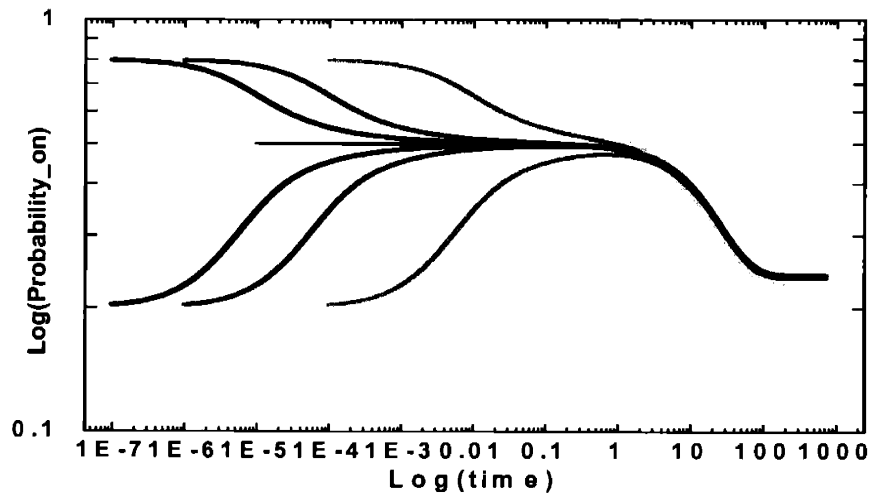
Figure 3.2.1(d) The green line is when $\alpha = 0.5$. The upper (lower) curves of black, dark gray, gray, and light gray are drawn when $\alpha = 0.9$ (0.1) with the identical on and off-time lower cut-offs are given 10^{-6}, 10^{-4}, 10^{-2}, and 10^{-1} sec.

As long as $t_{on}^{min} \cong t_{off}^{min}$ and $t_{on}^{max} \gg t_{on}^{min}$, the quasi-equilibrium is formed at

$f_{on}(t)$ = 0.5, independent of the value of α . The steady-state value is only a function of

t_{on}^{max} and t_{off}^{max} as in Figure 3.1(a). However, when the early symmetry is broken (i.e.

$t_{on}^{min} \neq t_{off}^{min}$), but retains the condition that $t_{on}^{max} \gg t_{on}^{min}$, the steady state value becomes

a function of both $t_{off}^{min}/t_{on}^{min}$ and $t_{off}^{max}/t_{on}^{max}$. In chapter 2, we assumed that t_{on}^{min} and t_{off}^{min}

are purely light-induced (an excitation period triggers t_{on}^{min} and t_{off}^{min}.) and $t_{on}^{min} \cong t_{off}^{min}$.

There is no direct experimental evidence that $t_{on}{}^{min}$ is only a function of the excitation

period, but it is clear from other experimental results that they are closely correlated (see

Chapter 4). The assumption of $t_{on}^{min} \cong t_{off}^{min}$ does not appear to be universal (see Chapter

6). We have observed numerous experimental time traces whose behavior suggests that

$t_{on}^{min} \neq t_{off}^{min}$. The next two sections will theoretically explore the cases of $t_{on}^{min} \neq t_{off}^{min}$.

3.2.2. $t_{on}^{min} < t_{off}^{min}$
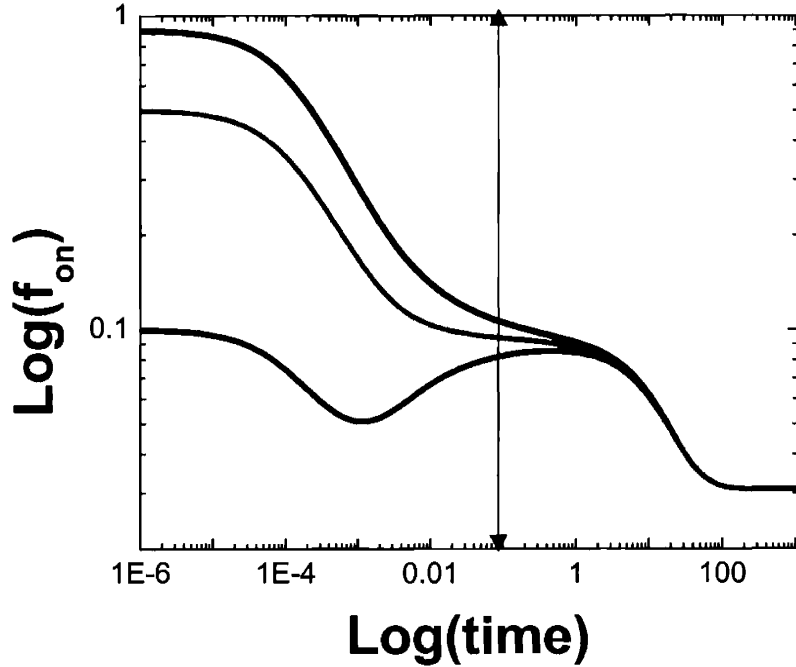
Figure 3.2.2. When $t_{on}^{min} = 10^{-4}$, $t_{off}^{min} = 10^{-2}$, $t_{on}^{max} = 10$, and $t_{off}^{max} = 10^2$ sec when $\alpha = $ (a) 0.1(red), (b) 0.5(green), and (c) 0.9 (black).

The next conditions to be explored are $t_{on}^{min} = 10^{-4}$ sec, $t_{off}^{min} = 10^{-2}$sec, $t_{on}^{max} = 10$sec, and

$t_{off}^{max} = 10^2$ sec with $\alpha = 0.1$, 0.5, and 0.9. In Figure 3.2.2, the steady state value appears

at $f_{on}(t) = 0.03$, which is significantly lower than the steady state value in 3.2.1 although

$t_{off}^{max} / t_{on}^{max} = 10$ in both cases. When $10^{-6} < t < 10^{-5}$ sec, $f_{on}(t) = \alpha$. The quasi-equilibrium

value reaches at 0.09 because $t_{on}^{min} < t_{off}^{min}$. This result implies that the conditions

$t_{on}^{min} < t_{off}^{min}$ or $t_{on}^{min} > t_{off}^{min}$ can be experimentally determined. Experimentally, if the

steady state value obtained assuming $f_{on}^{qe} = 0.5$ is smaller than the theoretically predicted value, then it would be that $t_{on}^{min} < t_{off}^{min}$.
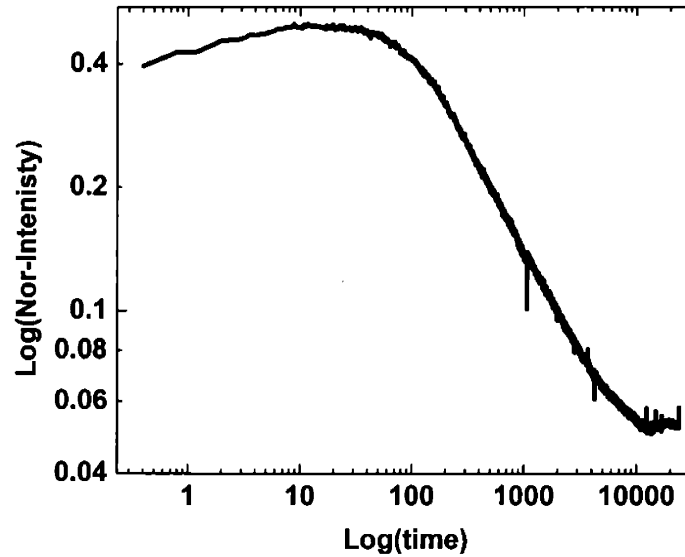
Figure 3.2.2(d) Log-log plot of the fluorescence time trace of a collection of CdSe(ZnS) QDs using an excitation intensity of 13kW/cm². The first absorption peak of the QDs/hexane solution was at 580nm and the diluted solution was spin-coated on a bare glass substrate. $t_{off}^{max} = 6,770$ sec and $t_{on}^{max} = 75$ sec are experimentally obtained. The steady state value, with the maximum intensity normalized to 0.5, is 0.055. With the assumption of $t_{on}^{min} \cong t_{off}^{min}$, the theoretical steady state is calculated to be 0.095. This implied $t_{on}^{min} < t_{off}^{min}$.

Although the normalization $f_{on}^{qe} = 0.5$ is not correct, the ratio ($f_{on}^{qe} / f_{on}^{ss}$) between the quasi-equilibrium state value (f_{on}^{qe}) and the steady state value (f_{on}^{ss}) should be conserved. $f_{on}^{qe}(= 0.500) / f_{on}^{ss}(= 0.055)$ for this experiment is 9.6, while $f_{on}^{qe}(= 0.500) / f_{on}^{ss}(= 0.095)$ for the calculated f_{on}^{ss} value is 5.3. This suggests that $t_{on}^{min} < t_{off}^{min}$. We estimate $t_{off}^{min} / t_{on}^{min} \cong 400$ using Equation 3.2.1. With this estimation

56

of $t_{off}^{min} / t_{on}^{min} \cong 400$ and the experimental ratio $t_{off}^{max} / t_{on}^{max} \cong 90$, the quasi-equilibrium

state and the steady state are $f_{on}{}^{qe} = 0.048$ and $f_{on}{}^{ss} = 0.005$, respectively.

### 3.2.3. $t_{on}^{min} > t_{off}^{min}$
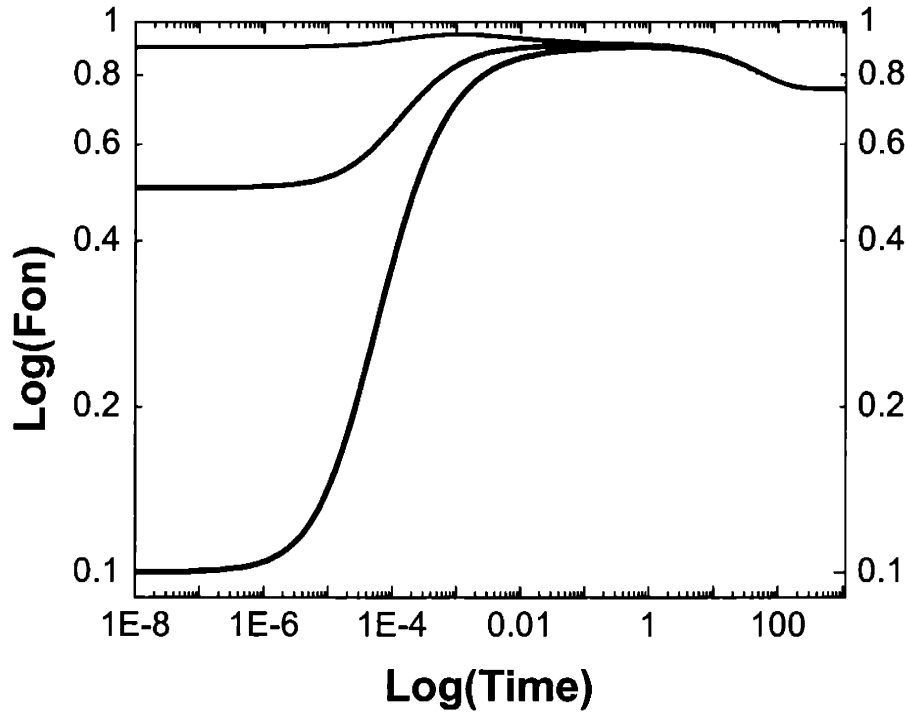
Figure 3.2.3. when $t_{on}{}^{min} = 10^{-2}$, $t_{off}{}^{min} = 10^{-4}$, $t_{on}{}^{max} = 10$, and $t_{off}{}^{max} = 10^2$ sec when α = (c) 0.9(green),(b) 0.5(red), and (a) 0.1 (black).

The final conditions tested are $t_{on}{}^{min} = 10^{-2}$, $t_{off}{}^{min} = 10^{-4}$, $t_{on}{}^{max} = 10$, and $t_{off}{}^{max} = 10^2$

sec with α = 0.1, 0.5, and 0.9. As shown in Figure 3.2.3(a)-(c), the quasi-equilibrium

state and the steady state values are 0.90 and 0.76, far different from the ones in Figure

3.2.1 and 3.2.2. Overall the $f_{on}(t)$ values are larger than the previous two and the ratio of

the quasi-equilibrium value to the steady state value is the smallest. Like the previous

two cases, when $10^{-6} < t < 10^{-5}$ sec, $f_{on}(t) = \alpha$. The reason for the overall increases in

$f_{on}(t)$ is that the average on-time is greater than the average off-time. QDs with this

optical property are bright, compared to other QDs with previous two conditions.
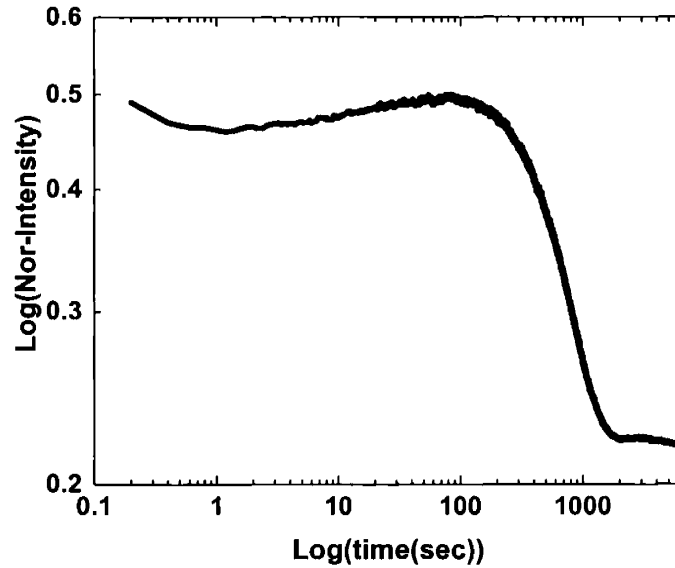
Figure 3.2.3(d) the log-log plot of the fluorescence time trace of a collection of CdSe(ZnS) QDs at the excitation period of 8kW/cm^2. The first absorption peak of the QDs/hexane solution was at 570nm and the diluted solution was spin-coated on a ITO/glass substrate. $t_{off}^{max} = 1450$ sec and $t_{on}^{max} = 31$sec were obtained. The steady state value, when the maximum intensity was normalized to 0.50, was 0.22. With the assumption of $t_{on}^{min} \cong t_{off}^{min}$, the theoretical steady state is calculated to be 0.13.

When $t_{on}^{min} \neq t_{off}^{min}$, the experimental steady-state value (when the quasi equilibrium state

is normalized to 0.5) should not match the theoretical value calculated from

experimentally obtained values of t_{off}^{max} and t_{on}^{max}. In Figure 3.2.3, the steady state value

was observed at 0.22 when the plot was normalized to 0.5. Although the normalization to

0.5 is not correct, the ratio ($f_{on}^{qe} / f_{on}^{ss}$) between the quasi-equilibrium state value

(f_{on}^{qe}) and the steady state value (f_{on}^{ss}) should be conserved.

$f_{on}^{qe}(=0.50)/f_{on}^{ss}(=0.22)$ for this experiment is 2.3, while

$f_{on}^{qe}(=0.50)/f_{on}^{ss}(=0.13)$ for the calculated $f_{on}^{ss} = 3.8$. This suggests that

$t_{on}^{min} > t_{off}^{min}$ and $t_{on}^{min}/t_{off}^{min} \cong 13$. With this condition, the real quasi-equilibrium state

and the steady state are $f_{on}^{qe} = 0.783$ and $f_{on}^{ss} = 0.345$ respectively for this time trace.

3.3. Conclusion

In summary, we have theoretically studied three cases of which the parameters, α, t_{on}^{min} and t_{off}^{min} were varied and we have observed how they appear in the early dynamics and affect the later dynamics of $f_{on}(t)$. All three cases have been observed in experiments and experimental examples were shown. We gained significant understanding about the effect of t_{on}^{min} and t_{off}^{min} to the quasi-equilibrium state and the steady state values. For all examples shown, we assigned the quasi-equilibrium and steady state values. As a result, we found that when $t_{on}^{min} < t_{off}^{min}$, the quasi-equilibrium and steady state values are lower than the values when $t_{on}^{min} \cong t_{off}^{min}$. In our example, surprisingly enough, t_{off}^{min} was estimated to be 400 times larger than t_{on}^{min}. With this condition, we found the quasi-equilibrium and steady state values for this collection of QDs should be 0.048 and 0.005, respectively. A collection of QDs in this condition is generally dark due to low f_{on}^{qe} and f_{on}^{ss}. On the contrary, with the condition of $t_{on}^{min} > t_{off}^{min}$, the quasi-equilibrium state and steady state values are higher than the values when $t_{on}^{min} \cong t_{off}^{min}$. Our example showed that t_{on}^{min} is 13 times larger than t_{off}^{min}. The quasi-equilibrium and steady state values for this collection of QDs were estimated to be 0.78 and 0.34, respectively. A collection of QDs with this collection is bright due to the high f_{on}^{qe} and f_{on}^{ss} values.

We now understand what makes a collection of QDs brighter, and if we get a microscopic understanding of these parameters, we should be able to engineer the optical

quality of QDs. However, there are a number of other issues that to be clarified. The symmetry of t_{on}^{min} and t_{off}^{min} appears to be heterogeneous within the same sample of QDs and the heterogeneity is exhibited in all types of QDs, such as bare QDs, core-shell overcoated QDs, and alloyed QDs. We will need to understand if the asymmetry in t_{on}^{min} and t_{off}^{min} is caused by the presence of a shell or the interaction of the QDs with the immediate substrate environment. We will deal with this matter briefly in Chapter 6 but we are not yet able to generalize results.

Chapter 4. Effect of the binning process on the fluorescence time traces of a collection of QDs

4.1. Introduction

In Chapter 2, the binned fluorescence intensity time trace of a collection of QDs (CQD) at high excitation intensity was explained with the time evolution of the probability, $f_{on}(t)$, which represents the probability to find a single QD in an on-state at time t. In fact, it was shown that the probability, $f_{on}(t)$, indicates the average fluorescence behavior for a single QD. Here we introduce a stochastic variable, $I(t)$, which is the fluorescence intensity time trace of a single QD as a function of time. The ensemble average of $I(t)$ will then be equal to $f_{on}(t)$. The stochastic variable, $I(t)$, begins to behave similar to $f_{on}(t)$ when a bin-size, t_b, is sufficiently large.

The probability, $f_{on}(t)$, used in the previous chapter was not binned. In experiments, a binned $f_{on}(t)$ describes the average fluorescence time trace of a single QD. In this chapter, we define the binned $I(t)$ and binned $f_{on}(t)$ as $b\text{-}I(t)$ and $b\text{-}f_{on}(t)$, respectively. $b\text{-}f_{on}(t) \cong f_{on}(t)$ when $t > t_{on}^{max}$. However, the early dynamics at the quasi-equilibrium state of $f_{on}(t)$ are not present in $b\text{-}f_{on}(t)$ when the short dynamics are hidden within a large t_b.

We learned from Chapter 2 that $f_{on}(t)$ for a CQD is completely constructed by 7 parameters. These are: the initial proportion of neutral QDs, α, the on- and off-time lower and upper cut-off, t_{on}^{min}, t_{off}^{min}, t_{on}^{max} and t_{off}^{max}, and the on- and off-time powers,

μ_{on} and μ_{off}. μ_{on} and μ_{off} are obtained from analyzing time traces of single QDs. μ_{off} can in principle be obtained from the power-law decay of the fluorescence time trace of a CQD, while μ_{on} does not appear. However, the experimentally obtained μ_{off} may be misleading when background signals are added to the fluorescence time trace of a CQD. Therefore, a correct subtraction of the background intensity is necessary to obtain the power-law decay as $1 - \mu_{off}$. Otherwise inaccurate values for t_{on}^{max} and t_{off}^{max} are obtained. In all chapters, we fix μ_{on} and μ_{off} to be 0.5, which is the average value obtained from experimental blinking statistics of single QDs dispersed either on glass substrates or embedded in solid polymer matrices. In the log-log representation of the fluorescence time trace of a CQD, we can easily find t_{on}^{max} and t_{off}^{max} values at the intersections of the flat $f_{on}(t) = 0.5$ line and the power-law line, and the power-law line and the flat steady state line, respectively, as shown in Chapter 2.

t_{on}^{min} and t_{off}^{min} cannot be observed in the time evolution of b-$f_{on}(t)$ in experiments that are performed at high excitation intensity (see Chapter 5) since t_b is larger than t_{on}^{min} and t_{off}^{min}. In the previous chapter, it was assumed that t_{on}^{min} and t_{off}^{min} are determined by the excitation cycle, which is defined as the mean time interval between two consecutive excitation of a single QD. In our experiments, the excitation intensity is typically on the order of 10 kW/cm^2, which gives an excitation cycle of $\sim$ 3MHz, using an absorption cross-section of 5×10^{-15} cm^2. If the assumption used in Chapter 2 holds true, t_{on}^{min} and t_{off}^{min} should then be $\sim$ 0.3 μsec.

The choice of t_b relative to t_{on}^{min} and t_{off}^{min} has a significant influence on the observed initial dynamics of the first region of the intensity time trace of the CQD. We therefore need a complete picture that shows how the choice of t_b affects the initial dynamics in the quasi-equilibrium state ($t < t_{on}^{max}$) appearing in b-$f_{on}(t)$. The quasi-equilibrium state is a temporary equilibrium state determined by t_{on}^{min} and t_{off}^{min}, as was theoretically described in Chapter 3. For simplification, we assume $t_{on}^{min} \cong t_{off}^{min}$ in this chapter.

One must first understand the fluorescence behavior of individual QDs in the quasi-equilibrium region where b-$f_{on}(t) = 0.5$ in their fluorescence time traces with the condition of $t_{on(off)}^{min} \ll t_b < t_{on}^{max}$. With $t_{on(off)}^{min} \ll t_b < t_{on}^{max}$, b-$f_{on}^{avg}(t) = 0.5$ leads to two possible scenarios. The first possibility is that at most 50% of the QDs in a CQD emit during t_b (since a QD either emits or does not emit, with equal probability). The second possibility is that the total amount of time during which every QD emits is $t_b / 2$. We show experimentally that the latter possibility is correct when $t_{on(off)}^{min} \ll t_b < t_{on}^{max}$. Finally, we both theoretically and experimentally show how t_b affects the binned fluorescence time traces, b-$I(t)$, of single QDs.

4.2. Experiments and Results

4.2.1. Fluorescence time traces of many single QDs at the quasi-equilibrium state

A dilute solution of the CdSe/ZnS core-shell QDs dispersed in hexane (first ABS peak at 605 nm) was spin-coated on a pre-cleaned glass coverslip. A 514 nm line from an Ar+ laser was used to continuously excite the sample at an excitation intensity of ~ 15 kW/cm^2.
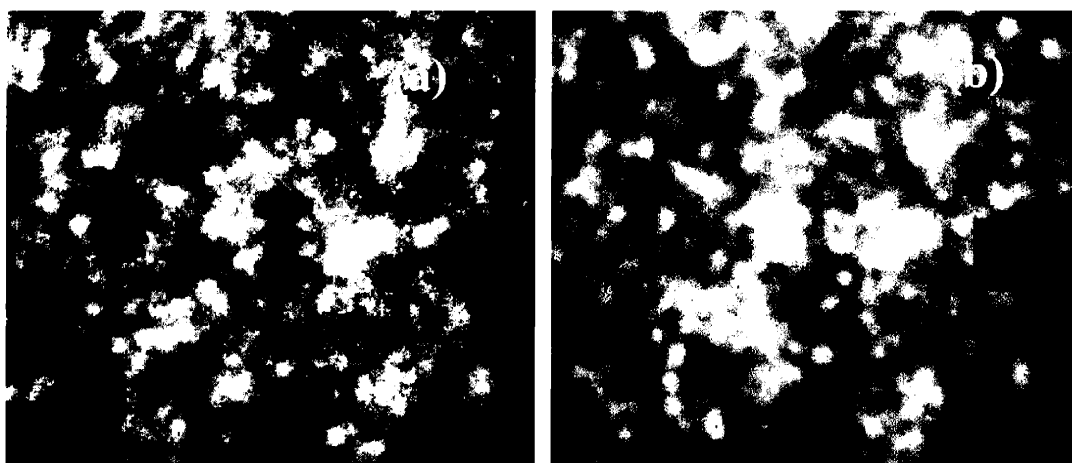
Figure 4.2.1. (a) A snap-shot fluorescence image with t_b = 0.1 sec at t = 20 sec. (b) The integrated fluorescence image from 0 to 10,000 sec. Nearly every individual QD is seen in both figures.

Figure 4.2.1(a) is a snap-shot image at the quasi-equilibrium state, taken from the time series of fluorescence images of a CQD with t_b = 0.1 sec. Every fluorescence image during t_b = 0.1 sec that is accumulated for roughly 2.5 hours yields the integrated image (within this time, the time trace reaches its steady state) as shown in Figure 4.2.1(b). Almost every QD shown in Figure 4.2.1(b) is matched with a QD in Figure 4.2.1(a). The brighter spots may come from aggregated QDs or several QDs which are closely located and that cannot be optically resolved. One may ask why nearly every QD is

observed at the quasi-equilibrium state. This is because $b\text{-}I(t)$ is close to $b\text{-}f_{on}(t)$ with the sufficiently large t_b. When t_b is not large enough, half of the QDs should emit as shown in Figure 4.2.1(a), since $f_{on}(t)=0.5$ for the collection of single QDs at the quasi-equilibrium. But, with a sufficiently large t_b, $b\text{-}I(t)$ behaves similar to $b\text{-}f_{on}(t)=0.5$, since numerous blinking events from a single QD are integrated within the t_b. Therefore, every QD emits during $t_b/2$ at each bin at the quasi-equilibrium state. Hence, the total number of QDs that can ever emit is observed at the quasi-equilibrium state as seen in Figures 4.2.1(a) and (b). The next section discusses the condition when t_b is considered to be sufficiently large in order to reach the state, $b\text{-}I(t) \sim b\text{-}f_{on}(t)=0.5$, by means of simulations and experiments.

4.2.2. $f_{on}(t)$ time traces for single QDs and the binning effect.
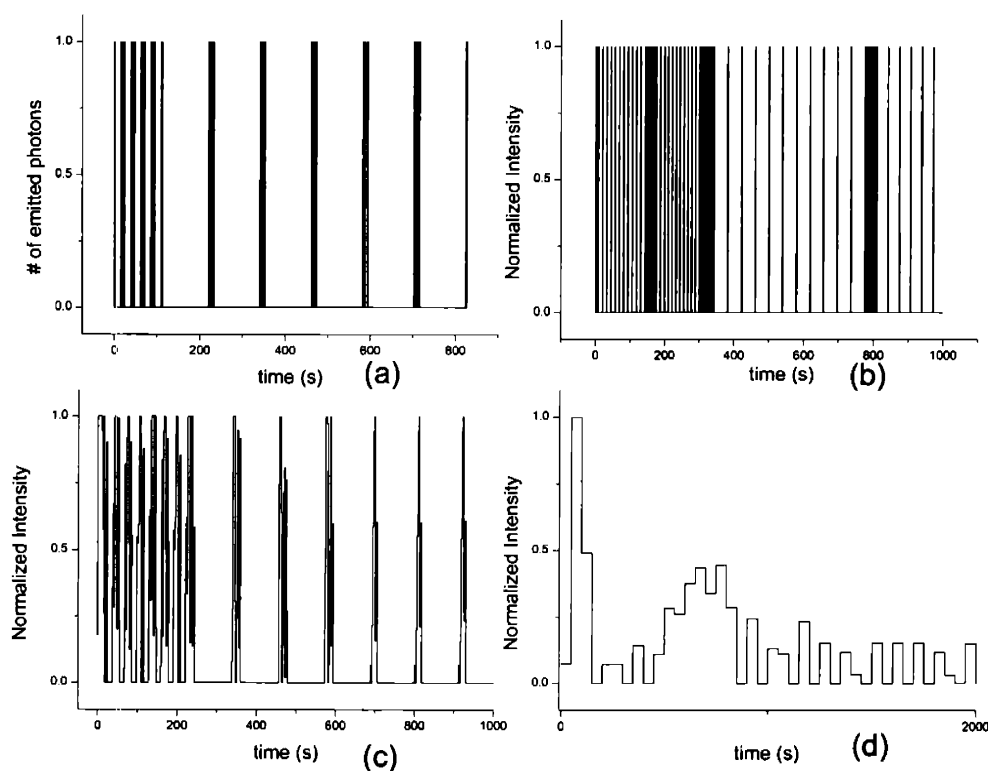
Figure 4.2.2. All time traces are constructed from power-law statistics with the conditions $t_{on}^{min} = t_{off}^{min} = 10^{-4}$ sec , $t_{on}^{max} = 10^2$ sec, and $t_{off}^{max} = 10^3$ sec . All the intensities in (b)-(d) are normalized to 1. (a) An arbitrary time trace, $I(t)$, for a single QD. Inside the black bars, very fast on and off-times are accumulated. (b) The time trace from (a) is binned with $t_b = 0.1$ sec and looks binary throughout the time range. (c) The time trace in (a) is binned with $t_b = 2$ sec. (d) The time trace in (a) is binned with $t_b = 50$ sec.

In Figure 4.2.1, every QD is observed in the quasi-equilibrium state when $t_b = 0.1$sec. If t_b were comparable to t_{on}^{min} and t_{off}^{min}, only half of the QDs would be observed at quasi-equilibrium state. Therefore, for a single QD, the choice of t_b strongly affects its fluorescence time trace. In this section, we simulate the time traces by varying t_b.

67

Figures 4.2.2(a)-(d) are theoretically constructed time traces with $t_{on}^{max} = 10^2$ sec,

$t_{off}^{max} = 10^3$ sec, and $t_{on}^{min} = t_{off}^{min} = 10^{-4}$ sec. A Monte-Carlo simulation was used to

generate binary intensity time traces for a single QD. Figure 4.2.2(a) is an example of a

simulated time trace. This time trace is a $I(t)$, the un-binned time trace. In Figure

4.2.2(a), y-values (intensity values) are either '1' (emitting state) or '0' (non emitting

state). Short and more frequent blinking events are observed in the early time of the time

trace before $t_{on}^{max} = 10^2$ sec. After t_{on}^{max}, longer on-times and even longer off-times

appear. A binned time trace, a $b\text{-}I(t)$, is shown in Figure 4.2.2(b) with $t_b = 0.1$ sec. The

single QD time trace continues to appear binary even when t_b is three orders of

magnitude larger than $t_{on}^{min} = t_{off}^{min} = 10^{-4}$ sec. In Figure 4.2.2(c), the time trace in Figure

4.2.2(a) is binned with $t_b = 2$ sec. The resulting binned time trace, a $b\text{-}I(t)$, appears less

binary. Figure 4.2.2(d), a $b\text{-}I(t)$, is constructed with $t_b = 50$ sec from the time trace in

Figure 4.2.2(a). t_b is $5 \cdot 10^5$ times larger than $t_{on}^{min} = t_{off}^{min} = 10^{-4}$ sec and appears long

enough to contain many on- and off- blinking events. The highest intensity in Figure

4.2.2(d) indicates the point when $b\text{-}I(t) \sim b\text{-}f_{on}(t) = 0.5$ is satisfied at the quasi-

equilibrium state with $t_b = 50$sec and $t_{on(off)}^{min} = 10^{-4}$ sec. Then approximately, the

condition for a t_b to reach the state $b\text{-}I(t) \sim b\text{-}f_{on}(t) = 0.5$ becomes $t_b \sim 10^6 \times t_{on(off)}^{min}$.

The fluorescence images of single QDs during a $t_b = 0.1$ sec in Fig. 4.2.1 are taken under

similar conditions as in Fig 4.2.2(d), where almost every single QD emits during half of

the time at a bin in the quasi-equilibrium state. The t_{on}^{min} and t_{off}^{min} values of single QDs at

an excitation intensity of 15 kW/cm^2 in Figure 4.2.1 are therefore extended as $t_{on(off)}^{min}$ =

$t_b (= 0.1 \text{ sec}) / 10^6 \sim 0.1$ μsec. The excitation intensity of 15 kW/cm^2 is converted to an

excitation period ~ 0.3 μsec. Therefore the speculated t_{on}^{min} and t_{off}^{min} values appear to be

on the same order as the excitation cycle. This may suggest that our previous assumption

in Chapter 2 that t_{on}^{min} and t_{off}^{min} are given by the excitation cycle is valid.

Therefore, if the excitation of a single QD at time $t = 0$ is properly initialized, with

varying excitation intensities between 10 and 30 kW/cm^2, similar features in the single

QD fluorescence time trace as those seen in Figure 4.2.2(d) should be observed. Figure

4.2.3 shows different single CdSe/ZnS QDs time traces. The QDs are embedded in a

PMMA matrix and an excitation intensity of 25 kW/cm^2 is used with $t_b = 0.1$ sec. This

excitation cycle corresponds to approximately 0.1 μsec. This cycle time is about 10

times faster than the typical period that is used to get blinking time traces of single QDs.

When the cycle time is shorter, the t_{on}^{max} and t_{off}^{max} values become smaller. (see Chapter 6)

Therefore the blinking time trace for a single QD no longer appears binary. Figure 4.2.3

shows that most single QD time traces, except the middle left panel exhibit similar

blinking features as the simulated time trace in Figure 4.2.2(d). Every trace corresponds

to a $b - I(t)$ of a single QD where the condition $b - I(t) \sim b - f_{on}(t) = 0.5$ is satisfied at the

quasi-equilibrium. The on-time events appear non-binary in Figure 4.2.2(d), compared to

typical blinking time traces at lower excitation intensities.
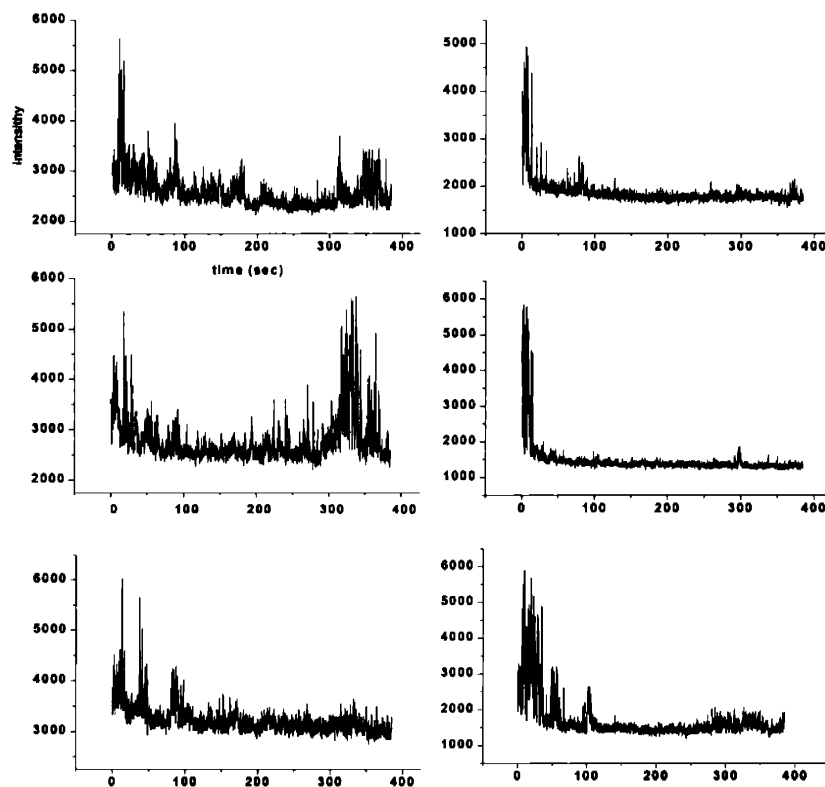
Figure 4.2.3. Each fluorescence time trace, a b - $I(t)$, was simultaneously obtained from single QDs, initializing the excitation time at $t = 0$. The excitation intensity was at 25kW/cm^2 with $t_b = 0.1$ sec. The different background intensity level comes from the inhomogeneous scattering from spot to spot in the substrate.

4.3 Conclusion

In this chapter, we defined a stochastic variable, $I(t)$, of a fluorescence time trace

of single QD. The ensemble average of $I(t)$ is then equal to $f_{on}(t)$. We further defined

the binned $I(t)$ and binned $f_{on}(t)$ as $b\text{-}I(t)$ and $b\text{-}f_{on}(t)$, respectively. From simulations,

it was found that $b\text{-}I(t)$ is close to $b\text{-}f_{on}(t)$ with the condition $t_b \sim 10^6 \times t_{on(off)}^{min}$. In

experiments where $t_b \sim 0.1$ sec and the excitation cycle ~ 0.3 μsec were chosen, $b\text{-}I(t)$

appeared closely as $b\text{-}f_{on}(t) = 0.5$ at the quasi-equilibrium state. By applying the

condition $t_b \sim 10^6 \times t_{on(off)}^{min}$, it was estimated that $t_{on(off)}^{min}$ values should be ~ 0.1 μsec

which is on the same order as the excitation cycle. Therefore, from this work, not only is

the condition that $b\text{-}I(t)$ reaches $b\text{-}f_{on}(t)$ with the choice of $t_b \sim 10^6 \times t_{on(off)}^{min}$ established,

but also the assumption in Chapter 2 that $t_{on(off)}^{min}$ is triggered by an excitation period was

validated. For further experiments, we suggest to obtain the precise range of t_b to satisfy

the condition $b\text{-}I(t) \sim b\text{-}f_{on}(t) = 0.5$ at quasi-equilibrium by varying the excitation period.

By doing so, we can also monitor the change in $t_{on(off)}^{min}$ values as a function of excitation

cycle, confirming that $t_{on(off)}^{min}$ are light-induced parameters.

Chapter 5. Fluorescence Behavior of QDs: from the 'Low' to the 'High' Excitation Regime.

5.1. Introduction

The quantum yield (QY) is defined as the ratio of the number of emitted photons to the number of absorbed photons. In experiments performed by Woo et al., it was shown that the fluorescence from CdSe QDs decays when a voltage is applied to charge QDs [1], which supports an earlier prediction by Efros et al [2] that a charged QD does not emit a photon. This hypothesis of 'a dark QD equals a charged QD' has been used to describe the phenomenon of fluorescence blinking in CdSe QDs [2-4].

In this chapter, that hypothesis is still employed. Given the definition of QY above, the contribution to the emitted photons from a collection of QDs in the context of fluorescence blinking is described. When there is no light excitation, a collection of QDs is composed of neutral QDs, charged QDs, and permanently dark QDs (QDs that cannot emit). It is assumed that while both the charged QDs and the permanently dark QDs still absorb photons, the former can be converted to neutral QDs as seen in the blinking time traces, and the latter type of QDs cannot change. Assuming that a neutral QD emits a photon when excited (i.e. the QY (of a neutral QD) is 100%) and the charged QD does not emit a photon when excited (i.e. the QY (of a charged QD) is 0%), then the QY from a collection of QDs can be expressed as the ratio of the number of neutral QDs to the total number of QDs (neutral QDs + charged QDs + permanently dark QDs).

The QY from a collection of fluorophores is usually measured at thermal equilibrium. At the thermal equilibrium state, the system (a collection of fluorophores) reaches equilibrium in an environment without interacting with any other external

72

perturbation (usually light). If a fluorophore is a 'two-level' system and there is no 'non-radiative' relaxation pathway, then thermal equilibrium can be reached once the collection of fluorophores relaxes to the ground state after excitation. Unless some fluorophores are permanently damaged, the QY from these fluorophores would reach 100%. However, for the case of QDs or any other multi-level systems with 'dark' states, this is not the case. When an electron-hole pair (EHP) is created within a QD by photo-excitation, the carriers do not necessarily radiatively recombine to relax to the ground state. In fact, whatever the inital state (charged or neutral), that state can be altered after absorbing a photon. If a CdSe QD is neutral prior to absorbing a photon, the created electron and hole either recombine or eject a carrier (either an electron or a hole, but an electron is speculated to be the better candidate due to its smaller effective mass, and lower tunneling barrier) out of the QD, leaving the QD charged. If a QD is initially charged, after absorbing a photon, the QD contains three carriers where two carriers (an electron and a hole) recombine, exciting the third carrier and resulting in no emission from the QD (this is called the Auger process). However, if the energy that excites the third carrier is high enough to eject the carrier outside of the QD, then the QD could become neutral. Alternatively, when three carriers are in a QD, a neighboring charge could experience a Coulombic force from the charged QD and move into the QD, making the QD neutral. However, we have no experimental evidence for such a scenario. Thus, upon absorption of a photon, an initially neutral QD can become either neutral or charged, and an initially charged QD generally becomes either neutral, depending on the energy transferred to the third carrier, or remains charged, with a low probability to become neutral by the alternative mechanism suggested above. Unlike the case of two-level

73

fluorophores, the state of a collection of QDs after interacting with photons is not identical to the previous state. Therefore the QY for a collection of QDs must be revisited. As an example, assume that at thermal equilibrium, approximately 30% of the QDs are neutral. We now define the QY measured at thermal equilibrium specifically as the thermodynamic QY (TQY). Upon photo-excitation, the number of neutral QDs may be different than 30%. As explained above, the state of QDs may have been changed in such a way that some neutral QDs become charged, and some charged QDs neutral. The interaction with light perturbs the initial state of the QDs. However, after passage of time, the collection of QDs relaxes to its initial equilibrium state; 30% of the total number of QDs is neutral again. We define this time interval as the thermal relaxation time (TRT). The initial ratio of neutral QDs cannot be measured by the absorption and emission experiments. In a typical QY measurement, the excitation intensity is low enough such that a collection of QDs can come close to reaching thermodynamic equilibrium between subsequent excitation-emission events. Therefore, the photoluminescence intensity is fairly constant as a function of time in this low excitation intensity regime. This infers that any perturbation due to photo-excitation vanishes before the next excitation. At higher intensities, the time between excitation events becomes comparable to or shorter than the TRT. At this point, the TQY values are affected by the blinking kinetics and evolve as a function of time. It is therefore necessary to connect the fluorescence behavior from a collection of QDs at the low excitation intensity, where a TQY value is measured, to the behavior at the higher excitation intensity where the probability, $f_{on}(t)$, that a QD is emissive at time t evolves as a function of time. (see Chapter 2) Then $f_{on}(t)$ evolves from a TQY value ($f_{on}(0) = $ TQY) ,governed by the blinking statistics of a single

QD. Therefore, at the high excitation regime, the TQY is no longer the main variable to demonstrate the 'brightness' of a collection of QDs.

We showed in the previous three chapters that the seven parameters that describe the blinking statistics determine $f_{on}(t)$ as a function of time. In this chapter, we will mainly focus on relating the fluorescence behavior of QDs at low excitation, represented by the TQY, to the probability, $f_{on}(t)$, that a QD is emissive at time t in the high excitation regime.

5.2. Experiments and Discussion

There have been no studies that connect the fluorescence behavior of a collection of QDs in the low excitation (LE) intensity to that in the high excitation (HE) intensity. An intrinsic photophysical parameter is required to distinguish the HE from the LE regime. This parameter is specified as the thermal relaxation time (TRT), and is defined as the passage of time that QDs perturbed by a photo-excitation, relax back to their initial thermodynamic equilibrium state.
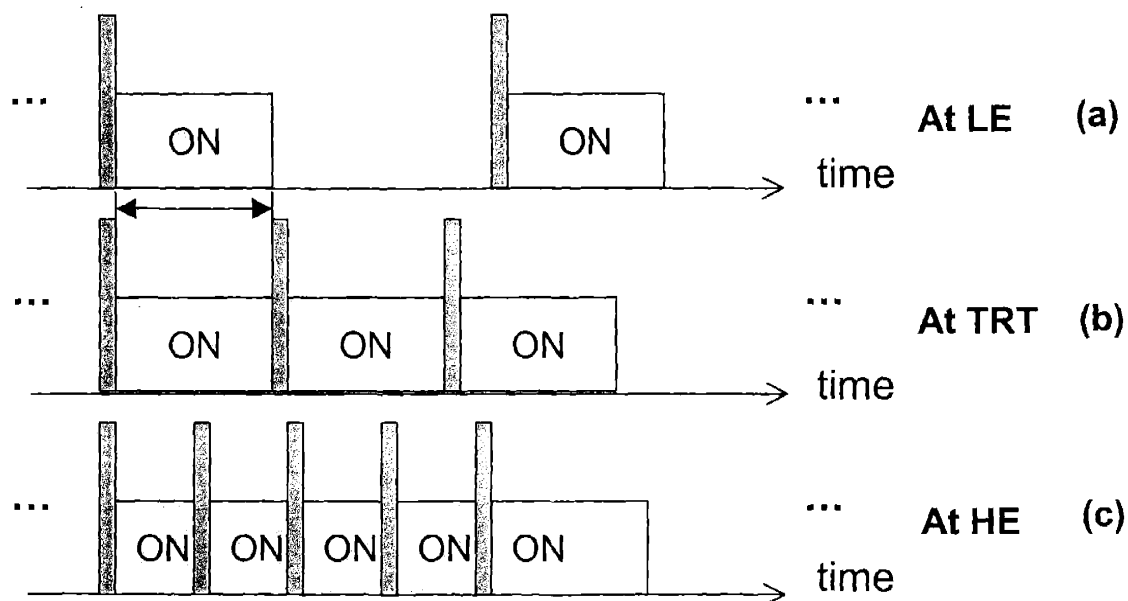

Figure 5.1. The green represents the light pulses (the spacing between the green bars can be calculated from the excitation intensity flux.) and the red box indicates the time that the state of a collection of QDs after a photo-excitation takes to relax to a thermodynamic equilibrium state. The double-sided arrow represents the thermal relaxation time (TRT). (a) The LE regime where the spacing between two excitation pulses is longer than the TRT (for continuous excitation, this spacing is the inverse number of the average rate of excitation). (b) The TRT point where the relaxation time is comparable to the pulse spacing. (c) The HE regime where the spacing between two excitation pulses becomes shorter than the TRT.

Possible sequential excitation-emission processes are illustrated in Figure 5.1(a)-(c), where the green and red colors represent the excitation pulses and the state of a collection of QDs resulting from photo-excitations, respectively. The LE sequence is represented in Figure 5.1(a) where the time interval between two consecutive excitation pulses is longer than the TRT. Therefore in this regime, the state created by the photo-excitation relaxes to a thermodynamic equilibrium state without any memory from the previous excitation. In the HE regime (Figure 5.1(c)) the relaxation from the perturbed state to the thermodynamic equilibrium state is not reached before the next photo-excitation occurs. In this regime, events such as a neutral (charged) QD becoming charged (neutral) and a neutral (charged) QD remaining neutral (charged) can all occur. The length of time that a QD remains neutral (therefore, emissive) or charged (not emissive) is governed by power-law distributions. An intermediate regime (Figure 5.1(b)) is achieved when the excitation period is on the order of the TRT.

In reality, absorption and QY measurements are typically performed in the LE regime where the QDs are dispersed in low concentration in a non-fluorescing solvent. At these conditions, the QY is constant as a function of time. When the continuous excitation rate is comparable to the inverse of the TRT, the collection of QDs becomes photo-excited before the thermodynamic equilibrium state is recovered. In the LE regime each state from successive photo-excitations is identical, and independent of each other. On the other hand, in the HE regime, the state of QDs driven by the photo-excitation is not the same as the previous state followed by the previous photo-excitation. In fact, the current state resulting from the photo-excitation is related to the previous state resulting from the previous photo-excitation in the HE regime. Since the duration of a QD that

keeps emitting or not emitting becomes the waiting times of on- and off-times, the fluorescence time traces of a collection of QDs are governed by the blinking statistics, independent of the initial TQY value. These blinking statistics of the on- and off- waiting time distributions have been reported to follow the power-law statistics with a power of 0.5. Since on and off-times are broadly distributed, the larger blinking events are rarely observed from experimental time traces of single QDs [3,4]. However, we have solved this problem by connecting the fluorescence time traces constructed from a collection of QDs to the blinking statistics of single QDs: the presence of a steady-state confirmed the existence of the off-time power-law upper cut-offs, t_{off}^{max}, as well as the on-time upper cut-off, t_{on}^{max}. (see Chapter 2)

In the HE regime, when a collection of QDs begins to be continuously excited with light, its fluorescence evolves as a function of time revealing the dynamics and the blinking statistics of a single QD. Detailed studies about this evolution are explained in Chapter 2. When a collection of QDs gets excited at $t = 0$ from a thermodynamic state, the emission yield of the first emission intensity value should represent the TQY. Then the QDs in the perturbed state from the previous excitation will again become excited. Therefore, in the HE regime, the time trace starts from the TQY and then evolves as a function of time, eventually reaching a steady-state determined by t_{on}^{max} and t_{off}^{max} (see Chapter 2). The fluorescence intensity time traces are analogous to the time evolution of the probability, $f_{on}(t)$, for a QD to be emissive at time t. (see Chapter 2) In fact, we can fully describe the fluorescence behavior of a collection of QDs at the HE regime except for the very early dynamics that result from the on- and off-time lower cut-off values,

t_{on}^{min} and t_{off}^{min} . (see Chapter 4) These fast blinking events are hidden during the first bin-size although we have a way to indirectly extract the ratio between the lower cut-off values. (see Chapters 3 and 4) As explained above, the first intensity of the intensity time trace, when properly normalized to describe the $f_{on}(t)$ value, should give the TQY value.
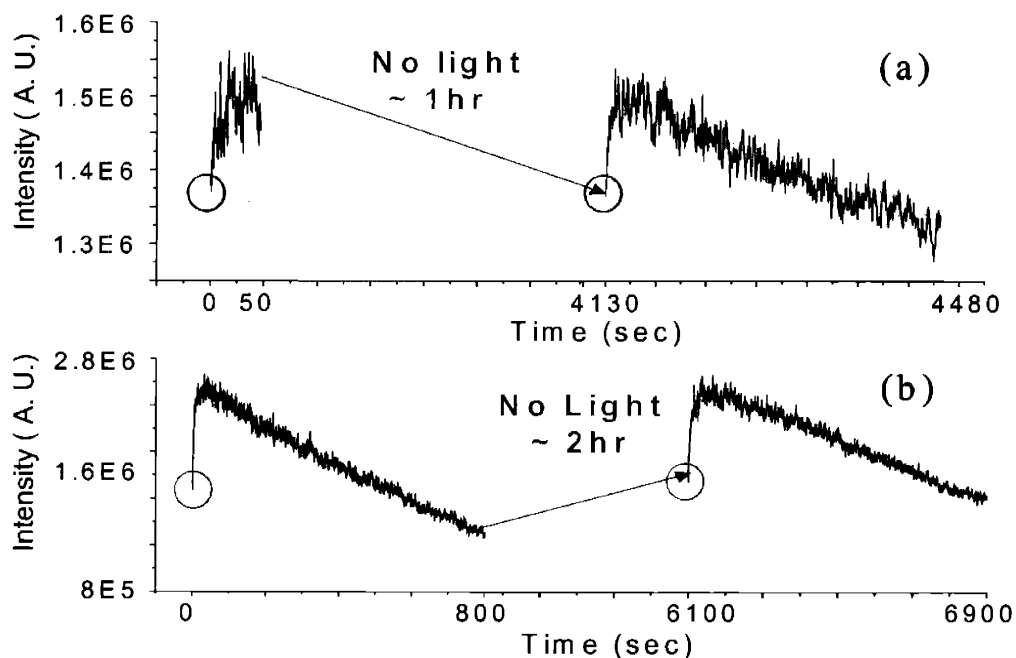

Figure 5.2(a) A collection of QDs dispersed in hexane was spin-coated onto a glass substrate. The collection of QDs was continuously excited from $t = 0$ sec to $t = 50$ sec and the excitation was then removed. A 514nm Ar+ laser was used to excite the QDs at the average intensity of 8 kW/cm^2. After 1 hour of darkness, the excitation was resumed and the previous initial intensity at $t = 0$ sec is recovered. Note that the fluorescence intensity is higher than the initial intensity at $t = 0$ sec. (b) Another collection of QDs were continuously excited with the same condition as in (a) from 0 to 800 sec. The excitation was resumed after 2 hours of darkness, and a similar time trace was obtained during the second excitation time trace.

However, in real experiments, the binning process (the time resolution of a detector) averages over many blinking events during a bin-time so that the first probability value is not exactly the TQY. (see Chapters 2 and 4) Generally, reducing the excitation intensity or having a smaller bin-size comparable to the smallest on(off)-times

would bring the first point probability value closer to the TQY[1]. In order to show that the first point in the intensity time trace represents the thermal equilibrium state of the QD sample in the dark (no excitation light present), we performed two experiments where the QDs were continuously excited, beginning at $t = 0$ until (1) the intensity remained higher than the initial intensity at $t = 0$ and (2) the intensity was lower than the initial one. The two experimental processes are illustrated in Figure 5.2(a) and (b), respectively. A 514 nm Ar^+ laser was used to excite collections of QDs (first absorption peak at 580 nm) which were dispersed in a hexane solution and then spin-coated on bare glass cover-slips. The samples were photo-excited using a far-field microscope setup. An air objective (100X, 0.95 N.A.) was used, and the excitation intensity was 8 kW/cm². If the first intensity value was to approximately represent the quasi-thermodynamic equilibrium state of the collection of QDs, regardless of the point that the excitation is stopped, the intensity should recover to its original value after completely relaxing to the thermal equilibrium state. As shown in Figure 5.2(a) and (b), the first intensity values after the dark periods are approximately identical to the initial value at $t = 0$. Therefore, we can conclude that the first point in the fluorescence intensity time trace roughly represents the quasi-thermodynamic equilibrium state of the QDs, which can be more accurately measured in the LE regime.

The effect of binning on the first point emission intensity value deserves further discussion. Experimentally the typical bin-size, t_b, is 0.1 ~ 10 sec. At the low excitation regime, the first point value (at $t = t_b$) is given from the TQY and this holds for any *i-th* point value (at $t = i \times t_b$). The emission intensity at each bin would still remain constant.

---

[1] See Chapter 3, this does not hold when $t_{on}^{min} > t_{off}^{min}$.

In the HE regime, when the on- and off-time lower cut-off values are significantly shorter than t_b, the previous TQY value integrated within a large t_b would not appear in the time traces and the time traces will be described by the evolution of $f_{on}(t)$ as a function of time. As blinking dynamics proceed in the HE regime, the neutral QDs that contributed the TQY value start to blink. Then the short on and off-events as well as the TQY value become integrated in the first bin. Experimentally this concept is well demonstrated in Figure 5.4(a), and (b). In Figure 5.4(a), we prepared dilute CdSe(ZnS) QDs solutions (0.05 absorbance at the first ABS peak) in hexane contained in a hollowed glass plate with a 0.3 cm thickness on top of which a cover glass is glued to prevent the evaporation of the solution as shown in Figure 5.3.
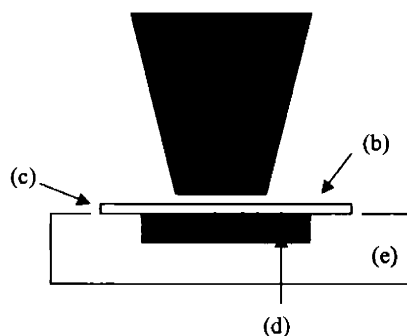

Figure 5.3 (a) Air Objective with N.A.=0.95, 100X (b) A cover-glass (c) Epoxy glue, and (d) QD solution inside the hollowed thick glass substrate.

Another sample was prepared with a solution of silica microspheres into which CdSe(ZnS) QDs were incorporated [5], dissolved in ethanol that was spin-coated on a glass cover-slip for the data displayed in Figure 5.3(b). Figures 5.4(a) and 4(b) show the integrated emission intensity (from $t=0$ to $t_b(=0.1$ sec)) as a function of the laser intensity. The illuminated sample spots were changed for each data point to initiate time traces at $t=0$.
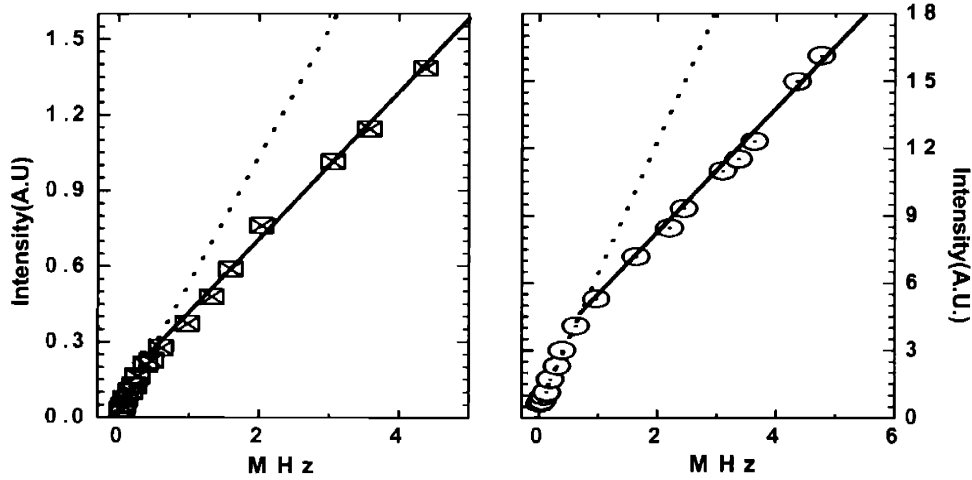
Figure 5.4. A collection of QDs (ABS peak at 580nm) (a) prepared in solution, and (b) prepared with the solution of silica microspheres into which CdSe(ZnS) QDs were incorporated, dissolved in ethanol that was spin-coated on a glass cover-slip. The QDs were shortly excited for about a t_b (= 1 sec) after being initialized at $t = 0$, and the emission intensity increased linearly with the excitation rate up to (a) 60 kHz and (b) 35 kHz, respectively. After these kinks, the emission intensity linearly increases with different slope of (a) 0.62 of the initial slope, and (b) 0.49 of the initial slope.
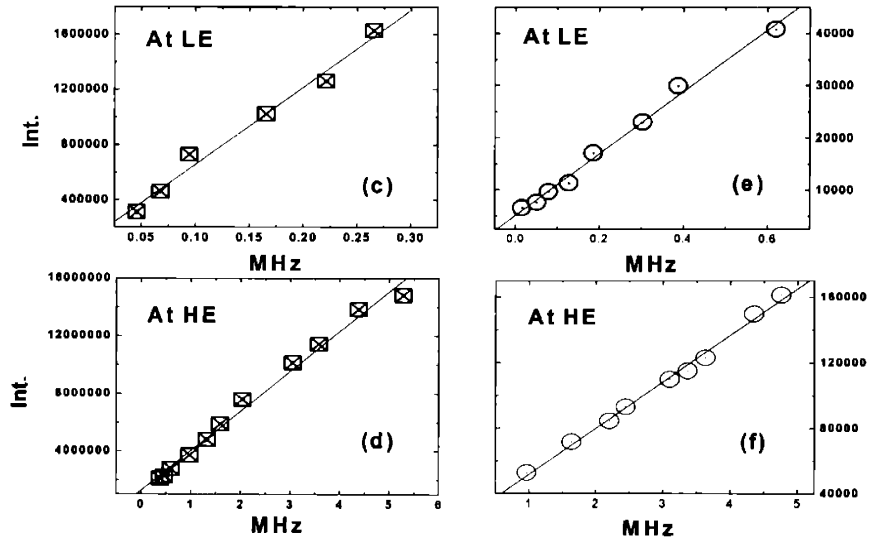

Figure 5.4. (c)-(f) demonstrates the zoomed-in regions of each of the following: the lower excitation region (c) and the higher excitation region (d) from the liquid samples in which the plots are fitted with the slopes of 5.6E6 ± 0.4E6, and 2.8E6 ± 0.3E6; the lower excitation region (e) and the higher excitation region (f) from the solid microsphere samples with the slopes of 5.9E5 ± 0.2E5, and 2.8E5 ±0.1E5. The excitation power, converted before the excitation cycle rates are, 14, 21, 29, 51, 69, 82,120, 145, 188, 303, 410, 493, 630, 945, 1,100, 1,360, 1,600, and 2,400 μW, for the liquid samples. And, 5,16, 24, 39, 57, 94, 120, 193, 300, 508, 680, 755, 960, 1,040, 1,130, 1,350, and 1,470 for the solid QD-microsphere samples.

The x-axes in both figures are converted to the excitation rate (i.e. the mean number of photons absorbed by a QD during one second). An absorption cross-section of 5×10^{-15} cm^2 was used to calculate the excitation rate. For each sample, the fluorescence intensity of QDs increases linearly with the excitation cycles until approximately 0.59 MHz in Figure 5.4(a) and 0.35 MHz in Figure 5.4(b). Figures 5.4(c)-(f) show close-up four regions: Figures 5.4(c) and (d) show the lower excitation (LE) region and the higher excitation (HE) region, respectively for the liquid samples in which the plots are fitted with slopes of 5.6E6 ± 0.4E6 and 2.8E6 ± 0.1E6. Figures 5.4(e) and (f) show the LE region and the HE region, respectively, from the solid QD-microsphere samples with slopes of 5.9E5 ± 0.2E5 and 2.8E5 ± 0.1E5. Beyond these two transition points of excitation cycles, the fluorescence intensities from two different samples of QDs increase with the slopes, approximately half of the previous slopes for both cases. For the QD solution and the QD-microsphere samples, the ratios of the latter to former slopes are 0.49 and 0.48, respectively. This is an experimental illustration of the theoretical processes demonstrated in Figures 5.1(a)-(c). Before and after the transition point (excitation cycle threshold), there exists the LE and HE regime, respectively. The transition point at 1.7 μsec in Figure 5.4(a) happens 1.6 times faster than that at 2.9 μsec shown in Figure 5.4(b). This is a reasonable result since a relaxation to the thermodynamic equilibrium state after each excitation is presumably faster in the hexane solution than in the solid state. The transition in the slopes demonstrates that the number of photons emitted by the neutral QDs becomes half of the excitation photons as fast blinking events begin to mix within a bin-size in the HE regime. If the excitation intensity was greater than that used for Figure 5.4, then slopes would increase more than

the half of the initial slope because previously dark QDs start to appear in the first bin-time.

5.3. Conclusion

In summary, the fluorescence behavior of QDs in the low excitation (LE) regime has been connected to that in the high excitation (HE) regime, both of which are separated by the thermal relaxation time (TRT). At room temperature, the thermal relaxation times of the QDs in hexane and QD-silica composite microspheres that were dissolved in ethanol, and spin-coated on glass substrates were measured to be 1.7 and 2.9 μsec, respectively. This study provides a thermal rate constant, the TRT, which should be incorporated in understanding the blinking mechanisms, especially when the excitation cycle is comparable to the thermal relaxation time (TRT).

5.4. References

1. Woo W-K, Shimizu KT, Jarosz MV, Neuhauser RG, Leatherdale CA, Rubner MA, Bawendi MG, Reversible charging of CdSe nanocrystals in a simple solid-state device. *Advanced Materials* 2002,**14**:1068-1071.
2. A. L. Efros and M. Rosen, Phys. Rev. Lett. **78**, 1110 ~1997
3. Shimizu KT, Neuhauser RG, Leatherdale CA, Empedocles SA, Woo WK, Bawendi MG: Blinking statistics in single semiconductor nanocrystal quantum dots. *Physical Review B: Condensed Matter and Materials Physics* 2001, **63**
4. 8M. Kuno, D. P. Fromm, H. F. Hamann, A. Gallagher, and D. J Nesbitt, J. Chem. Phys. **112**, 3117 ~2000
5. Y. Chan, J.P-. Zimmer, and M. G-. Bawendi, submitted. Incorporation of Luminescent Cadmium Selenide Nanocrystals into Monodisperse Silica Microspheres.

Chapter 6. Excitation intensity dependence of the upper cut-off values in fluorescence time traces

6.1. Introduction

The fluorescence intensity time traces of a collection of QDs undoubtedly hold the key to understanding the photo-dynamics of QDs in a well-defined environment. To date, no definitive microscopic models have been developed to explain fluorescence intermittency. This blinking effect is light-induced and results from complicated interactions between the bare or core-shell QD and its immediate environment. Although the dynamic feature in the fluorescence intensity time trace of a collection of QDs originates from these complex interactions, we can identify seven key parameters to fully describe the time traces. In fact, identifying these seven parameters and understanding the changes in the parameters with varying external conditions, such as the excitation power, the presence of overcoating shells, the energy structure of the immediate substrate material, and temperature will bring us closer to understanding the underlying mechanisms for the fluorescence blinking. The seven parameters are (see chapter3 3 and 4): (1) the quasi-thermodynamic QY (TQY) of the QD sample, α (2) the on-time lower cut-off, t_{on}^{min} (3) the off-time lower cut-off, t_{off}^{min} (4) the on-time upper cut-off, t_{on}^{max} (5) the off-time upper cut-off, t_{on}^{max} (6) the on-time power, μ_{on}, and (7) the off-time power, μ_{off}. μ_{on} and μ_{off} are fixed at 0.5 throughout in thesis, consistent with single QD blinking statistics obtained from experiments. α, as a quasi-thermodynamic QY (TQY) is the closest to a thermodynamic parameter and appears at first in the fluorescence time traces in the low excitation (LE) regime.(see Chapters 3 and 5). In most cases, α does

86

not play a significant role in the high excitation (HE) regime where the fluorescence time traces are binned. The parameters t_{on}^{min} and t_{off}^{min} dictate the early dynamics in the fluorescence time traces, starting from the TQY value to the end of the quasi-equilibrium state (see Chapter 3). On the other hand, the parameters t_{on}^{max} and t_{off}^{max} govern the long-term dynamics in fluorescence time traces that appear after the quasi-equilibrium state. However, t_{on}^{min} and t_{off}^{min} also affect the long-time dynamics if $t_{on}^{min} \neq t_{off}^{min}$ (see Chapters 3 and 4). Therefore, all cut-off values can affect the eventual steady-state value in the fluorescence time traces of a collection of QDs. (see Chapter 3) There are currently no studies that verify the relationship between t_{on}^{min} and t_{off}^{min}, and t_{on}^{max} and t_{off}^{max}.

All the cut-off values are light-induced, but they also appear to be affected by the presence of shells, different immediate environments, and temperature changes. All experiments in this chapter are done at room temperature.

The presence of the shell and different widths of shells affects the switching probability density distributions of a carrier in the core and also a carrier outside (including the surface of the shell) of the QD In this chapter, we describe how the excitation power affects t_{on}^{max} and t_{off}^{max} for three different kinds of QDs: CdSe, CdSe(ZnS), and CdSe(Cd$_x$Zn$_{1-x}$S). CdSe(ZnS) QDs are overcoated core-shell QDs, and CdSe(Cd$_x$Zn$_{1-x}$S) QDs are alloyed QDs with thicker effective shells. In this manner, we can understand the role that the shells and excitation powers play in the blinking statistics. However, the dependence of the excitation intensities on a particular type of QD was often difficult to reproduce experimenting due to heterogeneous properties within the

same sample. Thus, the early dynamics associated with t_{on}^{min} and t_{off}^{min} that lead to the

quasi-equilibrium state appeared to vary from one focus spot to another. These variations

in the early dynamics in some fluorescence intensity time traces were followed by

different t_{on}^{max} and t_{off}^{max} values that appeared inconsistent with the general trend shown in

the rest of the samples with identical external conditions. This result may suggest that

t_{on}^{min} and t_{off}^{min}, and t_{on}^{max} and t_{off}^{max} are closely related.

6.2. Experimental Results[2]

6.2.0. Sample Preparation

All the QD samples were excited with the 514nm laser line of a "Coherent" Ar^+ laser source. A home-built far-field microscope (with a 100X and 0.95 N.A. air objective) was used to excite and collect the fluorescence time traces of QDs. These time traces at room temperature were recorded with a TE-cooled intensified CCD camera (Pentamax). Sample preparations consisted of dispersing bare or overcoated CdSe QD solutions with low concentrations in hexane, and then spin-coating the resulting solution on a pre-cleaned glass cover-slip.

6.2.1. CdSe QDs

Figure 6.2.1 shows log-log plots of fluorescence time traces of a collection of CdSe QDs at different excitation intensities. After 3,000 seconds, the curves were smoothed to eliminate room light parasitic contributions to the time traces. In these experiments, the laser focus spot was roughly 20μm in radius and thus the excitation intensity for 1mW was 8kW/cm². The fluorescence intensity time traces from these samples gave $f_{on}^{qe} = 0.5$ at the quasi-equilibrium state in Fig 6.2(a). (see Chapter 3) Their t_{on}^{max} and t_{off}^{max}, and $t_{off}^{max}/t_{on}^{max}$ values are given in Table 6.2.1. When $f_{on}^{qe} = 0.5$, only the ratio, $t_{off}^{max}/t_{on}^{max}$, is needed determine the steady-state value, f_{on}^{ss}. As

---

[2] The results described in the tables are not universal to that type of sample. The comparison between samples can be generalized.

$t_{off}^{max} / t_{on}^{max}$ increases, f_{on}^{ss} decreases, making the collection of QDs poorer optical

emitters. The measured f_{on}^{ss} value was obtained by normalizing the quasi-equilibrium

state to 0.5. (see Chapter 2,3) We obtained an average $t_{off}^{max} / t_{on}^{max} = 280$ in the high

excitation (HE) regime (3-8mW range). This ratio is huge compared to those of core-

shell QDs and alloyed QDs, where surfaces are passivated to some extent, as will be

described in the next sections. The bare CdSe QDs have broader power-law distributions

than the other types of QDs. Moreover, the large $t_{off}^{max} / t_{on}^{max}$ gives $f_{on}^{ss} = 0.056$ from

calculation, which matches well with the experimentally obtained values which are also
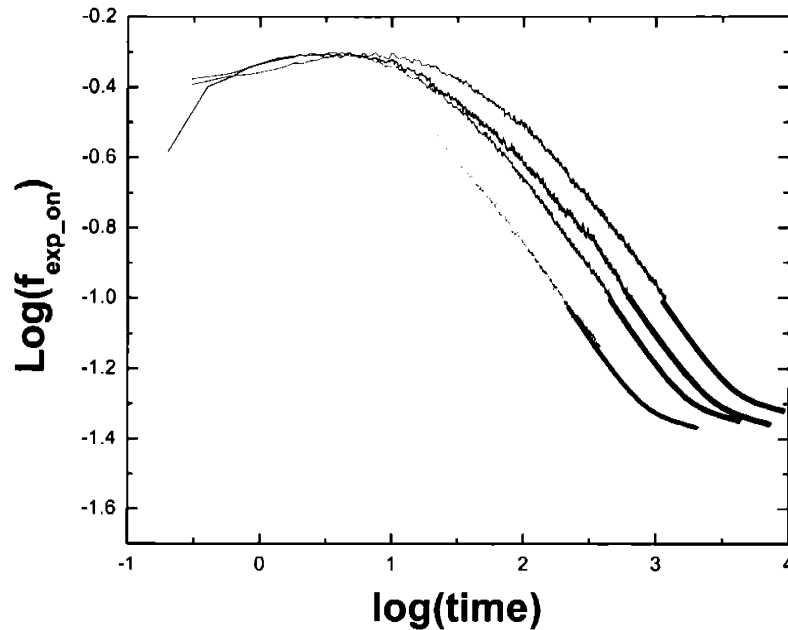
on average 0.056.

Figure 6.2.1. The log-log plot of the fluorescence time traces of CdSe QDs spin-coated on a glass coverslip. The excitation power values are 7.5, 5.6, 4.3, 3mW for green, blue, black, and red plots, respectively.

This result suggests that, at the steady state, an individual QD has only a 5.6 % probability of emitting during one bin (see chapter 4), indicating that a bare QD is a poor optical emitter. Since the fluorescence from a collection of bare QDs starts to decay early from t_{on}^{max} (~ less than a minute into the high excitation regime of 3-8mW), followed by a long decay to a low steady state, the bare QDs appear to "photo-bleach" faster than overcoated QDs. In fact, "photo-bleach" is not an accurate description of the photo-decay, since the photo-decay shown in the fluorescence intensity time trace is a purely statistical effect (see Chapter 2). The argument that t_{on}^{max} and t_{off}^{max} are intrinsic to a specific QD sample is well demonstrated by the experimental observation that the ratio, $t_{off}^{max}/t_{on}^{max}$ is conserved throughout the high excitation intensity range of 3-8mW. However, at very low intensities (0.09mW), this behavior differs from those shown in the higher excitation regime. This effect may suggest that the light-induced parameters, t_{off}^{min} and t_{on}^{min}, are increased to a thermal relaxation time as the excitation cycle becomes as slow as the thermal relaxation time. (see Chapter 5)

Power-law statistics are constructed from the waiting-time distributions for the on- and off-times. Therefore, the inverse values of the on- and off-times, $\left(t_{on}^{max}\right)^{-1}$ and $\left(t_{off}^{max}\right)^{-1}$, are equivalent to rates of switching the state from on to off, or off to on, respectively. In this way, $\left(t_{on}^{max}\right)^{-1}$ and $\left(t_{off}^{max}\right)^{-1}$ become the slowest switching rates between the on- and off- states. Figure 6.2.2 shows the evolution of $\left(t_{on}^{max}\right)^{-1}$ and $\left(t_{off}^{max}\right)^{-1}$ as a function of the excitation power.
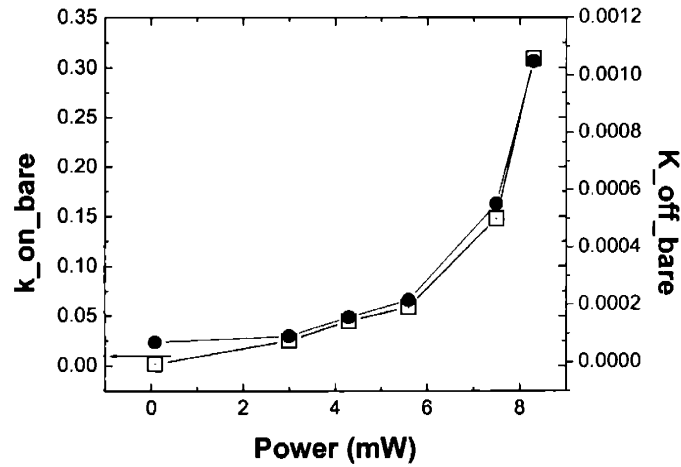
Figure 6.2.2. Excitation intensity dependence on $\left(t_{off}^{max}\right)^{-1}$ and $\left(t_{on}^{max}\right)^{-1}$.

k_on_bare(k_off_bare) = $\left(t_{off}^{max}\right)^{-1}\left(\left(t_{on}^{max}\right)^{-1}\right)$ for bare CdSe QDs. The black symbols

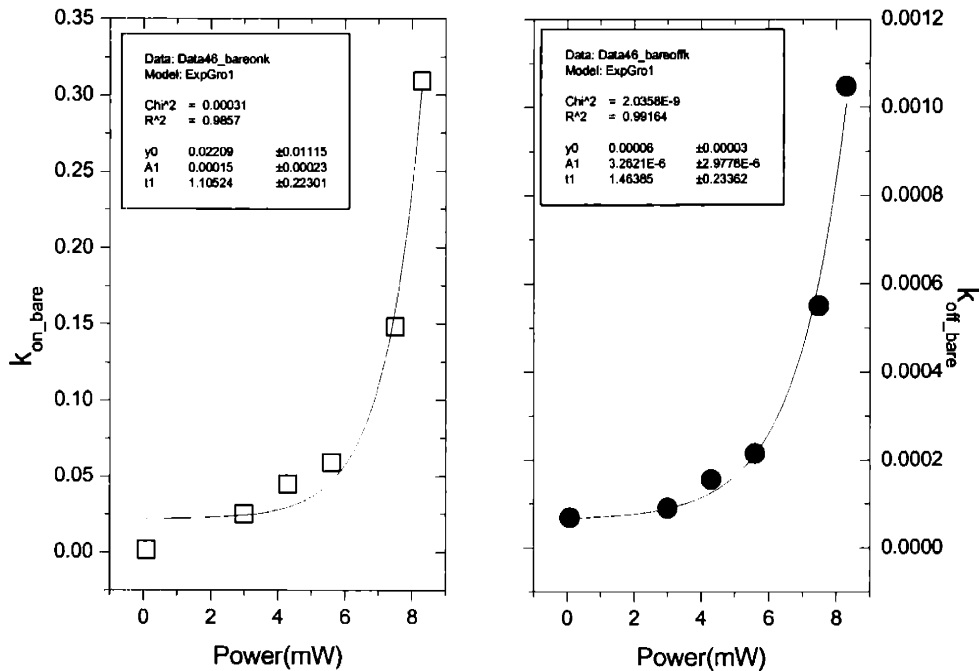are for $\left(t_{on}^{max}\right)^{-1}$ and the blues symbols are for $\left(t_{off}^{max}\right)^{-1}$.

Figure 6.2.3. Each plot in Fig 6.2(b) was fitted with an exponential curve, y = y_0 + A1·exp(x/f$_1$). As shown in the insets, the power dependent $\left(t_{off}^{max}\right)^{-1}$ and $\left(t_{on}^{max}\right)^{-1}$ for the bare QDs give f$_1 \approx$ 1.1mW and 1.5 mW.

In Figure 6.2.3, each plot is fit with an exponential function with the formula. The fits result in f_1 values of about 1.1mW and 1.5mW for the cases of $\left(t_{off}^{max}\right)^{-1}$ and $\left(t_{on}^{max}\right)^{-1}$, respectively. We discuss the possible mechanisms that may gie rise to this exponential dependence later in the discussion section.

Power (mW)	t_{on}^{max} (sec)	t_{off}^{max} (sec)	$t_{off}^{max} / t_{on}^{max}$	f_{on}^{ss} Measured/Calculated
0.09	602.6	14790	25	0.167
3	39.8	11220	282	0.056 / 0.057
4.3	22.4	6457	288	0.056 / 0.054
5.6	17	4677	275	0.057 / 0.056
7.5	6.8	820	269	0.057 / 0.058
8.3	3.2	955	295	0.049 / 0.052

Power (mW)	$\left(t_{off}^{max}\right)^{-1}$ (sec^{-1})	$\left(t_{on}^{max}\right)^{-1}$ (sec^{-1})
0.089	**0.0017**	**6.76E-5**
3	**0.025**	**8.91E-5**
4.6	**0.045**	**1.55E-4**
5.6	**0.059**	**2.14E-4**
7.6	**0.148**	**5.50E-4**
8.3	**0.309**	**0.00105**

Table 6.2.1.

6.2.2. CdSe(ZnS) QDs

Unlike for the case of the bare QDs, overcoated CdSe(ZnS) QDs displayed a variety of initial dynamics (from $t = 0$ to the end of the quasi-equilibrium). In addition, the heterogeneities within the same sample in the early dynamical features made it difficult to obtain intensity dependent measurements, and numerous runs had to be repeated to generalize the results. The upper cut-offs and the steady state values were highly susceptible to sample preparations, so repetition did not facilitate the data acquisition process. Figure 6.2.4 shows fluorescence intensity time traces of the collection of CdSe(ZnS) QDs (first ABS peak at 570nm) excited at intensities ranging from 0.07 to 7mW. The overcoated QDs feature longer brightening at low excitation intensities but the excitation cycle dependence on upper cut-offs appears similar to that of the bare QDs. However, the brightening shown in Figure 6.2.4 is not always present in the fluorescence time traces of the overcoated QDs.
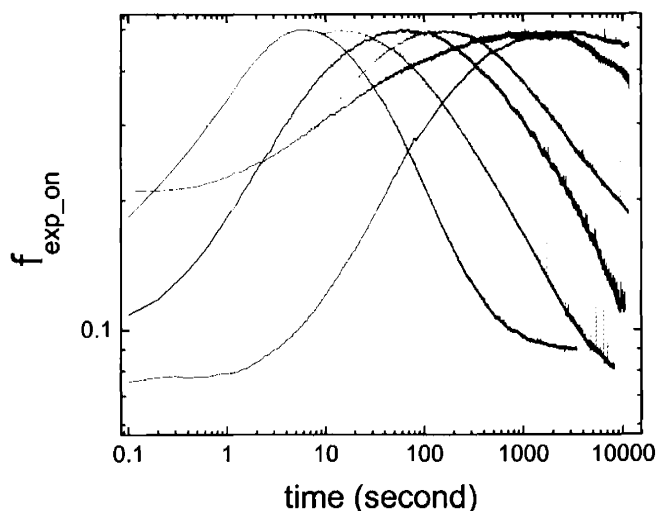

Figure 6.2.4. The fluorescence time traces of CdSe(ZnS) QDs. The excitation intensities for red, green, black, cyan, pink and blue curves are 7, 1.4, 0.75, 0.35, 0.08, and 0.07mW, respectively.

Figure 6.2.5 is constructed from different preparations of the same overcoated QD sample excited at multiple spots with varying excitation intensities. Differences in the time traces are clearly present, and the intensity dependence is not consistent from one sample (or spot) to the other (although the general tendency that $t_{off}^{max}, t_{on}^{max}$ decrease at higher excitation intensities remains true). However, it is interesting that traces that share similar dynamics at early times follow similar trends in the intensity dependence of the upper cut-offs. For example, the green curves in Figure 6.2.5 show similar early dynamics and their upper cut-offs decrease with increasing excitation intensity.
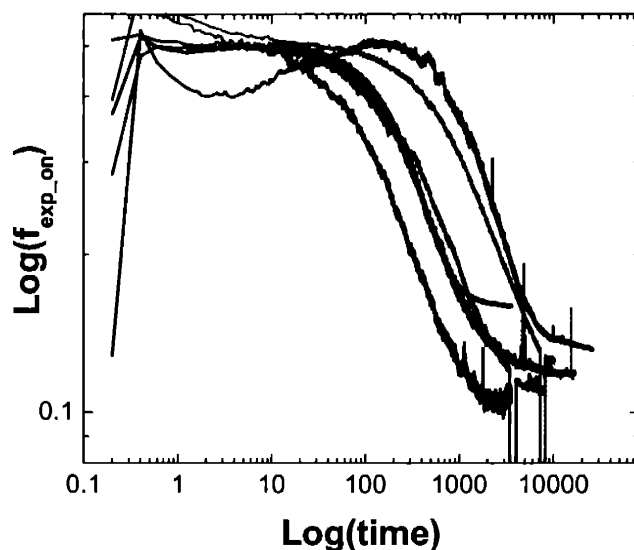

Figure 6.2.5. Log-log plots of fluorescence intensity time traces of CdSe(ZnS) QDs at different excitation intensities. The red curves are obtained from the same sample at the different spots. The left is from the excitation at 2mW and the right from excitation at 0.9mW. The green, blue and black curves are from the same CdSe(ZnS) QD sample. The green curves are from excitation at 2.2 and 3.6mW (left and right). The blue and the black are from 0.65mW, and 2mW excitation, respectively.

The red curves are obtained from the same QD samples at 2mW and 0.91mW. For the 2mW excitation, $t_{off}^{max}, t_{on}^{max}$, and $t_{off}^{max}/t_{on}^{max}$, are 1306 sec, 41 sec, and 32,

respectively. For the 0.91mW excitation, $t_{off}^{max}, t_{on}^{max}$, and $t_{off}^{max}/t_{on}^{max}$ are 3500 sec, 105 sec, and 33, respectively. The f_{on}^{ss} value calculated from this ratio ($t_{off}^{max}/t_{on}^{max} = 33$) is 0.148, and the measured value is 0.11. This result suggests that $t_{off}^{min} > t_{on}^{min}$ since the calculated f_{on}^{ss} value is larger than the measured value when the quasi-equilibrium state is normalized to 0.5. (see Chapter 3).

The green, blue and black curves are all from the same sample, but display qualitatively different early dynamics. The green curves are obtained using excitation powers of 2.2mW and 3.6mW. This time, $t_{off}^{max}, t_{on}^{max}$, and $t_{off}^{max}/t_{on}^{max}$ are 8229 sec, 301 sec, and 27 (2.2mW) and 2995 sec, 84 sec, and 24 (3.6mW), respectively. The measured (calculated) f_{on}^{ss} values for 2.2mW, and 3.6mW cases are 0.12(0.16), and 0.12(0.17), respectively. These results also indicate $t_{off}^{min} > t_{on}^{min}$.

The blue curve is obtained using an excitation power of 0.65mW. $t_{off}^{max}, t_{on}^{max}$, and $t_{off}^{max}/t_{on}^{max}$ are 8300sec, 556 sec, and 15, respectively. The smaller ratio at the lower excitation intensity is similar to that for QDs. The measured (calculated) f_{on}^{ss} values are 0.134(0.205). These values also imply $t_{off}^{min} > t_{on}^{min}$.

The black curve is obtained using an excitation power of 2mW. $t_{off}^{max}, t_{on}^{max}$, and $t_{off}^{max}/t_{on}^{max}$ are 1343 sec, 48 sec, and 28, respectively. $t_{off}^{max}/t_{on}^{max}$ is similar to that obtained for the green curves. However, the measured (calculated) f_{on}^{ss} values are 0.16(0.16), so this sample features $f_{on}^{qe} = 0.5$, implying $t_{off}^{min} \cong t_{on}^{min}$.

The next samples in table 6.2.2 showed very different values for $t_{off}^{max} / t_{on}^{max}$. As

$t_{off}^{max} / t_{on}^{max}$ was not constant over the intensity range, we assume that the sample spots

were heterogeneous. Presumably, the intensity dependence of the upper cut-offs would

be more clearly demonstrated if we had used more homogeneous sample spots. Figure

6.2.5 demonstrates the power dependence of $\left(t_{on}^{max}\right)^{-1}$ and $\left(t_{off}^{max}\right)^{-1}$. Figure 6.2.6 shows

the individual exponential growth fits to the curves. This time the power-dependent

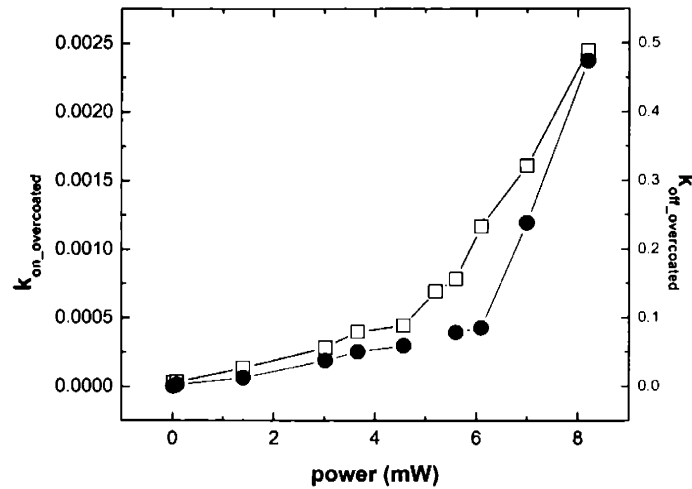$\left(t_{on}^{max}\right)^{-1}$ and $\left(t_{off}^{max}\right)^{-1}$ gives $f_1 \approx 1.5(2.9)\text{mW}$.

Figure 6.2.6. Excitation intensity dependence on $\left(t_{off}^{max}\right)^{-1}$ and $\left(t_{on}^{max}\right)^{-1}$.

$k_{on\_overcoated}(k_{off\_overcoated}) = \left(t_{off}^{max}\right)^{-1}\left(\left(t_{on}^{max}\right)^{-1}\right)$ for over-coated CdSe(ZnS) QDs. The

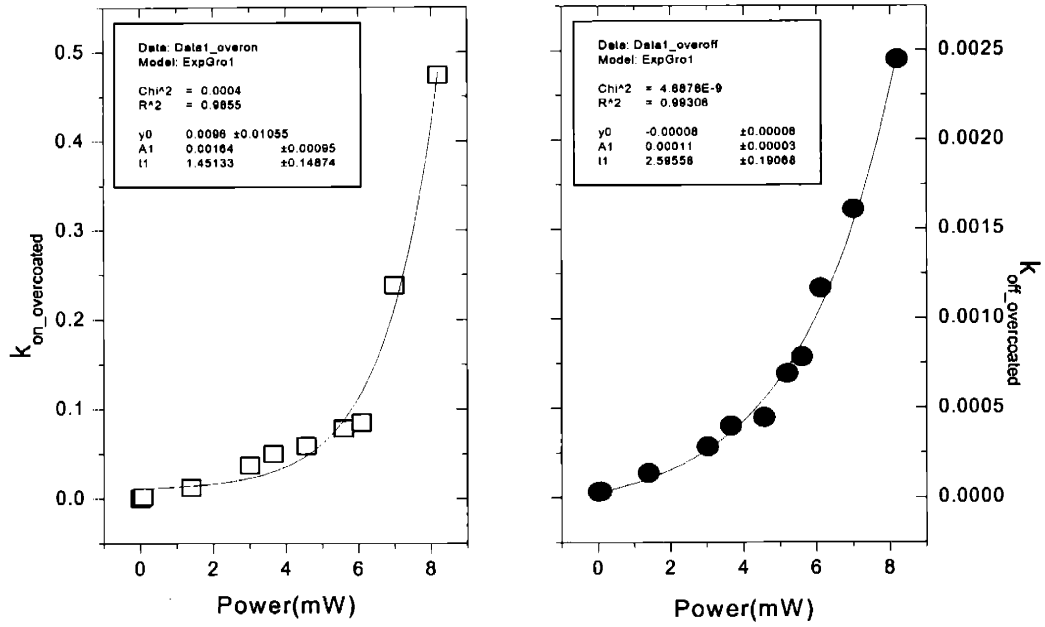black symbols are for $\left(t_{on}^{max}\right)^{-1}$ and the blues symbols are for $\left(t_{off}^{max}\right)^{-1}$.

Figure 6.2.7. Each plot in Fig 6.2.5 was fitted with an exponential growth. As shown in the insets, the power dependent $\left(t_{off}^{max}\right)^{-1}$ and $\left(t_{on}^{max}\right)^{-1}$ for the core-shell overcoated QDs bring both values of $f_1 \approx 1.5\text{mW}$ and 2.9mW.

Power (mW)	t_{on}^{max} (sec)	t_{off}^{max} (sec)	$t_{off}^{max} / t_{on}^{max}$	f_{on}^{ss} Measured/Calculated
0.02	34910	12601	2.8	/0.37
0.09	32296	482	67	/0.11
1.4	7507	83	91	0.054/0.095
3.02	3579	26.9	133	0.057/0.08
3.66	2530	20	127	0.058/0.082
5.6	1281	12.8	101	0.062/0.09
6.1	859	11.8	73	0.095/0.105

Power (mW)	$\left(t_{off}^{max}\right)^{-1}$ (sec^{-1})	$\left(t_{on}^{max}\right)^{-1}$ (sec^{-1})
0.02	2.86E-5	7.94E-5
0.089	3.10E-5	0.00207
1.4	1.33E-4	0.0121
3.02	2.79E-4	0.0372
3.66	3.95E-4	0.05
5.6	7.81E-4	0.0781
6.1	0.00116	0.0848

Table 6.2.2.

6.2.3 CdSe(Cd$_x$Zn$_{1-x}$S)

The alloyed QD samples studied in this section were purchased from Quantum Dot Corporation. The alloyed QD samples display high TQY (see Chapter 5) values above 80% due to their thick effective shells.
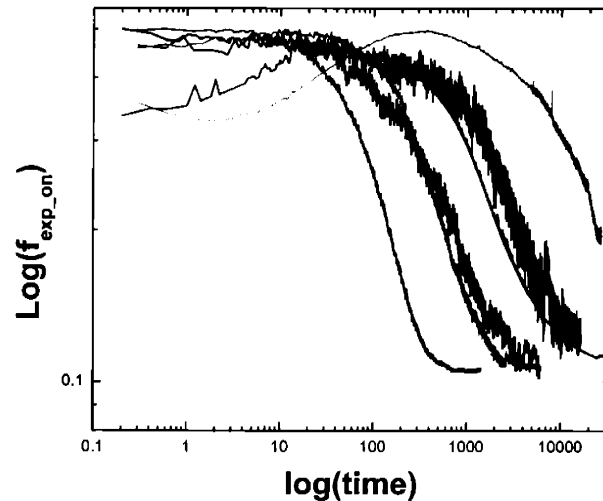

Figure 6.2.8. The fluorescence intensity time traces of CdSe(CdZnS) QDs. The blue, green, black, pink, red, and the cyan curves are from the excitation intensity at 4.7, 3.3, 3, 2.5, 1.7, 0.03mW.

The curves in figure 6.2.8 were taken in the excitation intensity range of 1mW to 5mW. When the excitation intensity is above 2mW, the quasi-equilibrium state is clearly displayed. In this range, the steady state value appears to be independent of intensity at 0.18. It is worth noting that the average value of $t_{off}^{max}/t_{on}^{max}$ for the alloyed QD samples is the smallest among all the QD samples studied so far. The value of $t_{off}^{max}/t_{on}^{max}$ for the alloyed QDs would result in the highest steady-state value, so that individual QDs would have ~18% emission yield at the steady state, if $t_{off}^{min} \cong t_{on}^{min}$. However, the steady state

value calculated from the experimental values of t_{on}^{max} and t_{off}^{max} is larger than the measured one, suggesting that $t_{off}^{min} > t_{on}^{min}$. When $t_{off}^{min} > t_{on}^{min}$, as demonstrated in Chapter 3, f_{on}^{qe} and f_{on}^{ss} become significantly reduced from 0.5. At the highest (6mW) and the lowest (0.03mW) intensities, f_{on}^{ss} deviates from the values obtained at different intensities. We speculate that at the lowest intensity, t_{on}^{min} and t_{off}^{min} are increased as large as the thermal relaxation time. At 6mW, when t_{on}^{max} approaches t_{on}^{min} and t_{off}^{min}, the fluorescence of a collection of QD does not have enough time to reach the quasi-equilibrium state. In this case, the quasi-equilibrium state will not appear, but there will be a fast transition to decay after time passes t_{on}^{min}. Then, normalizing the maximum intensities of those curves to the same value used for other curves will locate the steady state value at a different position from other values obtained from medium excitation intensities. Figure 6.2.9 shows the exponential increases of $\left(t_{on}^{max}\right)^{-1}$ and $\left(t_{off}^{max}\right)^{-1}$ as a function of excitation intensities, and Figure 6.2.10 describes the fits to each plot in Figure 6.2.9. This time, the exponential growth fits result in $f_1 = 1.53(1.81)$mW for intensity dependence of $\left(t_{on}^{max}\right)^{-1}$ and $\left(t_{off}^{max}\right)^{-1}$.
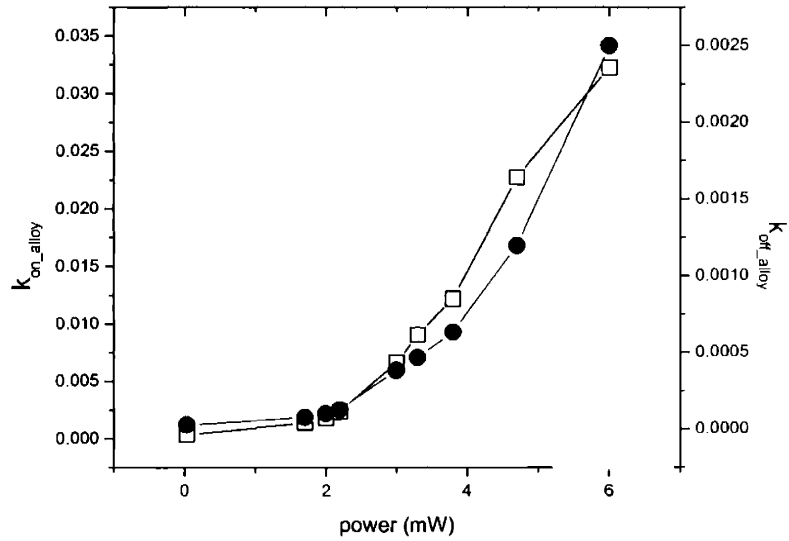
Figure 6.2.9. Excitation intensity dependence on $\left(t_{off}^{max}\right)^{-1}$ and $\left(t_{on}^{max}\right)^{-1}$.

$k_{on\_alloy}(k_{off\_alloy})$ $=$ $\left(t_{off}^{max}\right)^{-1}\left(\left(t_{on}^{max}\right)^{-1}\right)$ for alloyed $CdSe(Cd_xZn_{1-x}S)$. The black

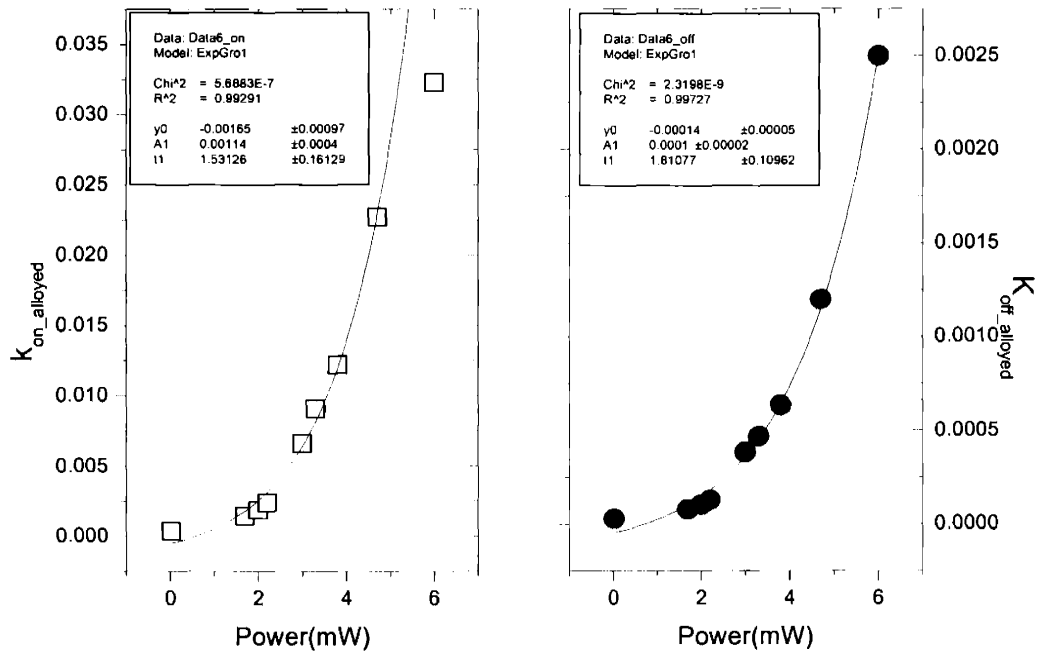symbols are for $\left(t_{on}^{max}\right)^{-1}$ and the blues symbols are for $\left(t_{off}^{max}\right)^{-1}$.

Figure 6.2.10. Each plot in Fig 6.2(h) was fitted with an exponential growth function. As shown in the insets, the power dependent $\left(t_{off}^{max}\right)^{-1}$ and $\left(t_{on}^{max}\right)^{-1}$ for the overcoated QDs result in $f_1 = 1.53\text{mW}$ and 1.81mW.

Power (mW)	On cut-off (sec)	Of cut-off (sec)	Ratio (off/on)	Steady State Value Measured/Calculated
0.03	2673	33870	12.7	0.191/0.219
1.7	694	12677	18.3	0.108/0.19
2	536	9630	18	0.112/0.191
2.5	418	7730	18.6	0.112/0.189
3	151	2605	17.3	0.109/0.194
3.3	110	2140	19.5	0.106/0.185
3.8	82	1580	19.3	0.106/0.185
4.7	44	835	19.0	0.105/0.187
6	31	400	12.9	0.117/0.218

Power (mW)	1 / On cut-off (sec^{-1})	1/ Off cut-off (sec^{-1})
0.03	3.74E-4	2.95E-5
1.7	0.00144	7.89E-5
2	0.00187	1.04E-4
2.5	0.00239	1.29E-4
3	0.00662	3.84E-4
3.3	0.00909	4.67E-4
3.8	0.0122	6.33E-4
4.7	0.0227	0.0012
6	0.0323	0.0025

Table 6.2.3.

6.3. Discussion

We first demonstrate one example of the comparison between fluorescence time traces of a collection of overcoated QDs and alloyed QDs. Figure 6.3.1 shows the fluorescence intensity time traces of collections of alloyed QDs and normal core-shell overcoated QDs at 6.5 mW, 0.07mW, and 2 mW, 0.02mW, respectively. Long brightening is not always observed in the normal CdSe(ZnS) QDs in the higher excitation regime (1mW ~ 7mW). Higher excitation intensities generally result in smaller values of t_{on}^{max} and t_{off}^{max} in the fluorescence time traces of a collection of all types of QDs. However, CdSe(ZnS) QDs are found to be very heterogeneous from sample to sample and from spot to spot in a given sample in this dependency.
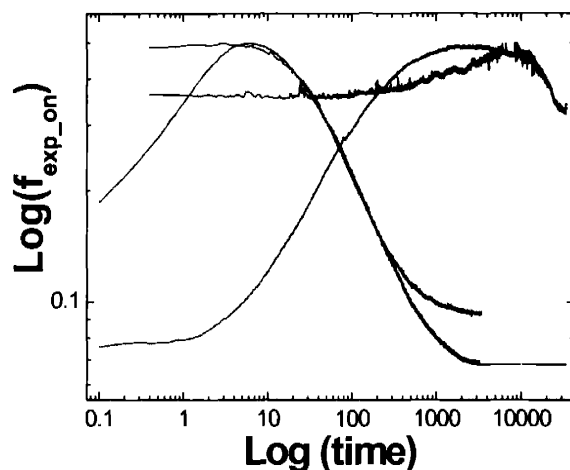
Figure 6.3.1. The log-log plots of fluorescence intensity time traces of CdSe(ZnS) (black) and CdSe(CdZnS) (violet) QDs at different excitation intensity values 1.8mW (left) and 0.02mW(right) for the CdSe(CdZnS) and 6.5mW (left) and 0.07mW (right) for the CdSe(ZnS).

105

Long brightening does not typically occur in the alloyed QDs in this intensity regime. In Figure 6.3.1, for example, there is a clear difference between alloyed and normal overcoated QD samples in terms of the extent of the initial brightening and the final steady state values. Because $t_{off}^{min} \neq t_{on}^{min}$, the steady state values, when arbitrarily normalized to 0.5, shown in experiments would be different from the steady state values, calculated from experimental values of t_{on}^{max} and t_{off}^{max} with the assumption of $t_{off}^{min} \cong t_{on}^{min}$. Due to the significant initial asymmetry, the steady state values would be located lower than 0.5 since the calculated value is larger than the measured one, implying that $t_{off}^{min} > t_{on}^{min}$ (see Chapter 3). The steady state value will then be larger for the alloyed QDs compared to the CdSe(ZnS) QDs due to larger $t_{off}^{max}/t_{on}^{max}$ and, speculatively, $t_{on}^{min}/t_{off}^{min}$. Since the bare QDs did not demonstrate asymmetry in the lower cut-offs except at the low power regime (<1mW), the initial symmetry in $t_{on}^{min}, t_{off}^{min}$ may be related to the tunneling width caused by the presence of the overcoating shell.

We will now discuss the excitation intensity dependence on $t_{off}^{max}, t_{on}^{max}$ for all three types of QDs with different of overcoating shell widths.
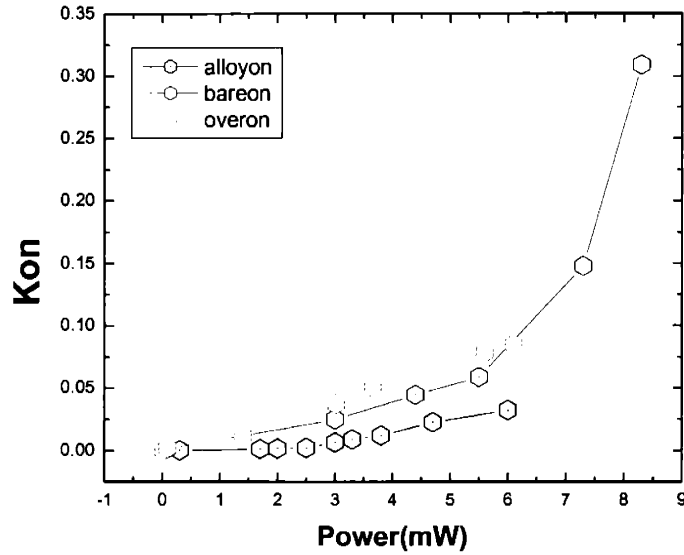
Figure 6.3.2. Excitation intensity dependence on $\left(t_{on}^{max}\right)^{-1}$ values for the CdSe(ZnS)(green), CdSe(red), and CdSe(CdZnS)(red) QDs.

Figures 6.3.2 and 6.3.3 display the values of $\left(t_{on}^{max}\right)^{-1}$ and $\left(t_{off}^{max}\right)^{-1}$ for CdSe, CdSe(ZnS), and CdSe(Cd$_x$Zn$_{1-x}$S) QDs. For both on- and off-times, the excitation intensity-dependences on $\left(t_{on}^{max}\right)^{-1}$ and $\left(t_{off}^{max}\right)^{-1}$ for all three samples were fit with exponential functions with excitation power in the range of 1mW~7mW. For $\left(t_{on}^{max}\right)^{-1}$ and $\left(t_{off}^{max}\right)^{-1}$, the exponential fit to each plot gave the exponents of 1.1, 1.5, and 1.5(mW), and 1.5, 2.9, and 1.8(mW) for the bare, core-shell overcoated, and alloyed QDs, respectively. By definition, $\left(t_{on}^{max}\right)^{-1}$ and $\left(t_{off}^{max}\right)^{-1}$ are the slowest switching rates, and therefore, they would result from the least probable switching mechanisms, such as a bi-exciton formation, or thermal activation of deep trap states by heating, with the

combination of the bi-exciton formation. For the discussion, we only attempt to make qualitative pictures.

We will first investigate the bi-exciton formation. Blinking statistics are usually obtained from single QDs that are excited by continuous excitation whose mean value is not typically large enough to create multiple excitons in a QD core. However, unlike for pulsed excitation, the number of photons from a continuous excitation source, arrives at a sample distributed according to a Poisson distribution. In the HE regime, the excitation period is chosen to be on the order of $0.1\,\mu\sec$. The fluorescence lifetime of a QD is measured to be $\sim 25\text{nsec}$[3]. Therefore, it is possible to excite a QD before the first e-h pair in the QD has relaxed, which results in creating a bi-exciton. With increasing the excitation rate, the mean value of photon arrival in the Poisson distribution approaches the fluorescence lifetime. The probability of exciting a second e-h pair before the first e-h pair has not recombined is the overlap integration of the single exponential emission lifetime distribution and the Poisson distribution of excitation photons. Therefore the overlapping region is approximately exponentially increasing as the mean value of the Poission distribution approaches the exponential lifetime.

The exponential increase of the slowest switching rates with faster excitation cycles can now be explained with bi-exciton formation, but different exponents obtained for $\left(t_{on}^{max}\right)^{-1}$ and $\left(t_{off}^{max}\right)^{-1}$ for the same excitation cycle suggest that there should be another mechanism to describe the difference between them. For the case of neutral QDs with a bi-exciton inside, one e-h pair (EHP) can recombine to excite a carrier, moving the

---

[3] . Fisher BR, Eisler H-J, Stott NE, and Bawendi MG: Emission Intensity Dependence and Single-Exponential Behavior In Single Colloidal Quantum Dot Fluorescence Lifetimes, *Journal of Phys. Chem. B* 2004, 108:143-148.

carrier outside of the QD and leaving the QD charged. A bi-exciton in a charged QD has dynamics that are different than in a neutral QD. When there are two excitons and one carrier, one EHP would recombine to excite a carrier out of the QD, leaving the QD neutral. While the prefactors of the exponential functions might describe the differences between these two mechanisms, the exponents should be identical for both $\left(t_{on}^{max}\right)^{-1}$ and $\left(t_{off}^{max}\right)^{-1}$. Our model may need to be augmented by considering different lifetime distributions of single QDs. Probably the bi-exciton formation and other effects are co-existent such that the excitation intensity depends on the smallest switching rates, $\left(t_{on}^{max}\right)^{-1}$ and $\left(t_{off}^{max}\right)^{-1}$.

Alternatively, we speculate that there could be a heating effect when a bi-exciton is formed. In the case of a charge QD, if the thermal energy due to a first EHP is not completely dissipated before a second EHP is created, then thermally assisted processes become accessible. Some deep trap states can be thermally activated so that a charge carrier in the QD (or a carrier in a trap state) can hop to the trap state (or to the QD), resulting in $\left(t_{on}^{max}\right)^{-1}$ and $\left(t_{off}^{max}\right)^{-1}$. As the ambient temperature increases with a faster excitation rate, $\left(t_{on}^{max}\right)^{-1}$ and $\left(t_{off}^{max}\right)^{-1}$ then follow an Arrhenius law. In order to validate this scenario, the thermal energy dissipation time should be calculated for each substrate where QDs are located on or embedded in, and we need to investigate the temperature increase as a function of the excitation rate.

From this position, we will make a comparison of $\left(t_{on}^{max}\right)^{-1}$ values between bare and alloyed QDs at a given excitation intensity. Since fluorescence time traces for

overcoated QDs were sample dependent, we will mainly focus on bare and alloyed QDs.

At a given intensity, $\left(t_{on}^{max}\right)^{-1}$ for bare QDs is higher than for overcoated QDs. This

finding suggests that due to their larger shell thickness and fewer impurity states inside

the shell, the switching rate (for a carrier in a QD to move from a QD to the environment)

is smaller for overcoated QDs than for bare QDs. The $\left(t_{on}^{max}\right)^{-1}$ value is the highest for

bare QDs since the shell is not present. Therefore, alloyed QDs stay in the quasi-

equilibrium state for the longest time.
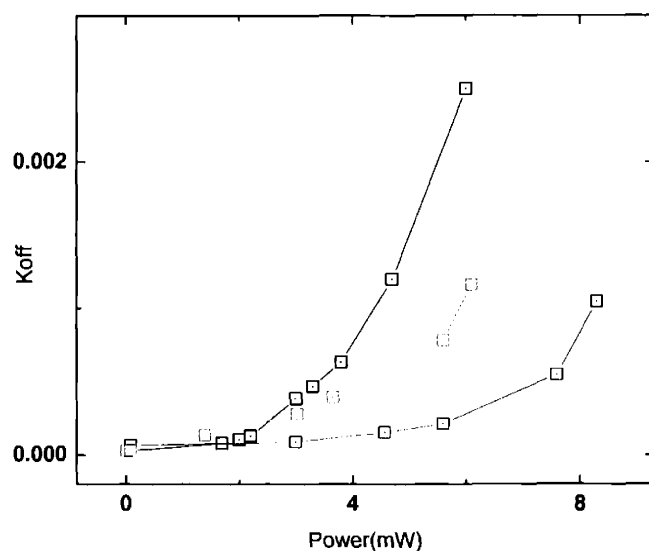
Figure 6.3.3. $\left(t_{off}^{max}\right)^{-1}$ for the bare, overcoated, and alloyed QDs at different excitation intensities.

Figure 6.3.3. is a graph of $\left(t_{off}^{max}\right)^{-1}$ as a function of excitation intensity. From a comparison of $\left(t_{off}^{max}\right)^{-1}$ between alloyed QDs and bare QDs, $\left(t_{off}^{max}\right)^{-1}$ for alloyed QDs appears more susceptible to the excitation light intensity than for bare QDs. It is not clear exactly why this is the case, but this finding can be interpreted in the context of the density of states of the carrier trap states. The off-time distributions are closely related to the spatial or energy distributions (or both) of the density of states for carriers trapped outside QDs. In the case of bare QDs, the absence of the shell increases the probability of a charge carrier being trapped in a nearby state in the surrounding environment, and bare QDs may have a broader density of states than alloyed QDs. The alloyed QDs have a thick shell, and any surface defect or impurity state on the shell may have a narrower density of states than those of bare QDs. Additionally, since most available trap sites are on the shell, the distance distribution between a trapped carrier and the core is concentrated at the surface of the shell, while for bare QDs, the distribution of distances of trap carriers could be stretched farther into the substrate environment. Finally, since the trap sites are mostly concentrated on the shell for the alloyed QDs, the presence of Coulomb interactions between a carrier in the core and a carrier in the trap site cannot be ignored.

Overall the off-time distribution as shown in Figure 6.3.3 for alloyed QDs exhibits smaller t_{off}^{max} values. Since alloyed QDs are characterized by larger t_{on}^{max} and smaller t_{off}^{max} than those values of bare QDs, alloyed QDs appear to be brighter. The f_{on}^{ss}

values are also higher for alloyed QDs than for other types of QDs. However, when

$$\left(t_{on}^{min}\right)^{-1} > \left(t_{off}^{min}\right)^{-1}, \; f_{on}^{ss} \text{ decreases.}$$
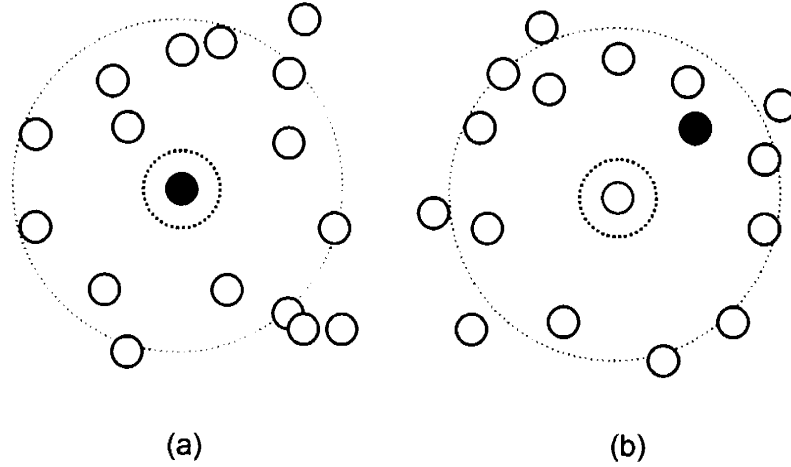

(a)   (b)

Figure 6.3.4. (a) The filled black circle is a charge carrier inside a QD. The first dotted circle is the edge of a QD. The empty black circles are trap sites. The next dotted circle corresponds to an effective distance that is the farthest distance that a carrier can hop from a dot to a trap site. (b) The empty red circle: a neutral QD. The first dotted circle is the edge of a QD. The empty black circles are trap sites and the filled black circle is a charge carrier in a trap site. The next dotted corresponds to an effective distance that is the farthest distance that a carrier can hop from a trap site to a dot. Figure (d) and (e) are independent images.

The reason why t_{on}^{max} is always smaller than t_{off}^{max} is illustrated in Figures 6.3.4(a) and (b). In Figure 6.3.4(a), the carrier inside the QD sees many possible places (black solid circles) to hop. However, once the carrier is outside of the QD, the QD (the red circle) is now only one of many possible places for that carrier to hop to. Thus, the probability to go back to the QD is smaller than to go out of the QD , resulting in

$$t_{on}^{max} < t_{off}^{max}.$$

6.4. Conclusion

In this chapter, we describe how the excitation power affects t_{on}^{max} and t_{off}^{max} for three different kinds of QDs: CdSe, CdSe(ZnS), and CdSe(Cd$_x$Zn$_{1-x}$S). We find that $\left(t_{on}^{max}\right)^{-1}$ and $\left(t_{off}^{max}\right)^{-1}$ increase exponentially with higher excitation intensity for all three kinds of QDs. At a given excitation intensity, bare QDs show a higher $\left(t_{on}^{max}\right)^{-1}$ value than alloyed QDs. We speculate that the absence of the shell in the bare QDs facilitates the switching behavior. For $\left(t_{off}^{max}\right)^{-1}$, alloyed QDs showed a higher value than bare QDs. We speculated that the trap density is concentrated on the surface of the shell for alloyed QDs while the trap density is stretched farther into the environment of the bare QDs. Therefore, the presence of the shell facilitates the switching process from off to on state.

Chapter 7. Estimating the number of QDs from Noise Analysis at Steady State.

7.1. Introduction

In Chapter 2, we showed that (1) the fluorescence intensity time trace of a collection of CdSe QDs, when the excitation is initialized at $t = 0$ sec, can be described by the probability that a CdSe QD is found in an on-state at time t, and (2) the time trace can be divided into three regions. This argument is applied to the fluorescence time trace, as seen in Fig 7.1(a), of a QD-silica composite microsphere. QD-silica composite microspheres are made using appropriately functionalized CdSe QDs dispersed in an ethanol solution that become incorporated into a growing shell around pre-formed silica microspheres. Fluorescence images of such microspheres are shown in Fig 7.1(b) [1]. Fig. 7.1(c) is the data in Fig 7.1(a) plotted on a log-log scale. In Fig. 7.1(c), the first short flat region (dark gray) is the quasi-equilibrium state that corresponds to $f_{on}(t) \cong 0.5$. This is followed by a second region that shows a power-law-like decay (gray) with a power of -0.5, starting roughly at t_{on}^{max}. The plot ends with a steady state (light gray) region with a mean value given by $f_{on}{}^{ss} = \dfrac{<t_{on}>}{<t_{on}> + <t_{off}>}$ (see Chapters 2,3), the ratio of the mean value of the on-time and the sum of the mean values of the on-time and off-time. Two conditions must be fulfilled to observe $f_{on}(t) \cong 0.5$ in the first region. The first condition is $t_{on}^{min} \cong t_{off}^{min}$, symmetric lower on-time and off-time cut-off values. The

second condition is $t_{on}^{min}, t_{off}^{min} \ll t_b < t_{on}^{max}$, the experimental bin-size must be sufficiently

larger ($\sim 10^5 \sim 10^6$) than t_{on}^{min} and t_{off}^{min} (see Chapter 4) and smaller than the on-time upper

cut-off. While the second condition is usually satisfied with a typical $\tau_b \sim$ (0.1 sec - 1

sec) of CCD detectors, experimental studies to date imply that the first condition is not

always met. In the $f_{on}(t) \cong 0.5$ region, the fluorescence intensity follows a Gaussian

distribution as seen in Fig 7.1(d). In the steady state, the central limit theorem holds and

the intensity profile is expected to be Gaussian as shown in Fig 7.1(e). As explained in

Chapter 4, every QD in a collection of QDs appears at quasi-equilibrium where

$f_{on}(t) \cong 0.5$. In other words, the total number of QDs, N_T, is observed at the quasi-

equilibrium state. Then the proportion of the average number of emitting QDs, N_S, at

the steady state, relative to N_T at quasi-equilibrium, can be theoretically determined by

the ratio of the $f_{on}(t)$ value at quasi-equilibrium, f_{on}^{qe}, to the value at the steady-state,

f_{on}^{ss}. For simplicity, we only focus on the case of $f_{on}(t) \cong 0.5$ at quasi-equilibrium.

Additionally, $\mu_{on(off)}$, the powers of on and off-time power-law statistics, will be fixed at

0.5. In addition, it is important to have the quasi-equilibrium state, well defined

experimentally at reasonable excitation intensities ($\sim$ 10~30kW/cm^2) so that both f_{on}^{qe}

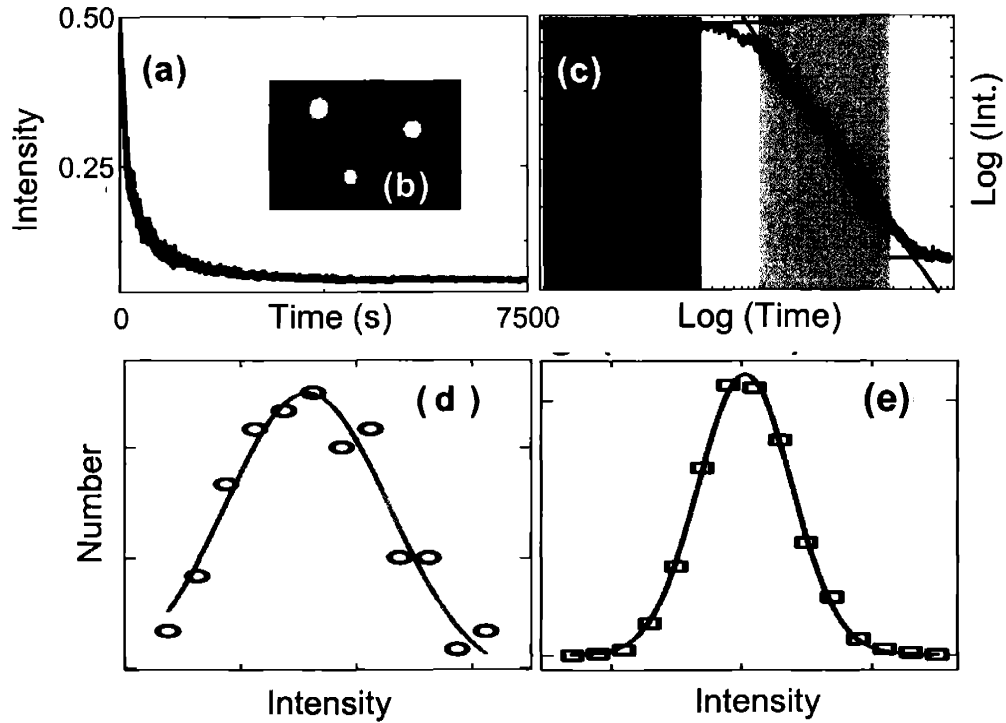and f_{on}^{ss} are well determined. (see Chapter 4)

Figure 7.1(a) Fluorescence intensity time trace of a QD-silica composite microsphere (b) fluorescence image of three microspheres excited at 514 nm. (c) Log-log plot of (a), where the three regions are indicated by dark gray ($f_{on}(t) \cong 0.5$), gray ($f_{on}(t) \approx t^{-0.5}$), and light gray ($f_{on}^{ss} = \dfrac{<t_{on}>}{<t_{on}> + <t_{off}>}$). (d)-(e) Fluorescence intensity distributions in the quasi-equilibrium region (dark gray) and the steady state region (light gray), respectively.

7.2. Fluorescence intensity fluctuation at the steady state

We define the ratio, N_S/N_T, where N_S and N_T are the number of QDs at steady state and at the quasi-equilibrium state, respectively.

$$\frac{N_S}{N_T} = \frac{\langle t_{on} \rangle}{\langle t_{on} \rangle + \langle t_{off} \rangle} \Big/ 0.5. \qquad (7.2.1)$$

Here, $\langle t_{on} \rangle$ and $\langle t_{off} \rangle$, the mean values of the on and off-times, are functions of t_{on}^{max} and t_{off}^{max}, respectively. In fact, as shown previously in Chapter 3, the steady state value depends only on the ratio, $t_{off}^{max}/t_{on}^{max}$. Figure 7.2(a) shows the evolution of N_S/N_T as a function of $t_{off}^{max}/t_{on}^{max}$. As the ratio N_S/N_T becomes larger than one (as $t_{off}^{max} > t_{off}^{max}$), the ratio decays with a power-law with a power of 0.5. This effect is due to $\langle t_{off} \rangle$ becoming dominant over $\langle t_{on} \rangle$ as $t_{off}^{max}/t_{on}^{max}$ increases. From previous experiments, $t_{off}^{max}/t_{on}^{max}$ values have always been larger than one, which results in a decay of the fluorescence intensity of a collection of QDs as a function of time.

The important point of this work is that the fluorescence intensity fluctuation of a collection of QDs at the steady state, which is the relative standard deviation of the fluorescence intensity at the steady state, is equivalent to the fluctuation of the number of QDs that are contributing to the emission at the steady state. If we assign a random number of emitting QDs in one bin at steady state to be N_p, an independent random variable, then the mean value of N_p is N_s. The resultant distribution of N_p follows

Poissonian statistics, where the standard deviation of N_p is given by the square root of the mean value, such as $\delta N_p = \sqrt{N_s}$. We define the noise of the fluorescence intensity at steady state as the ratio of the standard deviation of N_p to the mean value N_s.

$$Noise \equiv \delta(N_p)/N_s \equiv \sqrt{N_s}/N_s = N_s^{-0.5} = \sqrt{0.5/\frac{\langle t_{on}\rangle}{\langle t_{on}\rangle+\langle t_{off}\rangle}} \cdot N_T^{-0.5} \qquad (7.2.2)$$

$$N_T = \left(\frac{\langle t_{on}\rangle+\langle t_{off}\rangle}{2\langle t_{on}\rangle}\right)\frac{1}{Noise^2} \qquad (7.2.3)$$
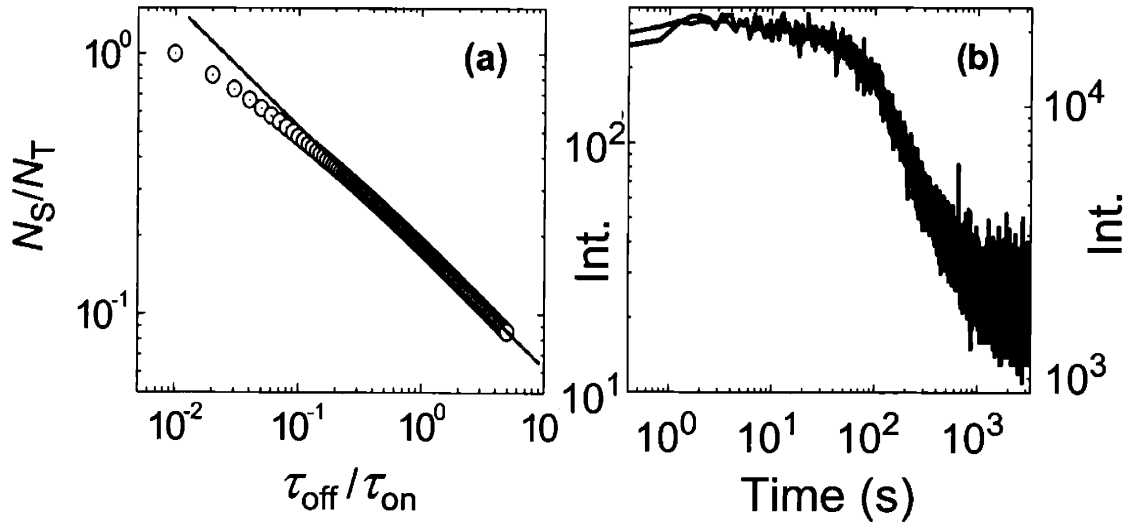
Figure 7.2. (a) $Log(N_S/N_T)$ versus $Log(t_{off}/t_{on})$. As the ratio, $t_{off}^{max}/t_{on}^{max}$, increases, N_S/N_T decays like a power-law with a power of -0.5. (b) Log-log plots of two fluorescence time traces obtained from the same sample (with the same $t_{off}^{max}/t_{on}^{max}$ values) of different numbers of QDs. (Dark gray trace contains a larger number of QDs than the black one.)

Figure 7.2(b) clearly demonstrates the difference in the intensity fluctuation obtained using different numbers of QDs. Both black and dark gray plots are fluorescence time traces of collections of QDs but containing different numbers of QDs sharing the common $t_{off}^{max} / t_{on}^{max}$ value. Obviously, the dark gray plot is obtained from a larger number of QDs as it is observed with significantly reduced intensity fluctuation.

However, it is not clear if the size of t_b affects the noise. In the next section, the effects of t_b, $t_{off}^{max} / t_{on}^{max}$, and N_S on noise are investigated by simulation and experimentation.

7.3. Mathematical description of the relative noise value

We have simulated intensity time traces for a collection of QDs with the conditions of (1) $N_T = 500$, (2) $t_{off}^{max} / t_{on}^{max} = 10^3 \, \text{sec} / 10 \, \text{sec} = 10^2$, $t_{off}^{min} \cong t_{on}^{min} = 10^{-4} \, \text{sec}$ and (3) t_b varying from 0.1 to 10 sec. Figure 7.3(a) shows the effects of t_b on noise at the steady state of the simulated time traces. As is seen in Fig 7.3(a), the center and the width of the Gaussian distributions scale linearly with bin-size. Therefore they do not affect noise. t_b can simply be regarded as a histogram bin-size of the Gaussian distribution. Therefore it does not affect the distribution. Figure 7.3(b) is a log-log plot of the data in Fig 7.3(a).

However, there can be Centroid errors that arise from the choice of the center of t_b. The range for significant Centroid error (10% - 10^{-2}%) occurs when t_b is comparable to the full width at half maximum (FWHM) of the distribution ($0 < \text{FWHM} / t_b < 1.5$). In Fig 7.3(a), the FWHM/t_b values are between 4.8 and 6.0, so that the Centroid error

119

due to the choice of t_b is negligible. Moreover, another Centroid error can be found when the number of events at the peak centroid is not large enough. When a small number of events are "histogrammed", a small t_b increases the uncertainty that the distribution can be fit with a Gaussian distribution. In experiments, if sufficiently long steady state traces are acquired, this effect can be ignored. Overall, the effect of t_b on noise can be negligible for a reasonable choice of t_b and sufficiently long data sets (long acquisition time for the steady state).
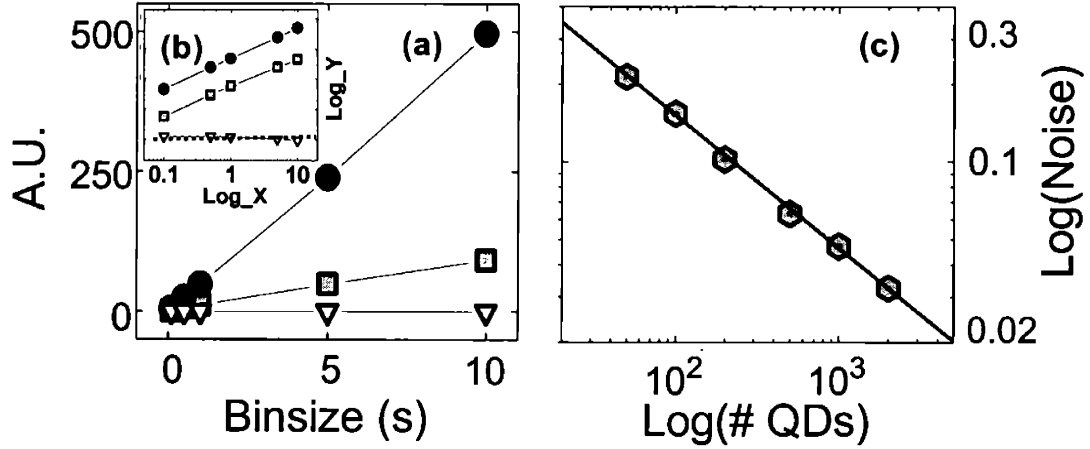
Figure 7.3. (a) The plots are obtained from the average intensity value (dark gray circles), the standard deviation (gray squares) of the intensity, and the ratio (white triangles) of the standard deviation at the steady state of the simulated time traces with the conditions $N_T = 500$, $t_{off}^{max} / t_{on}^{max} = 10^3 \, \text{sec}/10\text{sec} = 10^2$, $t_{off}^{min} \cong t_{on}^{min} = 10^{-4} \, \text{sec}$, by varying t_b values, 0.1, 0.5, 1, 5, 10 sec. (b) Log-log plot of (a). The dotted line indicates the theoretically calculated noise value. (c) Log-log plot of theoretical noise values vs. N_T at the steady state of the simulated time traces with the identical conditions of (a), but with $t_b = 0.5$ sec. The power-law slope is fitted to be -0.5.

Fig. 7.3(c) is a log-log plot of the noise at the steady state obtained from simulations using the same conditions as those in Fig. 7.3(a) but with t_b fixed at 0.5 sec and varying N_T. We find noise $\propto N_T^{-0.5}$ as in Eq 7.2.2. As a check, each N_T value used to simulate the time traces was successfully recovered from the measured relative standard deviation value at the steady state by using Eq 7.2.3. This method to extract N_T from the noise in the fluorescence time traces of a collection of QDs is not affected by the choice of the excitation intensity as long as the required conditions specified in Section 7.1. are fulfilled.

7.4. N_S dependence on the noise from experiments.

A dilute solution of CdSe/ZnS core-shell QDs (first absorption feature at 570nm) well dispersed in hexane was spin-coated on a glass coverslip. Figure 7.4(a) shows fluorescence intensity time traces of a collection of QDs varying the number of pixels of the CCD detector. Since the QDs are homogeneously dispersed in two dimensions, the number of QDs increases linearly with the number of pixels. Figure 7.4(b) shows a close-up of the steady state regions in Figure 7.4(a). Fig 7.4(c) shows the noise values as a function of the number of pixels. Although the density of QDs per pixel may not be perfectly constant in the experiment, we still find the power-law decay with a power of 0.5.

Additionally, we attempted to estimate the number of QDs in the microsphere shown in Fig 7.1(b) by using Equation 7.2.3. The estimated number of QDs per

microsphere by absorption measurement was 1,200 with potentially large error (i.e. a factor of 2 or 3)[1].
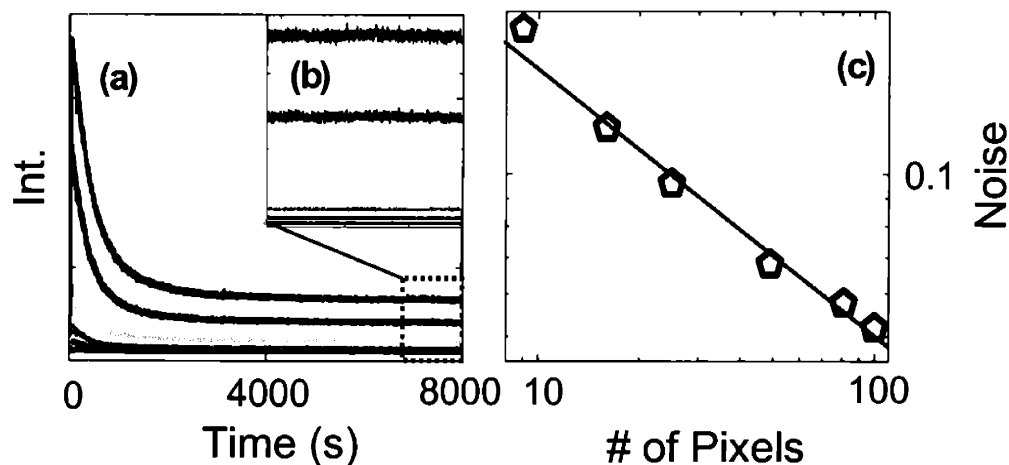

Figure 7.4. (a) Fluorescence time traces of a collection of CdSe(ZnS) QDs, accumulated in 9, 16, 25, 49, 81, 100 pixels (down to up) of the CCD detector. (b) Zoomed-in traces at the steady state. (c) Log-log plots the noise obtained at the steady state accumulated from each the pixel size (as specified as in fig (b)). The power-law slope was fit to be –0.51

The number of QDs in a microsphere was estimated using the noise at steady state as follows. Fluorescence time traces from 10 microspheres were observed. First common values of $t_{on}^{max} = 78 \sec$ and $t_{off}^{max} = 3,600 \sec$ were extracted from the fluorescence time trace of a microsphere. Second, the fluorescence time trace was normalized to 0.5, yielding an expected steady state value of 0.19. Using the experimental values of $t_{on}^{max} = 78 \sec$ and $t_{off}^{max} = 3,600 \sec$, we obtain the ratio, $t_{off}^{max} / t_{on}^{max} \approx 46$ which gives calculated steady state value at 0.19, identical to the experimental steady state value. This confirms that $f_{on}(t) \cong 0.5$ at the quasi-equilibrium state. A noise value of about 0.044 at the steady state was next obtained. The number of

QDs in the microsphere, N_T, was next estimated to be 2010 using Equation 7.2.3. The average number of QDs per microsphere from 10 microspheres was estimated to be 2,000. This value is within a factor of two within the error of that measurement. This simple method can be usefully exploited to estimate the number of QDs in their fluorescence time traces when it is not feasible to directly count the number of QDs.

7.5. Conclusion

The fluorescence intensity fluctuation (the noise) of a collection of QDs at the steady state is identical to the fluctuation of the number of emitting QDs at the steady state. Therefore, the number of emitting QDs during one bin-time at the steady state becomes a random variable that follows Poissonian (Counting) Statistics. The noise simply becomes a relative standard deviation around a mean value of emitting QDs at the steady state. The mean value of emitting QDs at the steady state is a function of on and off-time upper cut-off values and the total number of QDs. A simple mathematical formula that determines the noise was developed. The effect of binning on the noise was demonstrated to be negligible. The number of QDs incorporated in a silica microsphere was estimated to be within experimental error of the absorption measurement. In practice, this method could be very useful for estimating the number of QDs in QD containing microspheres or other QD containing systems.

7.6. References

1. Y. Chan, J.P-. Zimmer, and M. G. Bawendi, "Incorporation of Luminescent Cadmium Selenide Nanocrystals into Monodisperse Silica Microspheres," *Submitted.*

Inhee Chung

Education

Massachusetts Institute of Technology   Cambridge, MA

Ph.D. candidate in Physical Chemistry, degree expected: June 2004

Pohang University of Science and Technology (POSTECH)   Pohang, South Korea

B.S. in Chemistry, February 1999. Participated in undergraduate research programs resulting in published paper and thesis. Thesis: Recent Ultra-Short Laser Spectroscopic Methods in Studying Solid Surface

Research Experience

MIT, Department of Chemistry   Cambridge, MA

Advisor: Moungi G. Bawendi (December 1999 – present)

Thesis Title: Understanding and Engineering the Photophysics of Single CdSe Nanocrystals

- Created single molecule imaging microscopy set-ups to investigate fundamental optical and electronic properties of single and ensemble semiconductor nanocrystals.
- Developed statistical and theoretical models to interpret the optical properties of nanocrystals.
- Investigated the relationship between chromophores and environment, categorized to insulating amorphous, insulating crystalline, conducting amorphous, and conducting crystalline materials by constructing theoretical models and single molecule microscopy studies.
- Designed a novel imaging microscopy to probe three-dimensional orientation of single nanocrystals and applied this process to measure mechanical properties of plasma cell membrane.
- Created sophisticated device structures to monitor the electronic energy structures of the quantum confined nanocrystals.

POSTECH, Department of Chemistry   Pohang, South Korea
Advisor: Taiha Joo
Thesis Title: Recent Ultrashort Laser Spectroscopic Methods in Studying Solid Surface

- Investigated vibrational relaxation of – SH bonds on Ag surfaces by femto-second spectroscopy and designed a precise motion mechanical stage in Professor Joo's Laboratory (1998-1999)

- Designed an electrochemical sensor in Professor Park's Laboratory (Fall, 1996 – Spring, 1997)

- Participated in synthesizing bio-organic molecules and analyzed different isomers by HPLC in Professor Chung's Laboratory (Summer 1996)

Teaching Experience

MIT, Department of Chemistry   Cambridge, MA

Advanced Physical Chemistry Laboratory. Teaching Assistant.

Supervised and instructed students in the theoretical background and experimental techniques of pico-second transient-grating spectroscopy. Assisted each group of students with in-depth understanding the principle of time-resolved spectroscopy and with preparation for the final presentations. Graded final presentations with professors. (September 1999 – December 1999)

Thermodynamics and Kinetics. Teaching Assistant

Instructed students in the lecture material and prepared separate teaching materials. Helped write problem set solutions and exams. Assisted students individually with homework problems, exams or material they found difficult to understand. (February 2000 – May 2000)

POSTECH   Pohang, South Korea

Introductory class for beginning debaters. President of the Debating Society

Instructed new students to the debating society, the basic debating format used in U.K. parliament style, and how to develop arguments. (1996-1997)

Presentations

- Oral Presentations
  Chung I, Shimizu KT, Bawendi MG, "Single QDs Polarization Optical Microscopy." Harrison Spectroscopy Annual Seminar, MIT, Jan. 2001.

  Chung I, Shimizu KT, Bawendi MG, "Room Temperature 3-D Orientation Measurements of Single Quantum Dots Using Polarization Microscopy."American Physical Society, Seattle, Mar. 2001.

  Chung I, Bawendi MG, "Photoluminescence Dynamics of Single Nanocrystal Quantum Dots." American Physical Society, Austin, Mar. 2003.

  Chung I, Bawendi MG, "Does Single Colloidal Quantum Dot Optical Behavior Reflect Itself in the Optical Response of a Collection of QDs?" Material Research Society Meeting, Boston, Dec. 2003.

- Poster Presentations

  Chung I, Shimizu KT, Bawendi MG, "Room Temperature Polarization Studies of single Quantum Dots and its Application." Gordon Conference of Clusters, Nanocrystals & Nanostructure, Connecticut, Aug. 2001

  Chung I, Tracey J, Bawendi MG, "Single Colloidal Nanocrystal Spectroscopy and its Application." Nano scale Science and Engineering Center (NSEC) meeting at Harvard University, May 2002.

  Chung I, Bawendi MG, "Does Single Colloidal Quantum Dot Optical Behavior Reflect Itself in the Optical Response of a Collection of QDs?" Gordon Conference of Electronic Dynamics and Spectroscopy, Maine, Jul. 2003.

  Chung I, Lubchenko V, Silbey R, Bawendi MG, "Effect of the Environment on the Blinking Statistics of Single CdSe Quantum Dots." Material Research Society Meeting, San Francisco, Apr. 2004

Publications

Works in preparation are not listed here.

"Room Temperature Measurements of the 3D Orientation of Single CdSe Quantum Dots using Polarization Microscopy." Chung I, Shimizu KT, Bawendi MG, Proceedings of the National Academy of Sciences of the United States of America 2003, 100:405-408.

"Single Quantum-Dot Intermittency and Fluorescence Intensity Decays from Collections of Dots." Chung I, Bawendi MG 2003 (Submitted)

"Synthesis of All Possible Regioisomers of scyllo-Inositol Phosphate." Chung SK, Kwon YU, Chang YT, Sohn KH, Shin JH, Park KH, Hong BJ, Chung IH. Bioorg. Med. Chem. 1999, 7, 2577-2589

Acknowledgements

I wish to convey my sincere gratitude to all the people who have accompanied me and supported me in my life. I have felt so privileged and grateful since I have such a wonderful family. I am most thankful to my mother. You are the motivation of my life. I cannot thank you enough for being such a great mother and a best friend to me. You have been right beside me all the time and kept teaching me valuable lessons for my life. Your warmest heart and wisest advice have always saved me whenever I felt down or was lost. I also deeply thank my father for all his support and encouragement with never-ending trust in me. Moreover, you taught me how to view things realistically. Yunhee, my cute and lovely younger sister, always gave me big smiles with wit and sweetness. Finally, I am thankful to my grandmother, who has such a beautiful and pure heart and constantly shows her warmest wishes to me. If there is a reason I have never doubted the fact that I love my life, it is because all of you are with me in my life.

MIT has been a great place to learn about science and life with such amazing people that have greatly affected me. I consider myself very lucky to have had Professor Moungi Bawendi as my advisor. I have learned so many lessons from him in terms of science and also life. I have been always amazed by his shrewd insight and thoroughness in science. Having scientific discussions with my advisor has been a great joy. Moreover, his endless curiosity about any issue has given me the liberty to ask whatever questions I wanted, even if they were not always relevant to our research. For the first three years, while I was still very afraid of my advisor :), his main lesson to me was to be independent in research and in life. I once asked him when I would be ready to graduate and he answered: "when you don't need my help." I am not sure if, because I am graduating, I don't need your help any more, but I indeed have become quite independent, compared to myself in my first year. Thank you so much for all the lessons, advice and help!

I am also very grateful to all the members in the Bawendi group. As a laser lab person, I will first thank people in the laser lab A. I have to thank Jean-Michel first who has been a good friend to me. I am deeply thankful to you for all the help and for sharing such intriguing scientific discussions with me, and also for the times I was working late in the laser lab and you constantly woke me up by triggering my desire to see the results. When I was arguing with you about big and small issues right after you first joined this group, I didn't expect that you would become such a good friend. Thank you, man, for everything! I am also thankful to Ken for teaching me how to do the experiments when I first joined this group. I thank Antoine, who recently joined our group and helped me with experiments, also Brent, for all the help, former postdoc Hans and our newcomer, Hao. I also thank laser lab B people. Mirna, who has been a good friend since I joined the group: I am thankful to you for being such a listener whenever I had some issues, and for the invitations to events. I am thankful to Venda for all the help and cheerful conversations. I also thank David for his help, even with a dorm issue. I thank Catherine